L'impact de la croissance des plantes et l'absorption du potasse sur l'évolution minéralogique des argiles du sol

Eleanor Bakker

UNIVERSITÉ GRENOBLE ALPES

THÈSE

Pour obtenir le grade de

DOCTEUR DE L'UNIVERSITÉ GRENOBLE ALPES

Spécialité : **Sciences de la Terre, de l'Univers et de l'Environnement**

Arrêté ministériel : 25 mai 2016

Présentée par

Eleanor Bakker

Thèse dirigée par **Bruno Lanson**
et codirigée par **Fabien Hubert**

préparée au sein de **l'Institut des Sciences de la Terre**
et de l'école doctorale **Terre Univers Environnement**

The impact of plant growth and potassium uptake on clay minerals in soil

Thèse soutenue publiquement le **6 avril 2018**,
devant le jury composé de :

Philippe Hinsinger
Directeur de Recherches, INRA UMR Eco & Sols, Montpellier, Rapporteur

Stephen Hillier
Professor at the James Hutton Institute, Aberdeen, Royaume-Uni, Rapporteur

Laurent Charlet
Professeur au ISTerre, Université Grenoble Alpes, Grenoble, Président

Pierre Barre
Chargé de Recherche au Ecole Normale Superior, Paris, Examinateur

Fabien Hubert
Maître de Conférence au IC2MP, Université de Poitiers, Grenoble, Co-Directeur de thèse

Bruno Lanson
Professeur à l'ISTerre, Université Grenoble Alpes, Grenoble, Directeur de thèse

Résumé

Le potassium est un nutriment essentiel à la croissance et au développement des plantes. Les minéraux argileux dans les sols représentent un important réservoir de K disponible pour les plantes. L'extraction de potassium fixé à partir de l'espace interfoliaire des minéraux micacés 2:1 peut entraîner une augmentation de la distance feuillet à feuillet qui peut être mesurée par diffraction des rayons X . Des échantillons de l'expérience Morrow Plots continue avec du maïs ou du maïs-avoine-foin, provenant de sous-parcelles fertilisées et non fertilisées pour les années 1904, 1957, 1980, 1997 et 2013-2014, ont été soumis au fractionnement granulométrique séquentiel pour obtenir la fraction limoneuse (50-2 μm) et les sous-fractions argileuses (2-0,2, 0,2-0,05 et <0,05 μm). Les résultats granulométriques montrent une hétérogénéité significative malgré la petite taille de la MP, et un gain de sous-fraction $<$ 0,05 μm avec le temps. La modélisation des diagrammes de diffraction des rayons X a été effectuée pour obtenir une identification concluante de l'assemblage de minéraux argileux et évaluer l'impact de 110 ans d'agriculture continue et de différentes pratiques agronomiques de 1904 jusqu'à 2014. Un assemblage complexe de minéraux argileux a été identifié avec jusqu'à onze contributions différentes nécessaires pour reproduire les données expérimentales de sous-fractions de moins de 2 μm, y compris jusqu'à six couches mixtes d'illite-smectite-chlorite. L'analyse de phase quantitative pour toutes les sous-parcelles et toutes les années, a montré que l'assemblage minéral du Morrow Plots est similaire entre les différentes sous-parcelles, quel que soit le traitement agronomique. Aucune preuve significative d'altération ou de transformation des phases minérales argileuses n'a été observée au fil du temps. La nature dioctaédrique des minéraux argileux de la MP désavantage l'extraction du potassium et donc la dissolution est le mécanisme privilégié pour l'absorption du potassium et la perte de sous-fractions 2-0,2 et 0,2-0,05 μm est attribuée à ce processus.

Abstract

Potassium is an essential nutrient for plant growth and development. Clay minerals in soils represent an important reservoir of plant-available K. Extraction of fixed potassium from the interlayer space of micaceous 2:1 minerals can lead to an increase in the layer-to-layer distance which can be measured by X-ray diffraction. Samples from the Morrow Plots continuous corn and corn-oats-hay experiment, from fertilised and non-fertilised subplots for the years 1904, 1957, 1980, 1997 and 2013-2014 were subjected to sequential size-fractionation to obtain the silt fraction (50-2 um) and clay-sized subfractions (2-0.2, 0.2-0,05 and <0.05 um). Granulometric results show siginificant heterogeneity despite the small size of the MP, and a gain in <0.05 um subfraction with time. Full-profile fitting of X-ray diffraction patterns was performed to obtain conclusive identification of the clay mineral assemblage and to assess the impact of 110-years of continuous agriculture and different agronomic practices from 1904 to 2014. A complex clay mineral assemblage was identified with up to eleven different contributions necessary to reproduce the experimental data of <2 um subfractions, including up to six illite-smectite-chlorite mixed-layers. Quantitative phase analysis for all subplots and years showed that the mineral assemblage of the Morrow Plots is similar between different subplots, regardless of agronomic treatment. No significant evidence of alteration or transformation of clay mineral phases was observed over time. The dioctahedral nature of the clay minerals of the MP disfavours potassium extraction and thus dissolution of the entire crystal structure appears to be the favoured mechanism of nutrient extraction. The loss of 2-0.2 and 0.2-0.05 um subfractions is attributed to this process.

Acknowledgements

First of all I express my gratitude to my supervisors, Bruno Lanson and Fabien Hubert, firstly for choosing to accept me for the PhD position, and secondly, for the invaluable advice and guidance through my PhD and the mountains of work involved. I really appreciate the assistance you proivded and the confidence you had in me to complete the work.

Thanks also to my *rapporteurs*, Stephen Hillier and Philippe Hinsinger, for accepting the task of reading my manucript and providing insightful comments and ideas. I also appreciate the input of my *examinateurs* Michelle Wander, Pierre Barré and Laurent Charlet for taking the time to assess my work and for the questions and feedback that you have given me.

I would also like to thank Nathaniel Findling for all his help with sample preparation, his patience dealing with my basic French at the start of my PhD, for running so many XRD analyses for me, and most importantly for his care repairing the centrifuge when it had *tombé en panne*. I would also like to extend my thanks to Martine Lanson for performing CEC and elemental analyses for me, and all her other assistance in the lab. And further thanks to all the other interesting and wonderful people in ISTerre who were always welcoming, whether over a cup of coffee or celebrating with an inflatable unicorn.

A huge thank-you to all my friends and football crew in Grenoble and elsewhere for providing necessary distractions in the many moments we spent talking-laughing-drinking-dancing-relaxing-picnicking-playing. In no particular order, Natalie, Laura, Jess, Michelle, Nikos, Wilfrid, Paul, Eric, Maor, Jakes, Tobias, Thu, Benoit, Irene, Frans, Anca, Favio, Thu, Liva, Zane, Christian, Randy, Moritz, Catarina, Cyril, Igor, Marcelo, Margarita, Felix, Matt, Will, Linda, Miguel, and probably many others who I have forgotten (sorry!). Special thanks to Maor for market coffee, Rummikub, and for tolerating the worst of my stressed moods; to Laura as a wonderful and easygoing flatmate; to Natalie for general awesomeness and Princess provider; and to Irene for all the dirty jokes and quotes. And last but not least a big thanks to my family for all the conversations and support during my #PhDstruggle, it would have not been possible without you. Big thanks to Arwen for knowing the right things to say to kick me out of my ruts, to Dylan, Maria, and Willem (and cats!) for giving me a relaxing hideaway in Berlin and not complaining (much) that I spent all my time gaming, and to Benny and Kirstie for their massive confidence in me and the rational advice I needed.

Love you guys!

♡

Contents

List of Figures

List of Tables

Introduction

Figure 1.1: Potassium balls stored in oil to prevent reaction with water vapour in air.

1.1 Potassium

General information

Potassium (K) is a alkali metal with the atomic number of 19 and a molar mass of 39.0983 $gmol^{-1}$. It is one of the seven most abundant elements in the Earth's crust at about 2.6%, and the 20th most abundant element in the universe (Halka and Nordstrom, 2010). It is exceedingly reactive, so is never found as a pure metal, and must be stored in oil to prevent it from reacting violently with water vapour in air. Under normal conditions potassium has a single oxidation state, losing its outer electron to form the K^+ cation, which has an ionic radius of 1.38-1.69 Å depending on the degree of covalent-ionic bonding (Aylward and Findlay, 2002). It is commonly found in the form of salts such as potassium chloride (KCl), potassium nitrate (KNO_3) and potassium carbonate (K_2CO_3), which are

typically ionic in nature and relatively soluble in water. It is also found in feldspars and micas. There are three natural isotopes of potassium, stable ^{39}K and ^{41}K, and radioactive ^{40}K which is used as an dating method for crustal rocks, as it decays into the stable ^{40}Ar at a known rate (Aylward and Findlay, 2002; Halka and Nordstrom, 2010). While potassium was recognised as a unique chemical element as early as 1702, the pure metal was not isolated until 1807 by Humphrey Davy who extracted with the new method of electrolysis (at the same time extracting sodium) (Parsons and Dixon, 2013). He gave it the name *potassium* deriving from the common method of obtaining potassium salts in by burning wood in pots giving ash (pot-ash). Its chemical symbol, K, is taken from the German *kali* or *kalium*, which is in itself a derivation of the Arabic word for 'plant-ash' (which also gave the word alkali) (Mengel et al., 2001).

Potassium is an essential element for all forms of living organisms, and is one of the nine most common elements in the human body (by mass) with a suggested daily intake in the range of 3500-4700 mg per day necessary to maintain potassium levels (Halka and Nordstrom, 2010). Potassium plays a vital role in a number of functions in *homo sapiens*, including (and not limited to) propagation of electrical pulses in nerve and cardiac tissue, protein synthesis, and maintenance of cell-membrane potentials and of fluid/electrolyte balances (Halka and Nordstrom, 2010). A diet rich in fruit and vegetables is normally enough to maintain potassium levels, and use of mineral supplements can endanger health as a high concentration of potassium affects the regulation of cell water content and can have disastrous effects on nerve signalling to vital organs (Parsons and Dixon, 2013). Potassium is also an important plant nutrient and performs various vital functions.

Uses of potassium

Generally, pure potassium is seldom used due to its reactivity, and sodium compounds are used as a replacement where possible. Despite this, potassium compounds find a myriad of uses. Potassium cyanide (KCN) is famous for its historical role as a poison in various suicides and murders. More recently, potassium cyanide is used in large-scale gold mining operations, and is more often associated with the environmental concerns accompanying spills such as that of Baia Mare in 2000 (Batha, 2000). Potassium hydroxide, KOH, is a caustic agent used for soap production, and the manufacture of various drugs, alkaline batteries and for the unblocking of drains (Halka and Nordstrom, 2010). Potassium iodide, KI, is often added to table salt as a source of iodine, and also in

disinfectants. Some potassium salts are brightly coloured, such as potassium manganate ($KMnO_4$, purple) which is used as an antibacterial agent, chromate (K_2CrO_4) provides yellow colours for textiles and in ink, and yet another, dichromate (K_2Cr2O_7, orange) is used to preserve wood, develop blueprints, and colour glass (Parsons and Dixon, 2013). Potassium carbonate (K_2CO_3) is used in the glassmaking process, in brewing beer, and in fire extinguishers. While not an extensive list, various other potassium salts find their uses in gunpowder and explosives (KNO_3), fireworks and sparklers ($KClO_4$), and as a sedative (KBr) (Halka and Nordstrom, 2010).

However by far the most important use of potassium salts, in both production mass and significance, is the use of potassium in fertilisers. Potash, blood and guano have all been applied historically to soils to ensure adequate nutrient supply to plants, even before the unique role of potassium was recognised in 1860 (Marschner, 1995). Initially potassium was supplied through organic sources of manure and potash produced by the burning of wood, however following the discovery of large evaporite deposits in at Stassfurt in Germany in 1856 mineral fertilisation became the norm (Barker and Pilbeam, 2015). Worldwide, 40.7 million metric tonnes (Mt) were produced in 2015, and of this 90-95% went into the production of agricultural fertilisers (Jasinski, 2017a). Projections by the United Nations Food and Agriculture Organisation (UNFAO) expect increases in production of 43 Mt per year by 2020, due to increased demand for fertilisers in Asia and South America, and demand related to crops for ethanol-based fuel production (UNFAO, 2017).

Occurrence and extraction

Potash bearing deposits occur in the form of evaporite, which are created by the evaporation of ancient oceanic basins or lakes (Kesler, 1994). They primarily contain a mixture of sylvite (KCl) and halite (NaCl), and other potassium, sodium, magnesium and bromine minerals known as sylvinite (Foth, 1991). Worldwide deposits of potash are estimated at approximately 250 billion tonnes, with the largest deposits found in the Northern Hemisphere. Three countries, Canada, Russia and Belarus, accounted for 60% of world production and 85% of recoverable reserves in 2016 (Jasinski, 2017b). As these are soluble deposits, mining takes place underground, often at depths of 1,000 m or greater, and deposits must be protected from groundwater intrusions. For example, shafts are commonly lined with concrete and steel shields to prevent the influx of water. As sylvinite

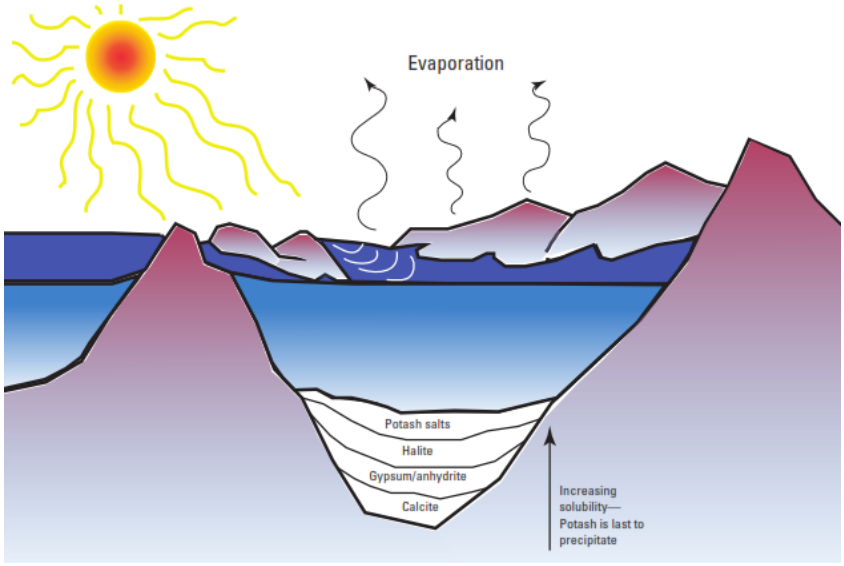

Figure 1.2: Schematic of evaporite formation from basin evaporation, from Kesler (1994).

is relatively soft, stability of mine shafts can also be an issue and closing of openings can occur within months. Thus, many mines do not recover all the mineral deposit but rather leave 55-65% behind to prevent collapse (Kesler, 1994).

In addition to underground mining, Israel and Jordan recover potassium from the Dead Sea, where the high salt concentration (approximately 8 times that of the Atlantic) makes such extraction commercially viable (Al-Harahsheh and Al-Itawi, 2005). Solution mining is a method which has replaced underground mining for deeper or more inaccessible reserves. This is performed by injection of freshwater into boreholes to dissolve the sylvinite, and the resulting solution is then brought to the surface, cooled and KCl precipitates out. Nevertheless, 94% of worldwide potash production involves exploitation of solid ores (Nielsson, 1986).

Processing of solid potash ores is performed to obtain fertiliser-grade levels of purity, for example in the United States products for agricultural applications must contain 60% K_2O (min) which is equivalent to 95% KCl (Kesler, 1994). The method of processing depends on physical and chemical characteristics. The typical process involves crushing and grinding followed by froth flotation, while differential precipitation is performed in cases where the ore is finely grained (Nielsson, 1986). Halite, NaCl, tends to be the largest by-product of refining processes. Potassium sulfate (K_2SO_4) and potassium nitrate (KNO_3) may also be produced for fertiliser needs. There is generally no easy

replacement for potash as a mineral fertiliser, as manure sources have low potassium values and need to be produced close to the location of use (Jasinski, 2017a). However current extractable reserves are sufficient to meet requirements for several decades and it is likely further underground deposits remain undiscovered or unexplored (Jasinski, 2017b).

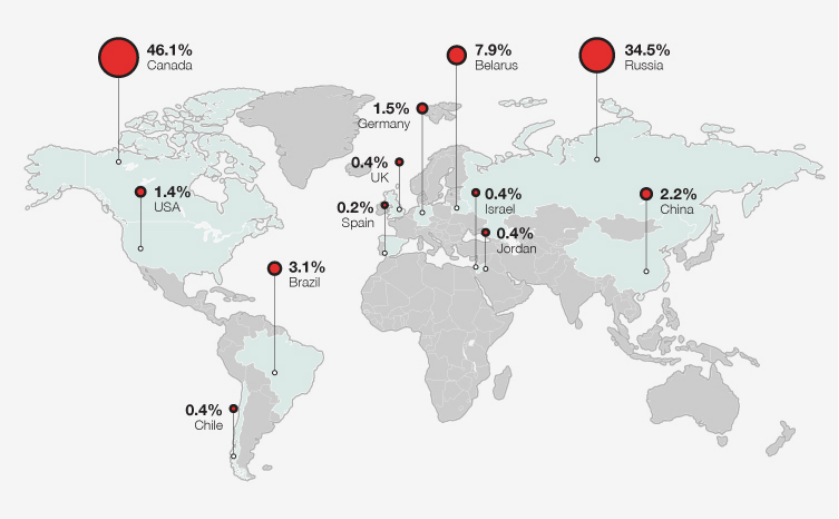

Figure 1.3: Map of worldwide distribution of proven potash reserves (Uralkali, 2017).

1.2 Potassium as an essential plant nutrient

Essentiality and use

The growth and yield of plants is directly related to the abundance of various factors, such as light, CO_2, moisture and a range of mineral nutrients. Mineral nutrients are required for specific enzymatic or metabolic roles, and can be classified as either *macronutrients* or *micronutrients*, depending on the plant requirements. There are six macronutrients, nitrogen (N), phosphorus (P), potassium (K), sulphur (S), calcium (Ca) and magnesium (Mg), and a number of micronutrients shown in Table 1.1 (Marschner, 1995). Potassium is the second most important of these nutrients (by weight) after nitrogen, with amounts for optimal growth being between 2-5% of the plant dry weight (Marschner, 1995). There is also an interaction between different mineral nutrients, with nitrogen uptake increasing with potassium availability, and as a result, potassium is frequently applied in mineral fertilisers, along with lime (L, $CaCO_3$ or other compounds to decrease pH), nitrogen and phosphorus (L-NPK fertilisers) (Foth, 1991; Marschner, 1995).

Table 1.1: Average concentrations of essential plant nutrients in dry plant shoot matter, adapted from Marschner (1995).

	Element	Symbol	μmol g^{-1} dry wt	%
Macronutrients				
	Nitrogen	N	1000	1.5
	Potassium	potassium	250	1
	Calcium	Ca	125	0.5
	Magnesium	Mg	80	0.2
	Phosphorus	P	60	0.2
	Sulphur	S	30	0.1
Micronutrients				
	Chlorine	Cl	3	-
	Boron	B	2.0	-
	Iron	Fe	2.0	-
	Manganese	Mn	1.0	-
	Zinc	Zn	0.30	-
	Copper	Cu	0.10	-
	Nickel	Ni	0.001	-
	Molybdenum	Mo	0.001	-

The essentiality of potassium has been proved via numerous laboratory experiments involving limited supply of potassium. Potassium is primarily present as ionic K^+, with a very small percentage incorporated into organic tissue, and is the most abundant cation in plant cytosol. It is involved in a large number of plant functions, including (but not limited to) (Barker and Pilbeam, 2015; Marschner, 1995):

- enzyme activation
- osmoregulation via
  - stomatal control
  - cell extension
  - phloem transport of sugars and starch
- protein synthesis
- photosynthesis and respiration
- ion absorption and transport (cation-anion balance)
- disease resistance

The role of potassium in photosynthesis directly correlates to increasing yields, as photosynthesis involves the transformation of light-energy into chemical energy and thus growth of plant tissues (Marschner, 1995). The role of potassium in osmoregulation plays a vital part in the drought and frost resistance of crops (Mengel et al., 2001). In legumes with an abundant supply of potassium (rather than deficiency), supply of potassium corresponds to improved transport of starch from leaf to other plant organs (Marschner, 1995).

Potassium deficiency and excess

Potassium deficiency is not easily recognisable, as the first sign is a retardation in the growth of the plant, such as poorly developed root systems or weak stalks, which contribute to lodging (non-vertical plant growth) (Mengel et al., 2001). A portion of this stunted growth is due to the role of potassium in cell turgor and extension, where an inverse relationship exists between potassium supply and cell-size of leaves, stems and storage tissues (potato tubers, carrots, etc.) (Marschner, 1995). Potassium deficient plants produce poor fruiting bodies, and have low frost, drought and disease resistance. As deficiency advances, further symptoms appear first in older leaves, as a yellowing (or scorching) of the leaf edges resulting from the transport of mobile potassium from older to younger plant tissues (Mengel et al., 2001).

Potassium deficiency is also linked to a number of non-visible chemical changes. One effect is poor water regulation and thus a higher water demand (Mengel et al., 2001). Additionally, soluble nitrogen compounds accumulate in the tissues of potassium deficient plants - perhaps related to the inhibition of certain protein synthetic pathways, or an effect on the activation of the nitrate reductase enzyme (Koch and Mengel, 1974). Accumulation of soluble carbohydrates and a decrease of starch content occurs, related to the reduced efficiency of the starch synthase in potassium deficient conditions (Marschner, 1995). A diamine, putrescine, also accumulates up to a factor of 80-100 times, as its synthesis is stimulated by the low pH arising under potassium deficient conditions. A divalent cation, putrescine compensates to a certain degree the K^+-deficit, and additional external supply was shown to prevent visual signs of potassium deficiency (Tachimoto et al., 1992).

Occurrences of potassium excess are rare with no specific symptoms other than possible depression of plant growth and yield. This is largely due to the well-regulated uptake of potassium by plants. Effects of oversupply of potassium tend to relate to a situation

Figure 1.4: Comparison of potassium deficient soy (*Glycine max*) leaves showing characterisitic yellowing of edges (left), next to soy receiving adequate potassium nutrition (right) (IPI, 2010).

called 'luxury uptake′ and suppression of the uptake of other cations such as Na^{+}, Mg^{2+} and Ca^{2+} as potassium competes strongly with these cations (ion-antagonism) and high quantities of Ca, Mg and Na are taken up at higher rates when potassium concentrations are low (Fageria, 1983; Foth, 1991).

Bioavailability and uptake

Plant uptake of mineral nutrients occurs through root uptake of ions in the soil solution. Root activity influences a volume in proximity to the roots which is defined as the rhizosphere (Hinsinger, 1998). The volume of the rhizosphere can vary widely depending on the mobility of the element considered, and may even vary widely for a single element, dependent on bulk soil properties and plant species and age, but is generally considered as several mm of soil closest to root surfaces (Marschner, 1995; Hinsinger, 1998). Chemical conditions in the rhizosphere can vary considerably from those of the bulk soil due to plant selective uptake of ions from the soil solution leading to depletion and/or accumulation, and release of plant exudates, such as organic anions and H^{+} (Marschner, 1995).

In the case of potassium, the relatively low concentration in the soil solution means that mass-flow processes (related to transpiration and plant uptake of water) are insuf-

ficient to meet plant potassium nutrient requirements (Marschner, 1995). This leads to a zone of depleted potassium concentration in the rhizosphere and the creation of a concentration gradient which may extend several millimetres from the root surface (Marschner, 1995). Due to the concentration gradient, plants are strongly reliant on diffusion processes for potassium nutrition, which for soils can be described using the *effective diffusion coefficient*, D_e. This is described in Equation (1.1) and is related to the diffusion coefficient in water (D_1), the water content of the soil (Θ), the tortuosity factor (describing the pathway that ions follow in the soil solution and pore space) (f), and the concentration of the ion in the soil solution, C_1, and the sum of ions both in the soil solution and which can be released from the solid phase (C_s) (Marschner, 1995).

$$D_e = D_1 \Theta f . \frac{C_1}{C_s} \tag{1.1}$$

Potassium uptake is also strongly related to the water content of the soil, which affects the distribution of nutrient uptake between top- and subsoil sources (Marschner, 1995). During times of drought, contact between roots and soil solution in the topsoil is limited, and thus a significant proportion of potassium nutritional needs are met through uptake from subsoil sources. For instance, (Fox and Lipps, 1960) showed that more than 60% of total nutrient requirements were met through subsoil uptake although this accounted for only 3% of overall root mass. Timing and intensity of rainfall events during the growing season is also associated with variations in root distribution between top- and subsoils, which again affects the distribution of nutrient uptake between the two (Marschner, 1995). A further association can be made between uptake and soil texture, which is a controlling factor for contact between plant roots and the soil matrix, however root-interception is a minor contributor to plant potassium nutrition.

Potassium cycling

Potassium contents in topsoils range from 11.7 to 26.3 mg g^{-1}, corresponding to 40,000 to 50,000 kg ha^{-1} (Foth, 1991). A simplified potassium cycle is shown in Figure 1.5 where the main inputs for soil potassium are fertilisers (chemical and manure), crop residues, and soil potassium minerals (atmospheric inputs resulting from deposition of dust particles are usually insignificant), while depletion occurs primarily through crop

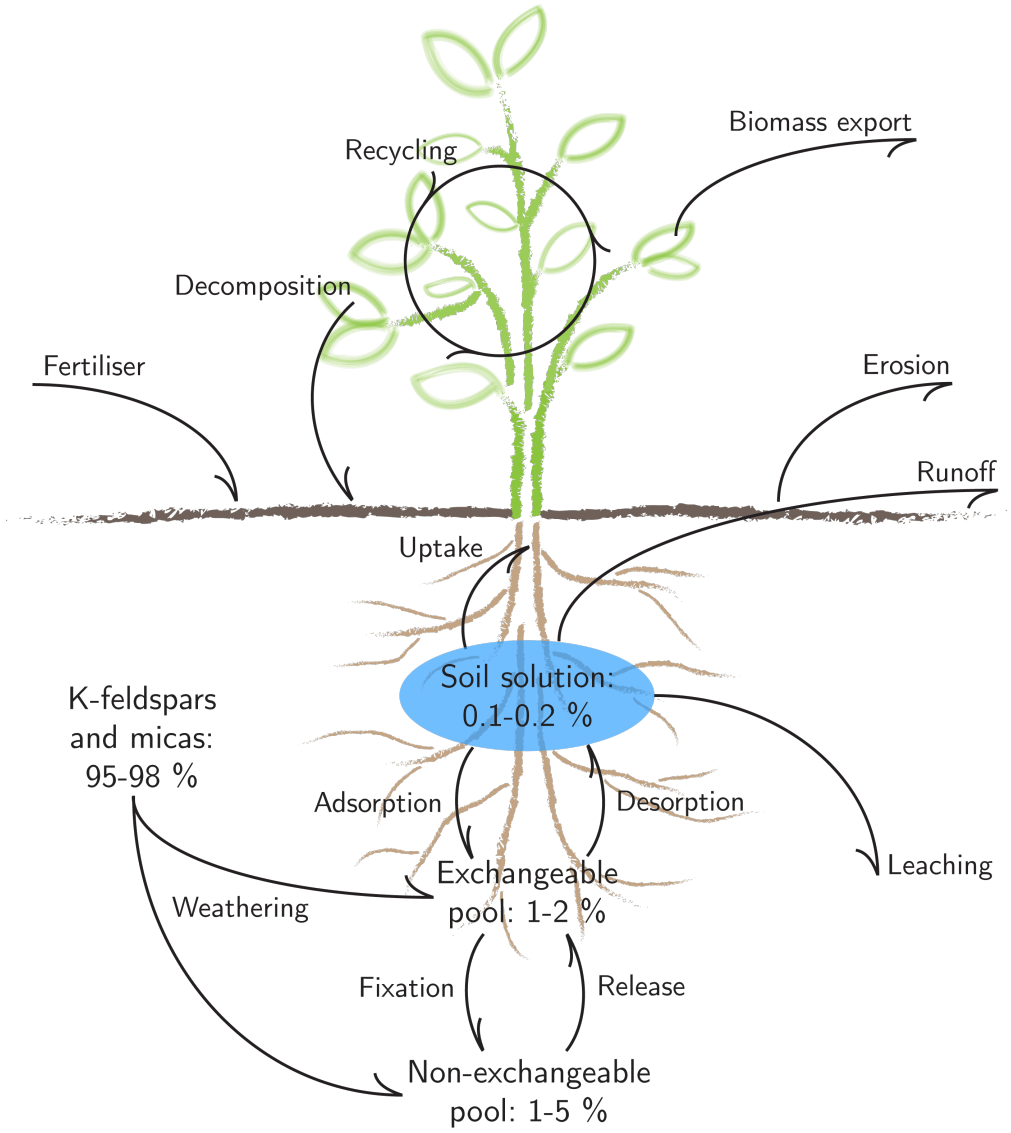

Figure 1.5: Simplified conceptual scheme of potassium cycling in soil (adapted from (Mengel et al., 2001; Sparks, 1987).

export, and erosion and runoff. Losses due to leaching tend to be minor, due to the potassium fixing capacity of many soils with the exception of very sandy soils (Mengel et al., 2001; Sparks, 1987).

In soils, 90-98% of this potassium is found in the crystal structure of K-feldspars and micas such as muscovite and biotite (Sparks, 2001). This potassium is released only slowly to plants through the weathering and dissolution of the mineral structure in contact with

the soil solution, releasing K^+ in addition to other cations (Velde and Meunier, 2008). Under natural conditions, mineral potassium is the most important source of potassium for plants, and thus soil fertility is strongly related to the soil parent material and the rate of weathering processes (Sparks, 1987). The second pool of soil potassium is so-called non-exchangeable potassium, which is fixed in the interlayer spaces of secondary 2:1 clay minerals (see Section 1.5.3), and accounts for 1-10% of soil potassium reserves (Sparks, 2003). The remaining 1-2% of soil potassium is in equilibrium between the soil solution (0.1-0.2%) and the exchangeable pool (Sparks, 2001). Potassium in the exchangeable pool consists of potassium adsorbed on mineral surfaces, such as that of kaolinite, and in the interlayer spaces of 2:1 minerals such as smectites, and associated with organic matter (Sparks, 1987). Exchangeable potassium is directly available to plants through processes of cation exchange (Mengel et al., 2001).

1.3 Soils and pedogenesis

Soil

Difference authors have descirbed soil in various ways. For instance, Joffe (1936) described soil as

"*...a natural body, differentiated into horizons of mineral and organic constituents, usually unconsolidated, of variable depth, which differs from the parent material below in morphology, physical properties and constitution, chemical properties and composition, and biological characteristics.*"

while Ramann (1928) used a definition of soil as

"*...the upper weathering layer of the solid earth crust.*"

In contrast, Hilgard (1921) chose to focus on the interaction with plants, giving

"*The more or less lose and friable material in which, by means of their roots, plants may or do find a foothold and nourishment, as well as other conditions of growth.*"

Despite these of the various definitions, soil can be characterised as a complex, open physical system, meaning that material or energy may be added to or removed from the

soil (Sposito, 2008). Soils represent the intersection of, and interface between, atmosphere, hydrosphere, biosphere, and lithosphere and are made up of assemblies of various solid components such as crystalline and amorphous phases, organic matter (humus), liquids, gases and organisms (Velde and Barré, 2009). One of the most important defining properties of soils is their anisotropy, in that there exists a spatial distribution of chemical and physical properties (Jenny, 1994). Other typical properties include colour, pH, and texture (Soil Survey Staff, 1999). The potassium content of soils is strongly dependent on the nature and quantity of the crystalline phases which make up the pools depicted in Figure 1.5 (Sparks, 1987).

Soil forming factors

Soil mineralogy is directly related to the pedogenesis of the soil - the formation of soil, over time, from parent rock. Using the approach of the Dokuchaev School of Soil Science, the five major factors which control the genesis of soils are typically considered: parent material (p), climate (c), relief (or topography, r), biota (b) and time (t) (Figure 1.6). These factors also indicate the openess of the soil system - climatic effects are dictated by the atmosphere and do not change dramatically when crossing the air-soil boundary. Different combinations of these factors lead to the development of soils with specific chemical properties. They also lead to the development of soil horizons, or strata, within a soil profile which recognise vertical transitions in the degree of weathering as soils are altered downwards from the original soil-rock interface.

Climate and topography

Climatic processes such as rainfall, wind and temperature determine worldwide distributions of soil. Overall, global air-flow and temperature variations tend to give high rainfall in zones close to the equator, followed by desert climates typified by high temperatures and extremely low rainfall bordering tropical zones which then graduate to temperate zones at higher latitudes (Figure 1.7) (Velde and Barré, 2009). The combination of high temperature and high rainfall can lead to an intense alteration, while lower rainfall and moderature temperature can lead to a significant deposition of organic matter (Jenny, 1994). This distribution of such zones of temperature and rainfall is next impacted by large-scale geological constraints such as the location and breadth of continents and mountain chains, particularly in the Northern Hemisphere (Velde and Barré, 2009). This shows that not only local, but global topography affects soil formation due to the effect on

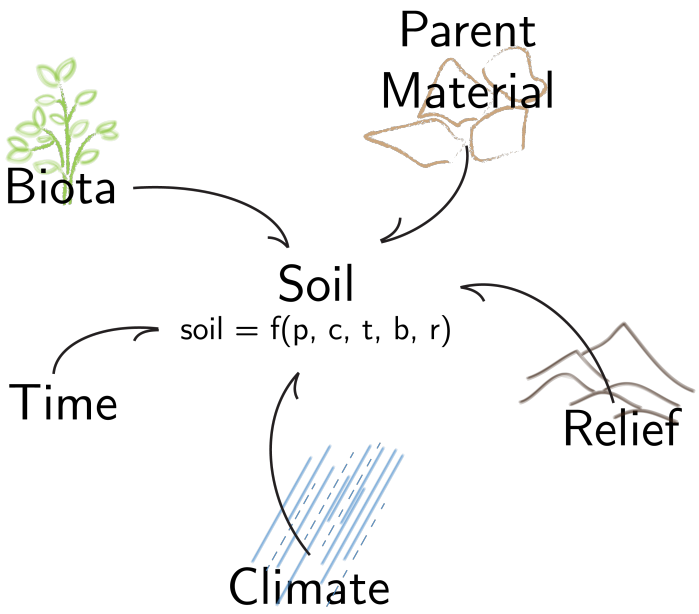

Figure 1.6: The genesis of soils is controlled by the five factors shown here, according to the equation of Jenny (1994).

the hydrosphere. For example, mountain chains redirect atmospheric flows of moist air in the atmosphere which then affects rainfall, while the flow of water and erosion/depostion of fine particles on a mountainside is different to that of a valley (Velde and Barré, 2009). Mountains also affect local climatic factors such as temperature and water-table depth Kutílek and Nielsen (2015).

The flow of water is the most important agent in soil formation, as its movement allows for the precipitation, dissolution and transport of substances within the soil system. Thus rainfall has a significant role, however this is attenuated by the amount of evaporation (related to temperature), evapo-transpiration rates of overlying vegetation and the permeability of underlying soil and rock horizons.

Parent material

The composition of the parent material has an influential role in determining a) the rate of weathering and b) the chemical composition of altered minerals (Meunier, 2005). The presence of silicon or aluminium rich parent material can lead to the formation of clay minerals, while other metal cations can influence soil colour and redox processes (Fe, Mn...), soil flocculation (Ca^{2+}, Mg^{2+}) or dispersion (K^{+}, Na^{+}), and acidic parent material again affects soil pH and dissolution rates (Jenny, 1994). These are important

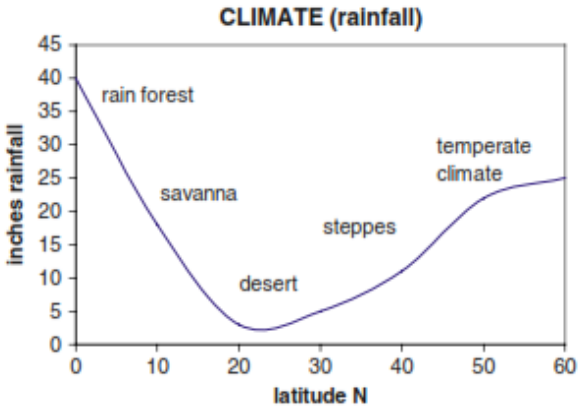

Figure 1.7: Depiction of how rainfall variation with increasing distance from the equator (Velde and Barré, 2009).

considerations given that approximately 50-66% of soil volume consists of solid material (Sposito, 2008). In the majority of soils more than 90% of this solid material is inorganic (or mineral) (Sparks, 2003). Weathering through physical disintegration of the parent rock may results from factors such as temperature-based, stress-inducing, volume changes which cause cracking and disruption of the compact rock matrix (Kutílek and Nielsen, 2015). Other methods of physical weathering are freeze-thaw cycles of fluid-filled cracks, growth of plant roots, and the action of wind and glaciers (Kutílek and Nielsen, 2015).

Other weathering processes are due to chemical decomposition, through the movement of water through fractures and faults in the rock leading to dissolution, transport, and reprecipitation of mineral elements within the soil system (Meunier, 2005). Chemical weathering depends strongly on the nature of the chemical bonds in the parent material - i.e. on the chemical composition - as these dictate slight differences in solubility and thus which minerals are most susceptible to weathering (Kutílek and Nielsen, 2015). The presence of trace elements or substutions in the crystal lattice also plays a role as these can involve a distortion in the lattice and a weakening of bonds surrounding the site of substitution (Wells and Norrish, 1968).

Biota

The presence and nature not only of vegetation but also of micro-, meso- and macrofauna in the soil ecosystem is closely linked to the formation of soils. Not only is the action of plant roots important to the physical breakdown of rock structures, their exudates and secretions in the rhizosphere can accelerate chemical alteration of minerals (see

Section 1.8.1), and additionally all vegetal matter incorporated in the topsoil undergoes the process of humification (Sposito, 2008). A specific example of how significant the impact of biota can be occurs in coniferous forests, where under certain conditions a special type of soil called a *podzols* or *podosols* can form . This occurs when the growth and accompanying decomposition of conifers causes acidification of the soil and leads to the leaching of all but the most insoluble elements, leaving a horizon enriched in quartz, and aluminium and iron sesquioxides (Righi and Chauvel, 1987).

Soils represent important habitats for microorganisms - one kilogram of soil can contain up to 10 trillion bacteria, 10 billion actinomycetes and one billion fungi, and large populations of organisms such as protozoa or nematodes (Sposito, 2008). Microorganisms in the soil are closely involved with processes such as the mineralisation of specific elements, in particular 'fixation′ of nitrogen and phosphorus from organic to inorganic forms, and in the secretion of glomalin-related soil proteins (glomalin is a fungal glycoprotein believed to be associated with soil aggregration) and humification (see also Section 1.5.1) (Sposito, 2008; Kutílek and Nielsen, 2015). Products of microbial metabolism are associated with accelerated weathering effects on certain minerals, such as potassium bearing minerals (Song and Huang, 1988). Biotic effects also include the action of animals and man, where modern agriculture impacts soil structure (through tillage), elemental cycling (fertiliser application), and by alteration of resident plant species, while animals such as worms impact soil porosity and aggregation (Kutílek and Nielsen, 2015).

Effect of time

The development of a 'well-developed′ or mature soil can take centuries or millenia. Weathering continues progressively over time and a soil considered to be relatively young (or immature) will have only slightly altered parent material and poorly developed horizons, representing an unstable state in soil formation, while a mature soil will generally have a well-developed sequence of horizons and have reached a final state of transformation (Jenny, 1994). The estimation of age or maturity is thus based on the differentiation between horizons but this relies strongly on the assumption that all other factors (t,p,c,b) remain constant during the measured period (Jenny, 1994). There is a strong interaction between time and the factors such as climate and topography, as these affect weathering rates and the deposition or removal of material (Velde and Barré, 2009).

Phases of soil formation

Due to the strong interactions between the factors of soil formation one cannot discuss young or old soils in absolute terms. In certain tropical zones, the high temperature and rainfall lead to the formation of thick soils with well-differentiated horizons extremely rapidly, geologically speaking (Foth, 1991). Conversely, the high temperature and low rainfall of deserts leads to a relatively slower weathering process (Foth, 1991). Thus, it is necessary to define the stages of soil formation.

- the first phase is the weathering of the parent material by chemical dissolution and physical decomposition
- the second phase involves arrival of biotic communities, which lead to some alteration of and interaction with mineral phases by organic molecules, and to the incorporation of organic matter into the soil matrix and the presence of leaf litter
- the third phase involves the redistribution of material within the system and the differentiation between different horizons (Jenny, 1994)

1.4 Soil structure and definitions

Soils have a hierarchichal structure which exists on an increasing scale from μm (crystallites and microaggregates) to km (horizons and pedons). The following section attempts to describe some of the variations in soil properties as a function of scale.

Particle aggregation

Starting with the smallest scale, clay particles flocculate to form micro-aggregates or 'quasicrystals′, which can be classed as crystallites (strongly oriented) or tactoids (irregularly oriented) (Meunier, 2005). Such interactions are governed by van der Waals and electrical double-layer phenomena. Organic molecules can be associated with such clay microaggregates, and are generally associated with external surfaces of the quasicrystals. These molecules are incredibly important to maintaining the micro-aggregate structure of soils and preventing the compaction into coagulated silts and clays (Kutílek and Nielsen, 2015). Associations of clay microaggregates and organic molecules contribute to soil microporosity, as the organic molecules prop open inter-particulate spaces. They also act to protect the organic molecules against attack by microorganisms (Singh et al., 2017; von Lützow et al., 2006). As both clay mineral surfaces and organic molecules tend to be negatively charged, these associations occur with the help of polyvalent cations such as

Fe^{2+}, Ca^{2+} etc., and also may use organic functional groups, e.g. amines (Meunier, 2005). As the size of microaggregates increases, they may also incorporate bacteria into the structure which may confer protective benefits to bacteria against larger soil organisms (Kutílek and Nielsen, 2015).

Further aggregation (formation of macroaggregates) occurs on a larger scales around matter such as fine root or hyphal material and larger particles of primary minerals (i.e. sand grains) (Huang et al., 2011). Polysaccharides are implicated strongly in cementation between larger aggregates, tending to accumulate in larger cracks and fissures where dissociation is most likely to occur (Velde and Barré, 2009). These largest associations, over 250 μm in diameter, are influential in determining soil properties such as mechanical strength and aeration status, as their overall organisation determines the meso- and macroporosity of the soil (Huang et al., 2011). Macroaggregates are also the most sensitive to mechanical disruption, in particular the type that may occur under tillage agricultural systems, but also stresses such as raindrop impact (Kutílek and Nielsen, 2015).

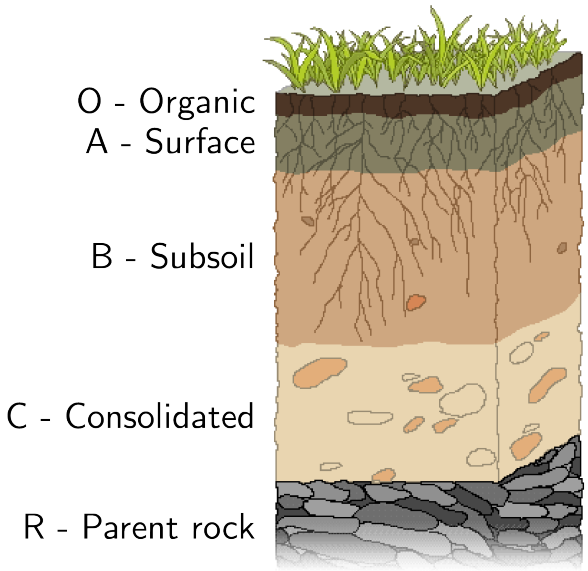

Figure 1.8: Schematic representation of soil horizons, showing how development consists of downwards progression of horizontal zones with different characteristics.

Definition of soil horizons

The next level of macroscopic soil organisation is that of soil horizons. Considering that alteration takes place roughly horizontally at the interface between solid-atmosphere,

zonation then occurs where certain characteristics exist within a defined range running parallel to the interface and corresponding to an extent of alteration of the parent material (Jenny, 1994). For example, the United States Department of Agriculture (USDA) uses the following primary designations:

- O - an organic horizon, which is dominated by detritus coming from a recognisably organic origin
- A - mineral-organic, composed primarily of mineral components which have been sufficiently altered to no longer represent the parent material, with some humified organic material present
- E - eluviated, characterised by concentrations of sand and silt particles due to the loss of clay-sized (<2 μm) particles
- B - formed below A, E, and O horizons, this is a clay rich horizon with concentrations of mineral phases conforming to significant levels of alteration or leaching
- C - represents consolidated or cemented or unconsolidated but pedogenically unaltered parent material
- R - consolidated and continuous parent material (bedrock)

Following these general classifications to identify different horizons in a profile, more specific classification can take place using suffixes to denote certain properties.

Pedon

The pedon is a unit of study which permits to investigate the soil properties below the surface, and is the largest unit still considered a soil. It is the smallest three-dimensional sample which allows a complete description of all pedogenetic properties. Such a description normally proceeds from a vertical profile and includes a characterisation of all soil horizons, boundary characteristics, and other elements such as colour, texture, pH, porosity, and the extent of root penetration, *inter alia*. The pedon also involves the precise location and description of the soil area. Pedons can also be organised on the large scale to provide a topographical indication of soil types and how they vary across polypedons across the countryside. These descriptions are based firstly on the nature of the horizons present, and are extended to take into account factors such as texture and moisture content. (Soil Survey Staff, 1999)

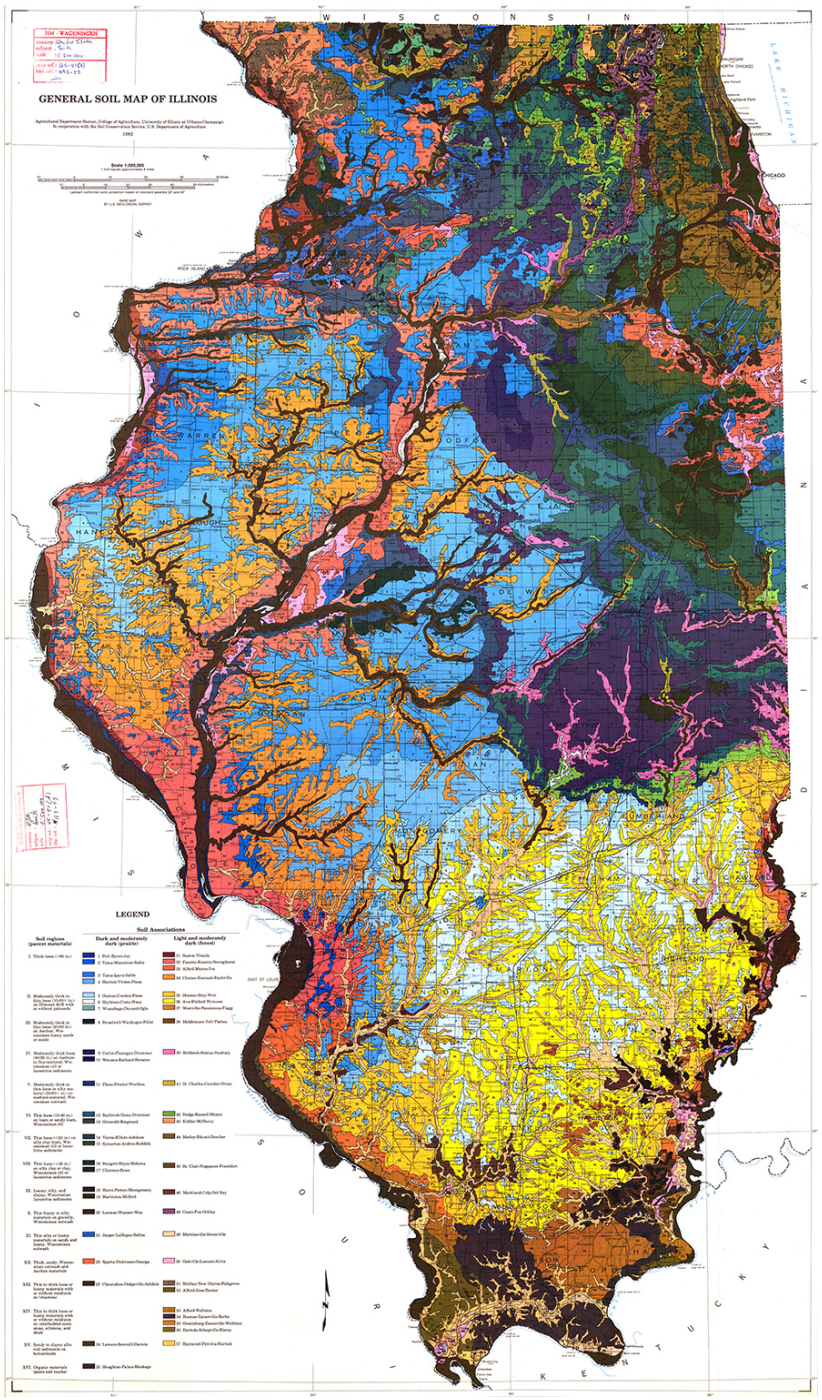

Figure 1.9: Soil map of Illinois showing the variation in soil classifications througout the state.

1.5 Soil components

Humus and humification

Soil acts as a support for living beings such as nematodes, bacteria, fungi, archaea, and higher and lower plants, and these organisms all contribute to a part of the composition of the organic matter in soils (Kutílek and Nielsen, 2015). The most simple is the presence of dead and decaying organic matter - leaf litter, branches and root material which play host to populations of bacteria and fungi which secrete organic substances to decompose specific components such as cellulose and lignin (respectively) (Sposito, 2008). Decomposition of the cellulose and lignin components is accompanied by the creation of new organic substances within the soil matrix. Other organisms such as ants and earthworms also play a role in the incorporation of organic matter into the soil due to physical movement of small morsels from the surface (Kutílek and Nielsen, 2015).

Once these larger elements of plant material are drawn beneath the surface, they are susceptible to the process of humification, which is a type of decomposition. Humification of different components of organic matter does not take place at the same rate. Sugars such as starch and glucose decompose quickly, while lignin and waxes are more resistant to decomposition, leading to the formation of soil humus consisting of a variety of organic molecules but always including high molecular weight carboxylic acids (R-COOH functional groups) which typify soil humus (Sparks, 2003). These acids are classified into three groups, called humins and fulvic and humic acids, based on solubility and molecular mass. These molecules are relatively stable in soils, enduring 10^2-10^3 years in soils (Kutílek and Nielsen, 2015). They tend to be negatively charged due to deprotonation of the carboxyl group, leading them to attract positive cations (Hinsinger et al., 2009). The humus content of soils is strongly dependent on vegetation type and temperature, due to the dependence of humification on bacterial metabolism which is in itself suppressed by decreasing temperature, however this likely varies by exact environmental conditions. (Sparks, 2003).

Inorganic soil constituents

The inorganic components of soils account for up to 50% of soil volume and 50-99.9% of soil mass, and includes both primary and secondary minerals. Their size, surface, and charge impact many important soil processes and equilibria. Primary minerals are directly inherited from the parent material in that they are minerals which have not been

Table 1.2: Concentration of the ten most abundant elements and selected metals in the Earth's crust, adapted from Wedepohl (1995).

Element	ppm	Element	ppm
O	472000	Mn	716
Si	288000	Ba	584
Al	79600	Sr	333
Fe	43200	Zr	203
Ca	38500	Cr	125
Na	23600	V	98
Mg	22000	Rb	78
K	21400	Zn	65
Ti	4010	Ni	56
C	1990	Cu	25

chemically altered since their deposition. This is in contrast to secondary minerals which are generally formed from weathering processes acting on primary minerals (Sposito, 2008). Soil minerals tend to be ionic solids, although most bonds tend to have a degree of covalency, and their structures are formed on the basis of Pauling's Rules governing the coordination (or arrangement) of ions based on the ratio of the ionic radii and bond-strength to minimise the charge and number of components in a crystal structure (Sparks, 2003). Silicate minerals and quartz are the most common minerals in the crust, as silicon and oxygen atoms (or ions) are the two most common elements found in the Earth's crust (Table 1.2). The most important potassium bearing silicate minerals in soils are feldspars, micas and clays minerals and the following sections cover their structure and properties.

Structural building blocks

The basic building block of silicates is the SiO_4^{4-} tetrahedron. This is formed from an arrangement of closely packed oxygen anions, in which four O^{2-} anions situated at the four apices of a tetrahedron, three at the base (basal oxygens) and one anion sitting on top of the three, termed the apical oxygen. This arrangement leaves a small central cation site, which can be occupied by small cations such as silicon, Si^{4+} (Figure 1.10a) in four-fold tetrahedral coordination. Some substitution of the central Si^{4+} is possible however

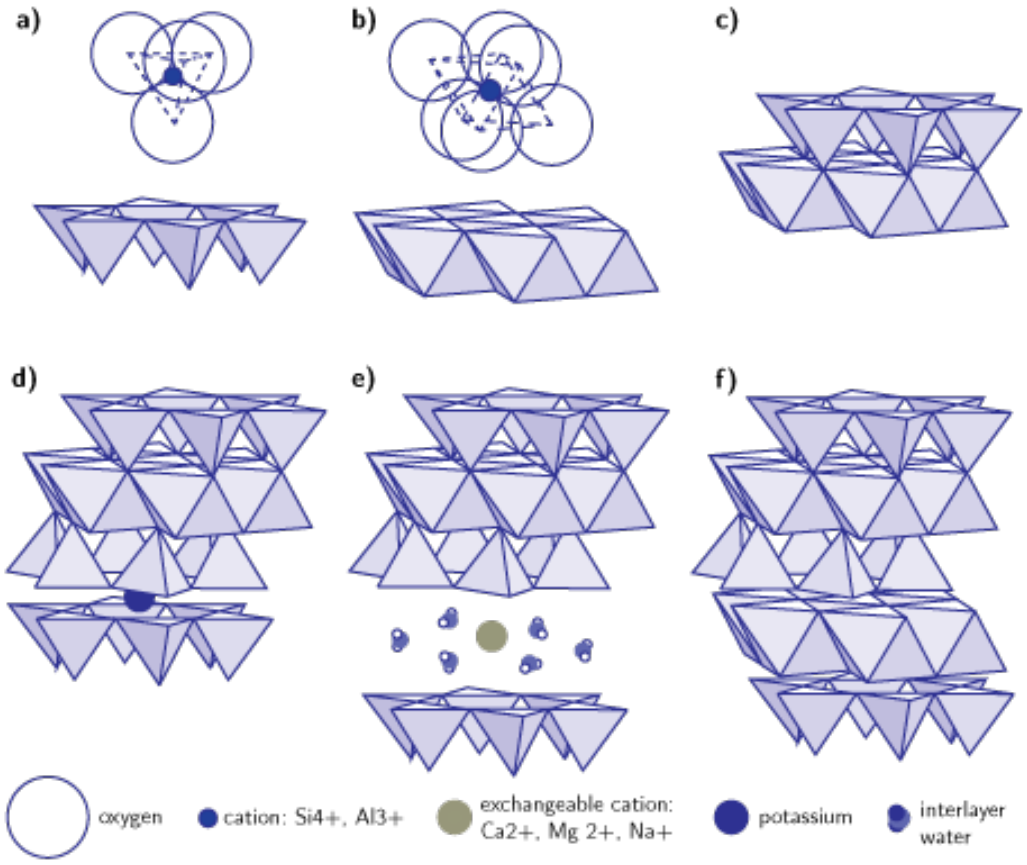

Figure 1.10: Structural components of common soil silicate minerals: a) example of a silicon cation tetrahedrally coordinated to four oxygen anions, and the tetrahedral sheet formed by corner-sharing of basal oxygen; b) octahedrally coordinated cation and the octahedral sheet formed by edge-sharing of octahedra, and examples of layer-silicate structures formed by combinations of tetrahedral and octrahedral sheets c) 1:1 layer (TO), d) 2:1 layer (TOT) non-expandable, 3) expandable 2:1 layer and f) 2:1:1 layer (TOT:O).

this is limited to cations with small ionic radius such as Al^{3+} as dictated by Pauling's Rules.

Larger cations are found in so-called octahedral sites. These are formed from planar arrangements of three O^{2-} anions, where each plane is rotated by 60 ° relative to the preceeding plane of anions. This leaves a cation site between six oxygen anions, giving six-fold octahedral coordination (Figure 1.10b). This site is commmonly populated by Al^{3+}, but is able to accomodate cations with greater ionic radii such as Fe^{3+}, Fe^{2+} and Mg^{2+}. Ions such as K^{+} or Ca^{2+} are prevented from occupying such sites due to their extremely large ionic radii.

These two substructures can then be assembled together in various ways to form different structures by sharing of the oxygen atoms. Figure 1.10 gives a basic view of some of these structures.

1.6 Minerals of interest

Feldspars

Feldspars are members of the tectosilicate family, in which SiO_4^{4-} tetrahedra share all four oxygen atoms in a three-dimensional array. Feldspar structure is based on chains of four-membered rings of tetrahedra, while individual chains are cross-linked. The general formula can be represented by $XAl(Al,Si)Si_2O_8$, where substitution of Al^{3+} for Si^{4+} in tetrahedral sites leads to incorporation of charge-balancing cations (X) such as Ca^{2+}, K^+ or Na^+ in interstitial sites within the tetrahedral network. The degree of substition and nature of interstitial cations can vary such that feldspars exists in a limited solid-solution series. These cations are surrounded by the silicate framework consisting of strong O-Si-O bonds. These bonds are resistant to weathering and as such feldspars release only slowly potassium held in interstitial positions, however attack by organic acids in soils (particularly in the rhizosphere) can accelerate the rate of dissolution ().

Phyllosilicates

Micas and clay minerals belong to the group of phyllosilicates whose name derives from the Greek phyllon, meaning leaf, as a reference to their layered structures. All members of the phyllosilicate family share the same two sheet structures, and different minerals are formed from different combinations of the two sheets. The two types of sheets are as follows:

- tetrahedral sheet: SiO_4^{4-} tetrahedra which share all three basal oxygen with adjacent tetrahedra, while protons are associated with apical oxygen atoms for reasons of charge balance. Different degrees of substition of Al^{3+} (or rarely Fe^{3+}) for Si^{4+} exist. Tetrahedral sheets are not found as independent minerals but are always associated with octahedral sheets
- octahedral sheet: two oxygen atoms are shared between adjacent AlO_6^{-9} octahedra in an edge-sharing arrangement. Protons are also associated with O^{2-} for charge balance. Al^{3+} can be substituted by a variety of atoms, and the sheets can be di-

or tri-octahedral, where in dioctahedral minerals only two of every three octahedra are occupied by M^{3+}. In trioctahedral minerals all three octahedra are occupied by M^{2+}. Octahedral sheets do exist as independent minerals in the form of metal hydroxides, but these are not silicates although they are structurally analogous to octahedral sheets.

Bonding between tetrahedral and octahdral sheets occurs through the sharing of tetrahedral apical O^{2-} ions and those at the corner of octahedra. This is accompanied by some distortion of the tetrahedral sheet to account for misfit between the dimensions of the two sheets. Substitution of tetrahedral or octahedral cations (Si^{4+} or Al^{3+}) may lead to charge deficiency termed the 'layer charge '. As a result of layer charge, interlayer cations are present to balance the charge and these are generally situated in the hexagonal cavities created by the rings of six tetrahedra in the tetrahedral sheet. Families of minerals can be characterised by the association of either one tetrahedral and one octahedral sheet (1:1 or TO) or by two tetrahedral and one octahedral sheets (2:1 or TOT sandwich), and further as TOT:O (2:1:1) where an additional octahedral sheet is found between TOT layers (Figure 1.10).

Micas and 2:1 clay minerals

At this point it is necessary to differentiate between micas and the clay minerals found in soils. This separation is done based on the definition of clay minerals by Guggenheim and Martin (1995) as

"*naturally occurring material composed primarily of fine-grained minerals, which is generally plastic at appropriate water contents and will harden when dried or fired. Although clay usually contains phyllosilicates, it may contain other materials that impart plasticity and harden when dried or fired. Associated phases in clay may include materials that do not impart plasticity and organic matter.*"

where their size is limited to particles with a diameter of less than two microns. This size limit is somewhat arbitrary, arising from the minimum particle size that was able to be investigated by classical optical and single-crystal microscopic methods before the invention of electron microscopy. However, despite their structural similarity, particles of muscovite and biotite are rarely found in the <2 μm fractions but rather in the silt (50-2 μm) and sand (2000-50 μm) fractions of soils. Micas tend to be primary minerals inherited from the parent material as they are commonly found in shales, granites and

Table 1.3: Clay mineral groups as defined by differences in layer charge and interlayer distance adapted from data in Brindley and Brown (1980). Where two names or structural formulae are given, the trioctahedral endmember is specified first followed by the dioctahedral end-member. Layer-to-layer distances are provided in hydrated conditions.

Family	Layer type	Structural formulae	Layer charge, meq $100g^{-1}$	Layer-to-layer distance, Å
Serpentine —kaolin	TO	$Mg_3Si_2O_5(OH)_4$ $Al_2Si_2O_5(OH)_4$	∼0	7.1-7.3
Talc —pyrophyllite	TOT	$Mg_3Si_4O_{10}(OH)_2$ $Al_2Si_4O_{10}$ $(OH)_2$	∼0	9.1-9.4
Micas	TOT	$(Al,Fe)_2(Al,Si)_4O_{10}$ $(OH)_2$.(K,Na,Ca)	∼1 or ∼2	9.6-10.1
Smectites	TOT	$(Al,Mg,Fe)_2(Al,Si)_4O_{10}$ $(OH)_2$.(K,Na,Ca)nH_2O	0.25-0.6	14.4-15.6
Vermiculites	TOT	$Mg_3(Si_3Al)O_{10}(OH)_2$.$(M^+,M^{2+})nH_2O$	0.6-0.9	14.4-15.6
Chlorites	TOT:O	$(M^{2+}_{3-y-z},M^{3+}_y,\square_z)$ $(Si_{4-x},M^{3+}_x)O_{10}$ $(OH)_2$.$(M^{2+},M^{3+})_3(OH)_6$	variable	∼14.1

schists, *inter alia*. During the weathering process they are thought to lose some of their interlayer potassium (among other slight compositional changes) to form illites, secondary minerals which are precursors to smectites and vermiculites (Moore and Reynolds, 1997). Smectites, vermiculites, illites and micas are members of a sequence of identical TOT structures, with one difference being increasing layer-charge through the series (Moore and Reynolds, 1997). These minerals generally tend to form interstratified crystallites where smectite layers may be found between layers of illitic nature, or vice versa. Chlorites are also commonly found interstratified with 2:1 layers (Brindley and Brown, 1980).

Layer stacking and disorder

These layered structures lead to some shared characteristics, such as a tendency to cleave along the horizontal plane between layers as a result of the weaker interlayer bonds. They also have similar platy particle morphology, which result from the stacking of many clay layers and where the number of layers determines the size or thickness of the crystal. However, the stacking of the layers can give rise to different degrees of

disorder within the crystal. As there is little energetic difference between different layer stacking configurations, and the interaction between adjacent layers is weak, layers can be translated or rotated with respect to one another (Drits and Tchoubar, 1990). If the TO or TOT layers are randomly stacked with no relation between the translational or rotational position of sequential layers, they give rise to a structure termed 'turbostratic'. This is common in smectites as there is little association between layers to determine their position relative to one another. If the translation and/or rotation between consecutive layers is both regular and fixed, and the magnitude of which corresponds to the symmetry of the silicate layers, then this gives rise to ordered, repeating stacked structures which are termed polytypes (Brindley and Brown, 1980).

1.7 Characteristics of 2:1 minerals

Layer charge

As previously described, cation substitutions within tetrahedral and octahedral sheet can lead to charge deficit and overall negative charge on the sheet. This type of charge is termed 'permanent charge', and is generally compensated for by interlayer cations. Selectivity for charge balancing cations may be displayed, roughly according to the following series:

1^+: $Li > Na > K > NH_4 > Cs$
2^+: $Mg > Ca > Sr > Ba$

Vermiculites are an exception to this series as they tend to prefer Mg^{2+} over Ca^{2+} (Meunier, 2005). This cation selectivity occurs based on the differences of size, hydration energy, and the amount and location of layer charge. Layers also have another type of charge described as variable charge, which arises from unfufilled -O or -OH bonds at the crystal surface. These bonds can be satisfied with additional OH^- or H^+ ions, meaning this charge can change depending on protonation or deprotonation as a result of local pH conditions, and it also controls dispersion and flocculation behaviour due to the attraction or repulsion between particles as a result of surface charge. Variable charge is most significant for minerals with little to no permanent charge such as kaolinite or talc, and loses importance as permanent charge increases (Brindley and Brown, 1980).

Cation exchange capacity

Layer charge and the presence of interlayer cations also leads to the concept of cation exchange capacity (CEC), which is the total amount of charge able to be transfered in a low-energy, reversible fashion (Meunier, 2005). It is expressed as centiequivalents of charge per kg of solid ($ceq_c kg^{-1}$), although milliequivalents of charge per 100 g ($meq_c 100g^{-1}$) is commonly used. Measurement also depends on a reference state of the material, i.e. oven- vs. air-dried, defined pH, as this may impact the nature of exchangeable cations. The CEC of different clay minerals varies according to the nature of the mineral. In smectites it is possible to exchange all the interlayer cations, as the interlayer space can be considered as an extension of the soil solution in the horizontal plane bound by TOT layers above and below (Martin, 1960; Sparks, 2003). In illites exchange is generally limited to ions held by variable charge located on the external edges of the clay particle. However, given favourable conditions and enough time, exchange of interlayer cations can occur in minerals where the interlayer cation is deemed to be fixed under favourable conditions, although the rate may be much slower due to limitations such as the opening of the interlayer space and the concentration of ions in solution (Mortland et al., 1956; Reed and Scott, 1962; Gaines, 1957). CEC plays an important role in determining the overall fertility of soils, as many exchangeable cations are important plant nutrients (Ca, K, Mg, Fe) (Huang et al., 2011).

Layer-to-layer distance

The interaction of layer charge and interlayer cations leads to the concept of layer-to-layer distance. Smectites, with a low layer charge of between 0.3-0.6 ceq kg^{-1}, have a relatively weak electrostatic interaction between charge-balancing interlayer cations and the TOT layers. This means that cations are able to enter and exit the interlayer space between TOT layers without dehydrating and losing their associated water molecules. This gives an interlayer space populated with both cations and water molecules, which can swell or shrink depending on local relative humidity, so these minerals are described as having a variable layer-to-layer distance. The extent of swelling (increase in layer-to-layer distance) is strongly dependent on three factors: a) the nature of the interlayer cations; b) the relative humidity of the surrounding environment; and c) the amount and location of layer charge (tetrahedral vs. octahedral) (Meunier, 2005; Sposito and Anderson, 1975; Brindley and Brown, 1980). The majority of the time, water is absorbed in single, double or triple planes (mono-, bi-, and tri-hydrated), although Li and Na can allow complete

dissociation of TOT layers, a state called 'exfoliated'. Water in the interlayer space can also be substituted with organic molecules, where saturation with ethylene glycol or glycerol and specific cations provides a series of diagnostic tests which can aid in determining the nature of the clay minerals present (Brindley and Brown, 1980; Moore and Reynolds, 1997). Substitution of interlayer cations with organic molecules to prop open the interlayer space is also a process used to create clay-organic hybrid materials, which may find uses in drug delivery or as barrier materials (Meunier, 2005).

As layer charge increases, as in vermiculite, this leads to TOT layers which are more closely held together by electrical double-layer effects. The layers are therefore less capable of expanding than smectites, and for example vermiculite when saturated with Mg^{2+} and solvated with glycerol will only expand to 14.5 Å rather than the 18 Å obtainable with smectites under the same conditions. Further to this, the layer charge of micas is so great that typically the interlayer cations have been completely dehydrated and can closely approach the layer surface in a so-called inner-sphere complex where there are no water molecules intervening between the cation and the mineral surface. This leads to strong electrostatic bonding which holds TOT layers together, and interlayer distance smaller than that of smectites at ∼10 Å. As a result illites and micas are not able to expand.

1.8 Setting of the study

Mineralogical transformations by plants

While potassium in the non-exchangeable pool (Section 1.2.4, Figure 1.5) has been typically considered unavailable for plant nutritional needs, Dyer postulated as early as 1894 that this potassium was potentially accessible for plant nutritional needs, and following this numerous studies have since shown that potassium is extractable from these interlayer sites (Reitemeier, 1951; Arnold and Close, 1961; Kuchenbuch and Jungk, 1982; Naderizadeh et al., 2010; Hinsinger et al., 1993). Differential uptake of potassium by Monterey pine seedlings depending on the mineral substrate was demonstratred by Boyle and Voigt (1973) over a period of six months. Hinsinger et al. (1992) reported the vermiculitisation of phlogopite up to 1.5 mm away from ryegrass roots could occur in as little as four-days. Further studies demonstrated potassium release from phologpite in 32-day experiments under ryegrass and rape, and related this to both reduced potassium concentration in the rhizosphere and the presence of protons inducing de-

composition based on the concurrent release of structural aluminium and magnesium (Hinsinger et al., 1993; Hinsinger and Jaillard, 1993). Barré et al. (2007a) went further and studied plant uptake on natural clay minerals (<2 μm fraction), using XRD peak decomposition to explain changes as a decrease in illitic nature following just 31 days of ryegrass growth, and these changes were shown to be reversible by potassium fixation when exposed to KCl solution (Barré et al., 2008a). Adamo et al. (2016) reported similar findings for the uptake of potassium by maize over 40 days, however over the course of a full growing cycle (130 days), potassium levels were unchanged even on non-fertilised plots.

As reversible equilibria govern the transformation of potassium between the three pools of soil solution, exchangeable, and non-exchangeable potassium, addition or removal of potassium causes the favouring of sorption or desorption. For example, depletion of soil solution potassium from 10^2 μmol L^{-1} to 2-3 μmol L^{-1} induced the depletion of exchangeable potassium and eventually non-exchangeable potassium causing reliance of non-exchangable potassium for nutrition despite considerable potassium reserves (Kuchenbuch and Jungk, 1982; Niebes et al., 1993). Notwithstanding such studies, extraction of interlayer potassium requires extremely small concentrations of potassium in the soil solution and potassium concentrations in many intensely cultivated soils are above this critical concentration (Hinsinger, 1998). However, Claassen and Jungk (1982) reported levels of 2-3 μm L^{-1} in the close vicinity (0.7 mm) of maize and ryegrass roots grown on a variety of soils.

Furthermore, the extent to which plants are able to extract non-exchangeable potassium is strongly dependent on species type, and even genotypes of the same species may have different uptake abilities (Schenk and Barber, 1980; Barber and Mackay, 1986; Marschner, 1995). These differences are attributed to changes in root morphology annd the nature of root exudates between species as, for example, maize releases oxalic and citric acids compared to wheat and sugar beet which also release amino acids that aid in extraction of interlayer potassium (Kraffczyk et al., 1984; Rengel and Damon, 2008). Song and Huang (1988) studied the effect of these acids on the rates of release of potassium from 20-50 μm particles and determined the series biotite > microcline $\simeq$ orthoclase > muscovite where the rate of release from biotite was 63 or 123 times greater than that from muscovite. Compared to the results of Feigenbaum et al. (1981), who found the rate of release of potassium from biotite was only 20 times that of muscovite for particles with the same size in a cationic resin, it is clear organic molecules in soils can play a large

role in mineral potassium release.

However these results highlight interesting differences in behaviour between dioctahedral and trioctahdral minerals. Following the report of Walker (1950) of the trioctahedral decomposition product from the weathering of biotite, a number of early laboratory studies focussed on the artificial weathering of micas and demonstrated that the rate of weathering of biotite is several times greater than that of muscovite (Mortland et al., 1956; Arnold, 1958; Mortland, 1958; Reed and Scott, 1962; Scott and Reed, 1962a). The difficulty of extracting potassium from dioctahedral micas was proven, as Scott and Reed (1962b) found that the concentration of KCl of 1 mmol L^{-1} was enough to inhibit the release of potassium from illites. While several authors proposed the kinetics of reaction were controlled by the diffusion of cations from particle edges to the centre and the concentration of potassium in solution, this is not enough to explain the differences in behaviour between di- and tri-octahedral micas (Scott and Reed, 1962a; Wells and Norrish, 1968; Chute and Quirk, 1967). Several explanations have been put forward, with Bassett (1960) suggesting the inhibition of the release from dioctahedral micas is due to the postion of hydroxyl ions around the hexagonal cavities in the tetrahedral sheet which hinder cation exchange. However, Robert and Barshad (1972) proposed that the relatively high tetrahedral charge of dioctahedral micas prevents expansion of the layer-to-layer space which is necessary for potassium extraction and exchange. Several of these studies also demonstrated that there are competing effects between complete dissolution of the mineral structure or simple exchange and release of interlayer potassium, where Feigenbaum et al. (1981) believe iron and manganese 'contaminants′ may play a role in destabilising the crystal lattice around substition sites and are preferentially released during decomposition. Feigenbaum et al. (1981) also reported on pH sensitivity, finding that dioctahedral muscovite is much more resistant to decomposition resulting from pH decrease than phlogopite and biotite, and in a further study found the rate of release of potassium from 5-20 μm illite particles was greater than that from <2 μm illite particles under the same conditions (Feigenbaum and Shainberg, 1975).

Long-term fertility experiments

A number of field experiments were set up in the 19^{th} and 20^{th} centuries to investigate the effect of long-term cropping and fertility treatments. Several authors have reported on the status of clay minerals and potassium in the soils of such experiments. Arnold (1960) stated

that the level of exchangeable potassium in soil from the Broadbalk continuous wheat plot at Rothamsted Experimental Station in the UK (established in 1843) was increased with potash fertilisation. This is simliar to Singh and Goulding (1997), who found that while the average potassium content increased from 1.01% to 1.10% or 1.20% from 1856 to 1987, for plots with and without potassium fertilisation, respectively, this difference was not visible in either the XRD data for the <2 μm or <0.2 μm fractions, seemingly indicating no mica transformation had taken place over 140 years. Conversely, Möberg and Dissing-Nielsen (1983) and Dissing-Nielsen and Möberg (1984) found potassium depletion as a result of continuous agriculture lead to a decrease in illite content with the formation of smectite and vermiculite accompanied by an increase in CEC, in the soils of two field experiments in Denmark. Tributh et al. (1987) also reported a decrease in illite and an increase in smectite in non-fertilised soils subjected to continous cropping for 30-115 years when compared to fertilsed soils from the same experiment (four different experiments/soil types were investigated). The authors demonstrated decreases in the intensity of illite peaks in <0.06 and <0.2 μm fractions, and that some depletion of illite in topsoil relative to subsoil also occurred. Velde and Peck (2002) went further, and studied soils from the Morrow Plots (est 1876, U. Illinois), interpreting XRD data using the peak decomposition method (Lanson, 1997) on <2 μm fractions to infer that large mineralogical transformation had occurred in the soil of unfertilised plots under continuous corn culture, which was explained as an increase in the proportion of minerals with smectitic nature. Studies of the soil of five different Swedish long-term agricutural experiments (Mollisols and Inceptisols) under straw and beet crop rotations and different potassium fertilisation regimes (plots also received P and K) demonstrated an effect of this potassium management on the amount of illitic layers, and the reversibility of such a reaction was dependent on other soil factors such as acidity (Simonsson et al., 2009).

Position of the study

Given these sometimes contradictory results, it is evident that a clearer understanding of the effect, on a mineralogical level, of potassium import and export by fertilisation and cropping on soil is needed. This is particularly important in light of the projected increases in fertiliser demand to improve yields of maize in Sub-Saharan Africa, and of maize and wheat in Eastern Europe (Mueller et al., 2012), which are required to meet increased nutrient demands of a projected population increase to 9.8 billion by the year 2050 (UNFAO, 2017). Similarly, such population expansion also threatens reserves of arable land, due to urban expansion of cities founded in agricultural zones (Bhadra and

Brandao, 1993; Norse, 1992). There is also increased competition for arable land reserves by forestry and grazing due to the twin pressures of CO_2 sequestration and increased meat consumption in developing countries (Bhadra and Brandao, 1993; Döös, 2002; DeFries et al., 2010; Lambin and Meyfroidt, 2011).

Furthermore, qualitative interpretation of XRD data limits the description of the mineral assemblage to well-crystallised phases with sharp and well-defined reflections and does not take into account the influence of highly-disordered and mixed-layers with small particle size. The contributions of such phases are not always evident when considering bulk $<2\mu$m fractions, and it is impossible to place compositional contraints on the layer-types. Whilst the peak decomposition method improves the description of the mineral assemblage to include the contributions of mixed-layers and attempts to place constraints on their composition, it does not take into account the full XRD profile and as such the results cannot be interpreted in a quantitative manner. More recent studies on hydrothermal and diagenetic sequences have applied a quantitative method of full-profile XRD fitting (Aplin et al., 2006; McCarty et al., 2004; Inoue et al., 2005; Drits et al., 1997b). Hubert et al. (2009, 2012) and Viennet et al. (2015) sucessfully demonstrated this approach could be adapted to evaluate the mineral assemblage of soils. Thus the present study was conceived to investigate the mineralogy of soils following 110-years (1904-2014) of continuous cropping and the anthropogenic effects of different fertilisation regimes and crop rotations have given different potassium levels in the plots, and this is expected to project into different mineralogies. Quantitative modelling will be used to provide insight into the absolute amount of potassium present in the soil minerals, and how this has changed over time.

Materials and methods

Figure 2.1: Tthe Morrow Plots experimental fields in September 2012, representing the typical post-harvest fallow state during which sampling took place in 2013 and 2014.

2.1 The Morrow Plots experiment

Description and location

The Morrow Plots are an agricultural field experiment which was established on the Urbana-Champaign campus of the University of Illinois (USA) in 1876. The experiment initially consisted of ten separate plots, with different crop rotations. Over time, seven of these plots were lost, until in 1904 only plots 3, 4, and 5, of the original ten plots remained. Plot 3 has been planted with corn (*Zea mays*) continuously since the inception of the experiment. Plot 4 was planted in a corn-oats (*Avena sativa*) rotation on a two-yearly basis, however in 1955 this was changed to soybeans (*Glycine max*) to better

reflect current agricultural practices of the central United States. Plot 5 is subject to a three-yearly corn-oats-hay rotation. Originally, the whole plots were left unfertilised (1876-1904), however in 1904 the plots were subdivided on a north-south basis and manure fertilisation was begun on southern halves. Hybrid corn crops were introduced in 1933 and at least one hybrid has been included in every corn cropping cycle since. Following this, in 1954, the plots were further subdivided to form eight subplots, and lime-nitrogen-phosphate-potassium (L-NPK) fertilisation was begun on certain northern subplots, and the hay cropping species was changed from red clover (*Trifolium pratense*) to alfalfa (*Medicago sativa*). Only a few minor adjustments have been made since this major adjustment in 1954, such as the introduction of a high L-NPK treatment in some southern subplots in 1967, although this treatment was stopped in 1989 at the same time a change was made from Mouldboard to Chisel plough.

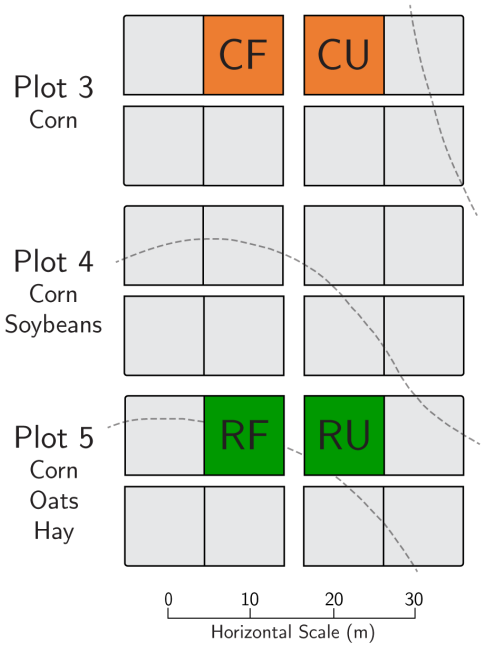

Figure 2.2: Schematic representation of the layout of the Morrow Plots, with the subplots included in the present study highlighted in orange and green. Dashed lines represent slope contours of 30 cm. Adapted from Odell et al. (1984).

Seeding densities have also been varied throughout the experiment. From 1904-1954, seeding densities across all non-fertilised continuous corn (Plot 3) subplots were 20,000 plants ha^{-1}, and for non-fertilised subplots of the rotations in Plots 4 and 5 the seeding

density was 30,000 plants ha^{-1}. The seeding density in all manure-treated subplots was 30,000 plants ha^{-1}. In 1955 the seeding density in subplots receiving L-NPK fertiliser was increased to 40,000 plants ha^{-1}, while in 1957 one subplot receiving manure treatment only was increased to 40,000 plants ha^{-1}. Following this, in 1967 the seeding density was increased to 60,000 plants ha^{-1} for corn and rotation subplots where high L-NPK treatment was introduced, and in 1977 all subplots receiving L-NPK fertiliser treatments were increased to this same seeding density. Finally in 2013 the seeding density for all subplots was standardised to 60,000 plants ha^{-1}, regardless of fertilisation regime and history. A complete description of the history of the experiment and information regarding fertilisation rates can be found in Odell et al. (1984) and Aref and Wander (1998).

The soil of the Morrow Plots is a Flanagan silt loam, or mesic Aquic Argiudoll, where 1–1.5 m of loess over a glacial till was developed under 4,000–6,000 years of prairie grassland vegetation (Endres, 2002). The plots are nearly level and the soil is black to dark brown. The climate is continental, an average temperature of of 11.1 °C for the period 1904-2014 with precipitation averaging 968 mm per year and snowfall 576 mm (essentially falling between December-March). Climate is subject to variation between monthly average low temperature of -7.7 to -5.2 °C in December-February, and monthly average highs of 28.0 to 30.0 °C from June-August (MRCC, 2018). Some chemical and physical characteristics are presented in Table 2.1. Soil samples for 2013 and 2014 were collected from the top 25 cm during fallow periods following autumn harvest (late September-October). Further samples were provided for the years 1904, 1957, 1980 and 1997 from the soil archives of the Department of Agriculture (U. Illinois). Whilst the Morrow Plots had already been under cultivation for 26 years in 1904, this represents the earliest available soil sample and thus serves as the initial state of the soil for this study.

Table 2.1: Selected chemical and physical properties of CU and RF subplots of the Morrow Plots experimental fields, adapted from (Odell et al., 1984).

Horizon	Depth, cm	Sand, 2000-50 μm	Silt, 50-2 μm	Clay, <2 μm	Bulk density, g cm^{-3}	Total porosity, %	Organic carbon, %	pH	Exchangeable cations, ceq$_c$kg^{-1} CEC	Ca	Mg	K	Na
CU													
Ap	0-23	9.0	66.8	24.2	1.45	45.3	1.32	5.1	17.6	8.8	2.3	0.2	0.1
A12	23-30	8.4	64.8	26.8	1.34	49.4	1.49	5.3	18.0	9.7	2.7	0.2	0.1
B1	30-38	5.6	58.7	35.7	1.43	46.0	1.20	6.0	23.1	13.4	5.5	0.1	0.1
B21t	38-56	5.2	54.8	40.0	1.5	43.4	0.62	6.5	26.0	15.8	7.5	0.1	0.1
B22t	56-76	7.6	57.6	64.8	1.57	40.8	0.54	6.7	22.7	13.6	7.1	0.1	0.1
B3	76-124	12.7	60.9	26.4	1.53	42.3	0.24	7.5	16.8	11.2	5.8	0.1	0.1
IIC1	124-147	26.7	57.1	16.2	1.75	34.0	0.21	8.1	-	-	-	-	-
IIC2	147-183	26.4	55.6	18.0	1.87	29.4	0.13	8.3	-	-	-	-	-
RF													
Ap	0.-25	6.4	67.1	56.4	1.39	47.5	1.94	5.8	21.5	10.4	4.5	0.4	0.1
A12	25-46	3.6	65.5	30.9	1.31	50.6	1.90	5.7	24.1	13.1	4.3	0.3	0.2
B1	46-58	2.8	62.9	34.3	1.40	47.2	1.24	5.7	25.8	14.3	5.7	0.4	0.1
B21t	58-74	1.8	58.0	40.2	1.61	39.2	0.58	6.0	28.9	16.2	8.6	0.5	0.2
B22t	74-94	2.7	63.9	33.4	1.64	38.1	0.28	3.6	25.7	15.2	8.3	0.5	0.1
B3	94-114	9.4	62.9	27.7	1.69	36.2	0.22	7.2	19.3	11.9	6.7	0.4	0.1
IIC1	114-175	15.3	71.1	13.6	1.57	40.8	-	8.1	-	-	-	-	-
IIC2	175-183	48.0	43.0	9.0	1.91	27.9	-	8.1	-	-	-	-	-

2.2 Experimental procedures

Preparation of samples for XRD

Typically, preparation of clay samples for XRD consists of concentration and purification via chemical pre-treatments such as hydrogen peroxide (H_2O_2), oxalic acid and dithionite to remove organic material, carbonates, and sesquioxides, in accordance with experimental procedures put forward by authors such as Jackson (1958). However, it has been suggested that treatment of this type may alter the structure of the clays (Moore and Reynolds, 1997; Velde et al., 2003). The soils used in this study have very low levels of carbonate and iron oxides, and previous work identified negative effects of peroxide treatment such as the appearance of quartz and feldspar minerals in <0.05 μm subfractions, in addition to an inferior yield of <2 μm fractions (Khan, 2013). Thus, dispersion of the sample took place in NaCl solution without any chemical pre-treatment, in line with more recent studies on soil clay minerals (Pernes-Debuyser et al., 2003; Khan, 2013; Viennet et al., 2015). This has the advantage of replacing all the exchangeable cations with Na^+, which enhances dispersion for the following steps.

Sequential fractionation was performed on the samples based on Stokes law and following the methodology presented by Laird et al. (1991) and Hubert et al. (2012) which involves repeated centrifugation steps to isolate first the 50-2 and <2 μm fractions and further to separate the <2 μm fraction into 2-0.2, 0.2-0.05 and <0.05 μm subfractions. Sonication is performed following each centrifugation cycle to enhance dispersion and the process is repeated until a clear supernatant is obtained (10-15 cycles depending on subfraction). The fractions obtained following centrifugation are saturated with either Ca^{2+} or K^+ using overnight exposure to $CaCl_2$ 1M solution, repeated three times with centrifugation and renewing of the salt solution on each repetition. Calcium was used as calcium saturated expandable clay minerals have a relatively homogeneous saturation state at room temperature and 40% relative humidity (RH). Saturation with K^+ was also carried out using KCl 1M and the same procedure. To avoid particle loss it is necessary to wash saturated subfractions by dialysis.

Oriented slides were prepared for XRD via the pipette method, where a clay slurry is dropped on a silica slide and allowed to sediment. This permits a deposition of particles which is relatively homogeneous and uniform, with a generally good orientation of particles to maximise the $00l$ series. XRD was performed on such slides of Ca-saturated samples in

both air-dried (AD) and ethylene-glycol (EG) solvated states at 40% RH in a controlled humidity chamber. Patterns were also recorded for K-saturated samples following heat treatment at 150 and 350 °C for four hours. This allows to contrast between layer types with TOT or TOT:O nature. Random powder diffraction of 50-2 μm fractions and selected <2 μm powder was also performed to obtain information on the bulk mineralogy of the silt fraction.

Chemical analyses

Cation exchange capacity (CEC) analysis was performed on complete <2 μm fractions for 1904, 1957 and 2014, and on 2-0.2, 0.2-0.05, and <0.05 μm subfractions of 2014 samples using the cobalt hexamine method (Orsini and Remy, 1976; Dohrmann and Kaufhold, 2009). The organic component was measured via CHN analysis of the <2 μm fractions of these samples, in addition to analysis of major and trace elements via inductively coupled plasma mass and optical emission spectroscopy (ICP-MS and ICP-OES).

2.3 Analysis by X-ray diffraction

Characterisation of clay minerals is typically performed using XRD. This is due to the small size of clay crystals, <2 μm, which means they cannot be characterised by traditional methods such as optical microscopy, while techniques such as electron microscopy may not characterise a representative number of particles. Additional constraints exist due to the complex nature of clay phases, which are often mixtures and mixed-layers, leading to difficulty interpreting the results of chemical or compositional analyses when compared to those for a pure phase. The advantage of XRD is due to the non-destructive manner of analysis, and as XRD analysis is performed on thousands or millions of crystallites at a time, bulk compositional and structural information can be obtained for the specimen analysed.

Principles of XRD

Analysis of a sample by XRD uses of a monochromatic beam of X-rays which is directed at a sample and the angle of incidence between the beam and the sample is varied over a certain range. A detector is positioned to capture any reflected X-rays that result from

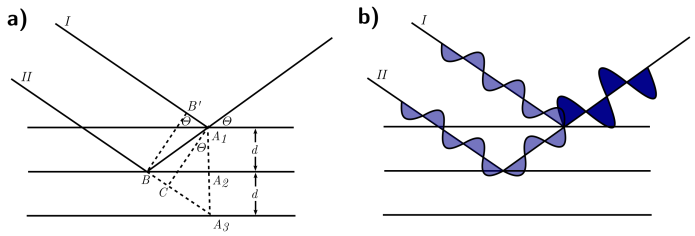

Figure 2.3: Conditions which result in a) diffraction (or reflection) of an X-ray beam from a set of lattice planes and b) an example of constructive interference arising from the path difference where I-II = 1λ. (Borchardt-Ott, 2012)

the interaction between the X-rays and the atoms within the unit-cell of the crystals (the unit-cell is the smallest repeating structural unit) due to the similarity of the unit-cell dimensions and the wavelength of X-rays (e.g. Cu Kα 1.54 Å). When certain conditions are met, the interaction results in diffraction of the X-ray beam in a coherent, in-phase manner where the diffracted waves have the same vector direction, wavelength and amplitude, and the waves interfere constructively. This occurs when the conditions satisfying Bragg's Law (Equation (2.1)) are met.

$$2dsin\Theta = n\lambda \tag{2.1}$$

Using Bragg's Law, the position of diffraction maxima, Θ, can be related to the distance, d, between the planes of atoms in the sample and thus to determine the atomic configuration of the atoms in the unit-cell. λ, a constant, is the wavelength of the incident x-rays and n an integer number of wavelengths which allows for the presence of higher-order reflections (harmonics) for a given d value (a complete mathematical derivation can be found in Moore and Reynolds (1997). The intensity of the diffraction maxima is modulated by the arrangement of atoms in the unit cell and their scattering power, which is determined by their electronic configuration. As such, different modulation of intensity occurs based on the exact configuration and the value of Θ, which alter the amount of constructive or destructive interference between diffracted waves. Thus, analysis of not only the position but the intensity of diffraction maxima can be used to identify the composition and configuration of atoms within the unit-cell.

XRD of clay minerals

The sharpness of reflections is also proportional to the number of planes of atoms which are diffracting coherently, so it is linked to the ıcrystallinityȷ of the sample. This is particularly relevant in the case of diffraction from clay minerals which have very small crystals, and even the largest crystals of clays can consist of many smaller crystallites, each of which has a different number, N, of planes of atoms diffracting coherently. Small values of N lead to broad and diffuse reflections, while large N values give sharp, well-defined peaks. The presence of stacking defects between layers in clay minerals, also leads to peak broadening due to variations between the positions of planes of atoms when moving from layer to layer. Thus the reflections from clay minerals tend to be much more diffuse and broad than those of crystalline materials with ordered structures. Furthermore, the structure of clay minerals is essentially identical when looking in the a-b plane horizontally through the tetrahedral and octahedral sheets. Random powder of clay minerals often performed to distinguish between trioctahedral and dioctahedral minerals which can be discerned by differences in position of the 060 reflection, where the sample is prepared so as to give the maximum possible number of different orientations of crystals and the associated atomic planes and d-spacings. The largest structural difference for clays is the layer-to-layer distance in the c-axis perpendicular to the layer. Thus to emphasise the effects of the difference in layer-to-layer distances, diffraction of clay samples often takes place from oriented slides, where the sample is prepared in such a way as to maximise the orientation of the clay particles. This gives rise to a pattern which consists primarily of the basal, or 00l, series of reflections which, in the case of a discrete mineral, can be broken down into the 001 reflection corresponding to the layer-to-layer distance and a rational series of higher order reflections, i.e. 002, 003, 004,. . . ,00n, which result from higher order reflections (Equation (2.1)). In the case of mixed-layers this series is not commonly rational (certain mixed-layer compositions or species may result in a rational series, e.g. corrensite).

Quantitative analysis of samples

Initially, XRD data is subject to a background subtraction, which corrects for the possible influence of the silica glass slide on diffracted intensities, and to a correction for the thickness of the sample (Moore and Reynolds, 1997). Full-profile fitting of <2 μm subfractions takes place using the Sybilla programme developed by Chevron^{TM}. Full details of the parameterisation of the model are found in the following section, and as such will not be repeated here. This section will provide a brief overview of the modelling

procedure. In Sybilla, phases are added independently on the basis of the position of the diffraction maxima. Rational series which arise from discrete phases are identified, and mixed-layers added on the basis of Mering's rule, which states that the intensity of a given reflection in a mixed-layer will be found at a d-spacing between those corresponding to the reflections of the discrete phases which make up the mixed-layer. Attempts are made to identify mixed-layers which would appear to have a large proportion of a single layer-type, and gradually increase the compositional complexity of introduced phases if the simplest phases are not enough to fully describe the sample. A direct comparison between AD and EG samples is made and concurrent refinement of the two structural models takes place to converge to a single structural model that provides a good description of the sample in both AD and EG states.

Initial modelling approach

An initial model was defined for the samples from the Morrow Plots by Khan (2013) which involved full-profile fitting of AD and EG samples as described above. The proposed model involved the use of three-component mixed-layers, of the nature A-smectite-smectite (A-SS) where the parameter W_a described the proportion of the first layer-type. The two different smectite layer-types allow to represent the different hydration states of smectite with either one plane (S_1) or two planes (S_2) of interlayer water (or glycol in EG conditions). The mixed-layers used in this model were R0, which denotes that the interstratification was random – the nature of the layer-type of a selected layer has no influence on the nature of its nearest neighbours. To fit <0.05 μm subfractions the width of the 001 reflection, particularly towards 10 Å, was described using a R0 kaolinite-S_1S_2 mixed-layer (K-Exp, W_a ∼50–60) and intensity from this phase was the primary contribution to the large, broad maxima centred near 3.3 Å in AD conditions, shifting to 3.4 Å in EG solvated samples. R0 illite-S_1S_2 (I-Exp, W_a ∼60) provided intensity in the low-angle side of the 001 reflection at 15.3 Å in AD conditions, in addition to contributions to the maxima at 5 Å and adding to the high-angle shoulder at 3.3 Å. A R0 chlorite-S_1S_2 (Ch-Exp, W_a ∼35-40 was used to account for the high-intensity of the 001 reflection which was not able to be described by the I-Exp and K-Exp phases alone. The maxima at 7.25 and 3.58 Å were described using a discrete kaolinite phase. The shoulder on the 001 reflection near 10 Å, and maxima 4.99 and 3.33 Å complete a rational series which was described by a discrete illite phase. For the fitting of the 0.2-0.05 and 2-0.2 μm fractions the same assemblage was used with the addition of discrete chlorite. An example of this model is provided in Figure 2.4.

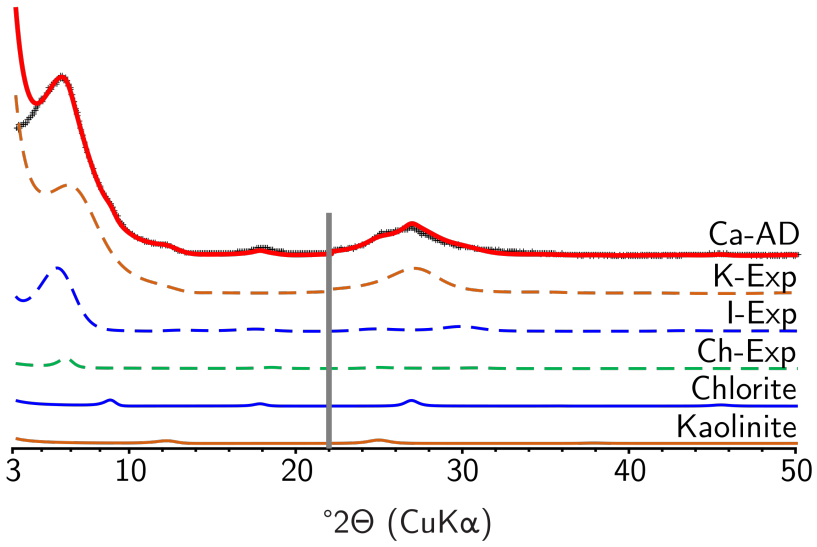

Figure 2.4: An example of the fit obtained using the initial model of Khan (2013) for 2014 CF <0.05 μm Ca-AD sample. Best fit is shown as a solid red line and experimental data as black crosses. The contributions of the individual phases are indicated on the figure. Descriptions of the K-Exp, I-Exp and Ch-Exp notation can be found in Section 2.3.4. Solid grey bars indicate where intensity in the high angle region has been increased by a factor of two.

This model was used to fit the sample series from 1904 to 2014, and was able to provide a good description of the experimental data, with R_p values typically <6% for <0.05 μm subfractions (misfit increased with size due to the presence of quartz and feldspar impurities) (Figure 2.7). However, a comparison with XRD data for K-150 samples was made to attempt to provide additional constraints on the nature of the proposed mixed-layers. Based on the layer composition of the phases proposed in this model, certain changes could be predicted to occur with K-saturation and heating. These predictions can be made from the basis of Mering's rule, which bases the position of the $00l$ reflection of a mixed-layer between the reflections of the component layer-types, and studies on the hydration behaviour of smectites when saturated with different cations (Méring, 1949). In particular, K-saturation and heating leads to dehydration and collapse of the interlayer space for the majority of smectite layers (a minor proportion of S_1 layers may remain) (Ferrage et al., 2005b). Such collapse gives a 2:1 layer phase with a d-spacing resembling that of illite/mica at ~10 Å. Thus, the K-150 treatment should reasonably be expected to result in the collapse of intensity of the I-Exp 001 reflection from ~15 Å in Ca-AD samples to close to 10 Å. A similar collapse of the Ch-Exp mixed-layer should result in an increase of intensity between 10 and 14 Å, and the collapse of smectite layers

in K-Exp would cause an intensity increase between 7 and 10 Å. Observation of these predicted changes would imply the model is accurate.

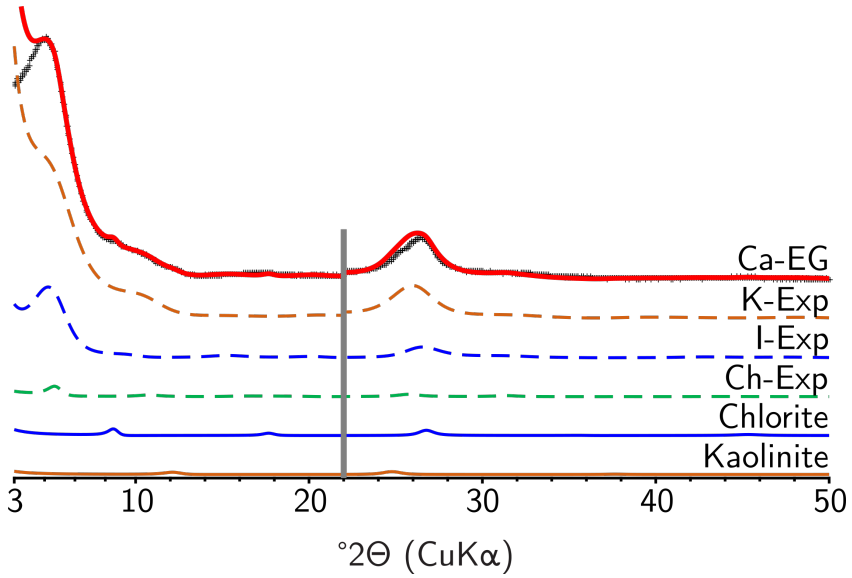

Figure 2.5: An example of the fit obtained using the initial model of Khan (2013) for 2014 CF <0.05 μm Ca-EG sample. Best fit is shown as a solid red line and experimental data as black crosses. The contributions of the individual phases are indicated on the figure. Descriptions of the K-Exp, I-Exp and Ch-Exp notation can be found in Section 2.3.4. Solid grey bars indicate where intensity in the high angle region has been increased by a factor of two.

Inclusion of K-150 samples

However, comparison between Ca-AD and K-150 samples of the present study (Figure 2.6) shows these predicted differences are not observed. Although a gain of intensity near 10 Å does occur, the collapse of the 001 reflection is incomplete and leads to the presence of a relatively broad reflection at 13.2 Å. The position of this reflection is consistent between the 2-0.2, 0.2-0.05 and <0.05 μm subfractions. There is no gain of intensity of between 7 and 10 Å. This can only be interpreted as the absence of a K-Exp mixed-layer. The incomplete collapse of the 001 reflection on K-150, and even K-350, treatments indicates that there are a significant proportion of chlorite layers in the mixed-layers present in the sample. This would suggest the layer-composition of the I-Exp and Ch-Exp mixed-layers needs to be adjusted to better match the experimental data. Following this, the experimental data was assessed according to the description outline in the following subsection.

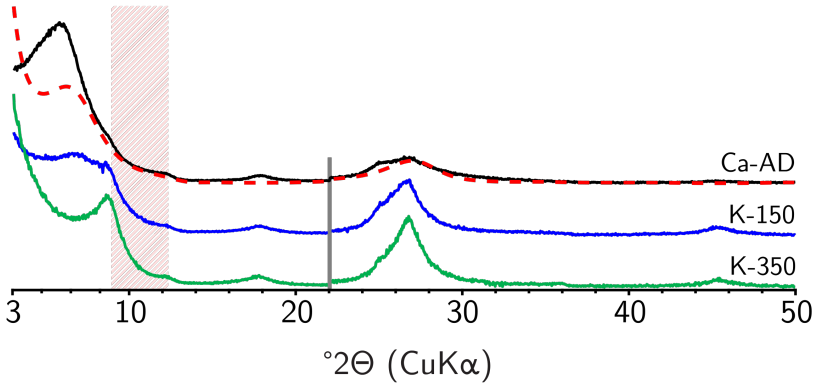

Figure 2.6: Comparison of experimental data in Ca-AD (black), K-150 (blue) and K-350 (green) conditions. The contribution of the K-Exp phase is shown in dashed red, and the shaded region represents the interval in d-spacing where an increase in reflected intensity would be expected in K-saturated conditions, based on the presence of the K-Exp phase. The solid grey bar represents where intensity has been multiplied by a factor of two in the high-angle region.

Simulation of XRD patterns

Mineral identification and full-profile modelling of the XRD profiles of 50-2 μm fractions was carried out using Rietveld refinement and the Profex interface for BGMN software (Doebelin and Kleeberg, 2015) for the range 8-90 °2Θ. For 2-0.2, 0.2-0.05 and <0.05 μm subfractions simulation was performed between 3.5-50 °2Θ using the Sybilla programme developed by Chevron^{TM} (Aplin et al., 2006), using the mathematical formulation reported by Drits and Tchoubar (1990). This modelling is based on the direct comparison between experimental and calculated $00l$ XRD reflections, and fitting takes place via trial-and-error determination of structural factors to arrive at a single structure model which fits the profiles obtained from each treatment according to the multi-specimen technique which has been previously adapted for soil samples ((Drits et al., 1997b; Sakharov et al., 1999b,a; Hubert et al., 2012, 2009).

Discrete or mixed-layer contributions were added independently, and factors such as layer-type and proportion and stacking sequence refined. The model allowed for the presence of smectite with either one, two, or zero planes of interlayer water (noted as S_1, S_2 and S_0 respectively) with layer-to-layer distances of ∼12.5, ∼15.0 and ∼10.0 Å respectively in the AD state. Under glycolation, these layer-to-layer distances were set at 12.9 and 16.8 Å (Ferrage et al., 2005a,b). While in the K-saturated state the majority of S_1 and S_2 layers collapse to ∼10 Å, for the minority of layers which remain expandable the same layer-to-layer distances were used. The z-coordinates of Moore and

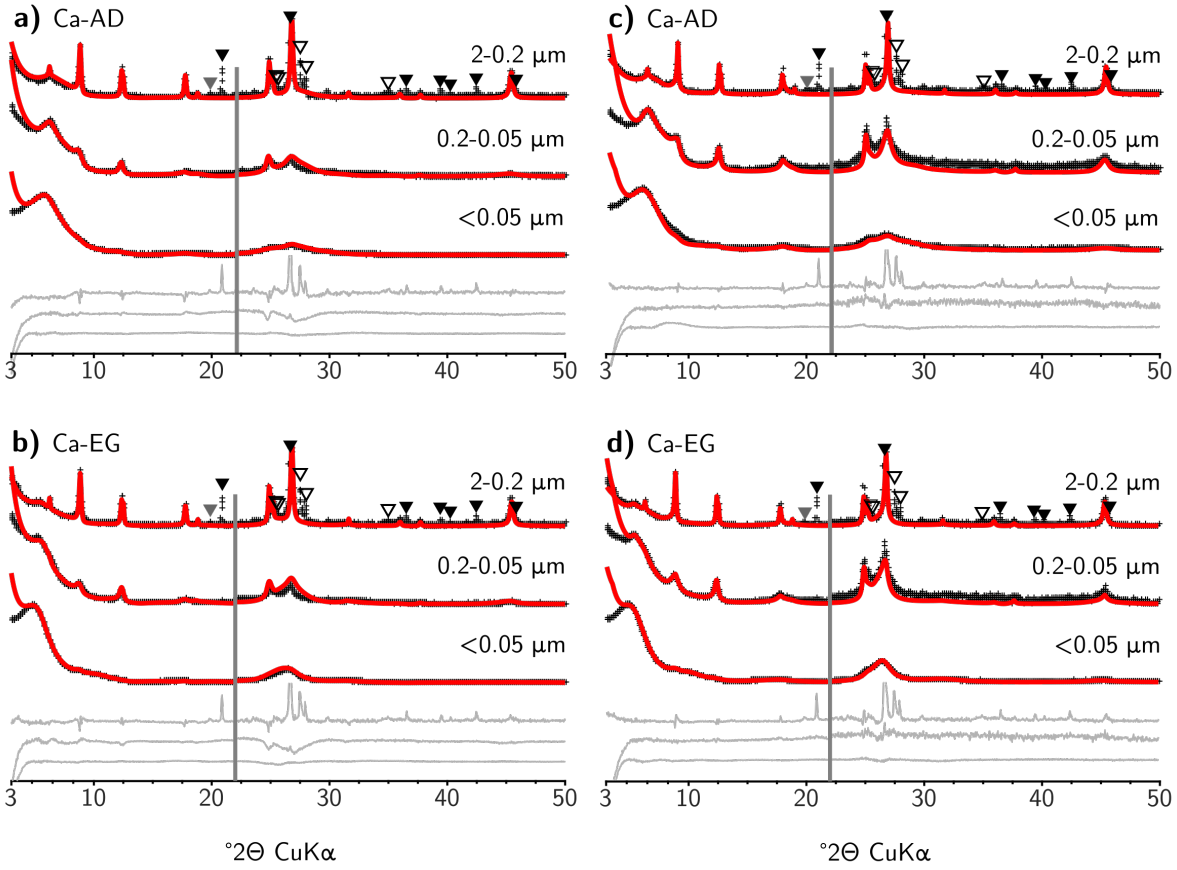

Figure 2.7: Comparison of the best fits achieved with the different models for all three subfractions of 2014 CF subplots. The initial model using K-Exp is on the left, while the final model is shown on the right. Solid red lines represent the best fit and black crosses experimental data. Light grey lines at the bottom of each plot represent difference plots. Solid black and outlined triangles indicate reflections arising from quartz and feldspar impurities, while solid grey triangles show *hk* reflections, and were excluded from the modelling process. High quartz intensities at 26.6 Å have been removed for clarity.

Reynolds (1997) were used for the distribution of atoms within the interlayer space of these layers. Octahedral iron occupancy and the number of interlayer cations and water molecules were also treated as adjustable parameters. Sigma-star (σ^*), which represents the distribution of particle orientation, was assumed to be identical for all phases within a given model, however it was allowed to vary between models for different samples or subfractions. Distribution of coherent scattering domain (CSD) sizes was assumed to be log-normal about an adjustable mean (Drits et al., 1997a). This approach relies on differences in layer-to-layer distances and structure factors of expandable layers arising from the different treatments (AD/EG) and leads to the determination of the proportion or weighted concentration of each independent phase in the sample, where agreement of

the proportions of each phase between the different treatments was achieved to within 5%.

I

Identification of the mineral assemblage and pedogenetic influences of the Morrow Plots

Soil development under continuous agriculture at the Morrow Plots fields via X-ray diffraction profile modelling

3.1 Introduction

Clay minerals are ubiquitous in soils and result from the weathering of primary minerals, thus the nature of the parent mineral and the climate can have a strong bearing on the nature of the soil clay mineral assemblage and the rate of weathering (Meunier, 2005; Velde and Meunier, 2008; Velde and Barré, 2009). Furthermore, clay minerals in soils may be affected by physical distribution processes within the profile, such as eluviation or illuviation, or by subsequent chemical modification. For example, acidic environments may lead to dissolution of minerals and the fixation of aluminium in the interlayer space of expandable 2:1 minerals with a subsequent loss of soil fertility (Righi, 1982; Ranger et al., 1991; Huggett, 1998; Bain and Griffen, 2002; Bortoluzzi et al., 2008, 2012). Further, the actions of plants may have an influence on clay mineral structure through uptake of mineral nutrients, which depends on clay mineral composition and proximity to plant roots, and the soil solution chemistry (Arnold and Close, 1961; MacLean and Brydon, 1963; Marschner, 1995; Mengel et al., 2001; Vetterlein et al., 2013; Mouas-Bourbia et al., 2015; Adamo et al., 2016). In particular, several studies have contrasted the effects of different vegetation and agronomic processes, such as an increase of illite content in fertilised soils which had been under cultivation for 200 years when compared to adjacent native forest, or decreases in soil organic matter and aggregation in cultivated Humic Luvisol (Chenu and Plante, 2006; Cornu et al., 2012). Bortoluzzi et al. (2012) reported the vermiculitisation of illite in a sub-tropical regosol, despite fertiliser inputs during 40 years of grape cultivation. Similarly, Bain and Griffen (2002) reported increased vermi-

culitisation in the top horizon of a temperate arable soil when compared to adjacent forest and grassland of the same pedogenetic origin (brown forest soil with gleying or Inceptisol).

The complex nature of soil clay minerals arises from their variation in size, morphology, degree of interstratification, and composition (Badraoui et al., 1992; Pernes-Debuyser et al., 2003; Hubert et al., 2009; Caner et al., 2010; Hubert et al., 2012). Long-term field experiments such as the Morrow Plots represent a unique opportunity to look at the long-term effect of intensive agriculture as a pedogenetic factor on soil clay minerals to unravel some of this complexity. Initially established to investigate the impacts of different agronomic practices such as crop rotation and fertilisation treatments on soil fertility and crop yields, the well documented history of the Morrow Plots provides the opportunity to isolate the mechanisms of plant-induced mineral weathering. Previous studies on plant-mineral interactions have focussed on plant uptake of potassium, an essential plant nutrient, from clay minerals, as extraction of potassium from the interlayer space of non-expandable 2:1 minerals (illite and micas) is accompanied by structural changes which can be observed using XRD analysis (Hinsinger et al., 1993; Velde and Peck, 2002; Barré et al., 2007a,b; Adamo et al., 2016). Furthermore, a number of results have been reported from various field experiments on changes indicating that long-term cropping may impact the level of exchangeable potassium in soils, which is closely related to the clay mineralogy. For example Arnold (1960) and Singh and Goulding (1997) reported an increase in potassium content in the soils of the Broadbalk continuous wheat experiment, but Singh and Goulding (1997) did not observe any changes in XRD that indicated changes in clay mineralogy. Möberg and Dissing-Nielsen (1983) and Dissing-Nielsen and Möberg (1984) reported a decrease in both potassium and illite content in the soils of two agricultural experiments in Denmark. Simliarly, Tributh et al. (1987) reported a decrease in illite content and increase in smectite content in soils which accompanied 35-130 years of continuous cropping.

However these studies used qualitative assessment of XRD data, which restricts interpretation to sharp, well-defined reflections and is unable to extract comprehensive compositional information on the nature of mixed-layers which may be present. More recent studies have attempted to identify clay mineral evolution using the decomposition method initially proposed by Lanson (1997) in combination with partial simulation of XRD patterns (NEWMOD, Reynolds Jr. (1985)) to characterise soils under various soil management systems (Velde and Peck, 2002; Pernes-Debuyser et al., 2003; Barré et al.,

2007a, 2008a; Li et al., 2011; Mouas-Bourbia et al., 2015; Adamo et al., 2016). This method is based primarily on the position of reflections in the low-angle region (20-7 Å), and these reflections are decomposed into pseudo-Voigt functions to separate the contributions of both discrete phases and mixed-layers. This method improves both the evaluation of mixed-layers in a given sample and their evolution in a series of comparable samples. These studies are nonetheless confined to interpretation of only a portion of the experimental XRD pattern and the information obtained cannot be considered quantitative. Development of the full-profile modelling methodology, used in conjunction with the multi-specimen approach (Drits et al., 1997b; Sakharov et al., 1999a,b) has been successful in characterising the full clay mineral assemblage of a range of soils or diagenetic sequences (Inoue et al., 2005; Aplin et al., 2006; Hubert et al., 2009, 2012; Viennet et al., 2015). This technique was used to provide a comprehensive description of the mineral assemblage of the cultivated soil of the Morrow Plots. The aim of this study was to investigate the effects of plant growth as a pedogenetic factor in temperate-zone agricultural soils by characterisation of physical and chemical properties, and of mineralogy as a function of time using full-profile XRD modelling.

3.2 Materials and methods

Sample collection, particle size distribution, chemical analyses and analysis of XRD patterns were performed as described in Chapter 3. The results described and discussed in the following sections were collected from RU subplots.

Table 3.1: Results of CEC and elemental analyses for selected fractions from 1904, 1957 and 2014 samples. Note the low value reported for Ca is due to the analysis performed on samples that were previously Na-saturated.

Year	Fraction	CEC (ceq_c/kg^{-1})	C	H	N	K_2O	Na_2O	MgO	CaO	TiO_2	Fe_2O_3	MnO	P_2O_5	SiO_2	Al_2O_3
									%						
1904	<2 μm	45.5	6.47	1.56	0.56	2.15	0.25	1.78	0.08	0.79	8.56	0.07	0.28	45.57	17.25
1957	<2 μm	47.9	6.18	1.49	0.57	2.18	0.22	1.78	0.07	0.82	8.33	0.08	0.29	46.56	17.3
2014	<2 μm	55.2	5.79	1.59	0.6	1.83	0.15	1.91	-	0.65	8.85	0.06	0.32	43.09	18.10
	2-0.2 μm	22.1													
	0.2-0.05 μm	58.6													
	<0.05 μm	82.2													

3.3 Results

Particle size distribution

The results of the size-fractionation of samples from 1904 to 2014 are reported in Figure 3.1, normalised to 100%. Average recovery for all samples was 94.9% of the starting weight. The 2 mm-50 μm fraction accounts for 6-8% of the sample mass for all samples from 1957-2014, while the 50-2 μm and <2 μm fractions account for 63-66% and 27-30% respectively. For 1904 these values are 4, 61 and 35% possibly indicating grinding of the sample. In the <2 μm subfractions (Figure 3.1b) the proportion of 2-0.2 μm fraction is relatively constant at 32-34% for the samples covering the period 1957-2014 while for 1904 the proportion is 39%. The proportion of the <0.05 μm subfractions varies almost linearly from 37% in 1957 to 46% in 2013-14. Similarly, the proportion of 0.2-0.05 μm subfractions varies from 29% to 22% in the same timeframe and that of 2-0.2-0.05 μm from 39 to 35%.

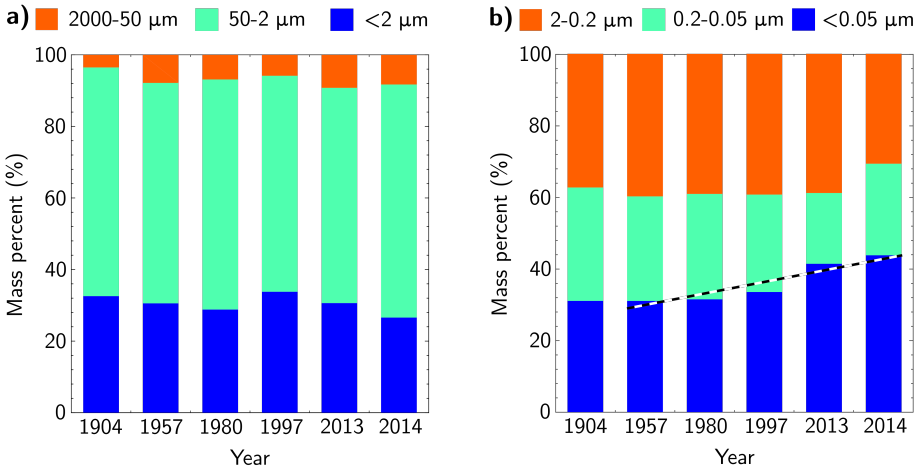

Figure 3.1: Results of particle size-fractionation for a) sand-silt-clay fractions and b) <2 μm subfractions. Despite significant variation, the <2 μm fraction remains relatively stable, while the proportion of <0.05 μm subfraction increases over time primarily at the expense of 0.2-0.05 μm subfractions.

Chemical Analyses

Results of the CEC and elemental analyses are shown in Table 3.1. They demonstrate an increase of 17% in the CEC from 47/48 meq/100g in 1904 and 1957 to 55 meq/100g in 2014. The results for the subfractions in 2014 show a variation with size from 81

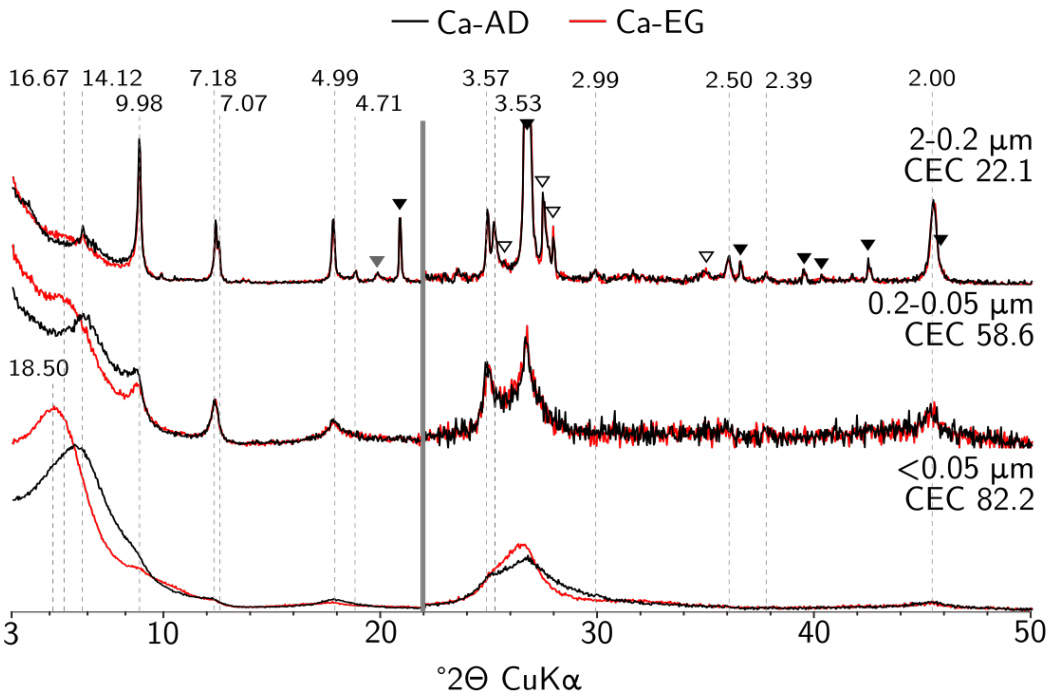

Figure 3.2: Comparison of experimental XRD profiles for Ca-AD and Ca-EG samples for the three subfractions from 2014 RU subplot. AD samples are shown in solid black lines and EG samples as solid red. Quartz reflections are indicated by solid black triangles, whilst open triangles those of feldspars and solid grey hkl reflections. Dotted grey lines indicate the positions of major reflections, with d-spacings provided in Å. The solid vertical grey bar represents an increase in intensity of the high-angle region by a factor of two.

meq/100g for the <0.05 μm subfraction to 14 meq/100g for 2-0.2 μm subfraction. The elemental analyses show a slight but consistent decrease in C content from 1904 to 2014 while N levels remain relatively constant through the same period, leading to a decrease in the C/N ratio. For remaining elements, K, Na, and Si contents decrease with time, while those of Al, Fe and Mg increase slightly.

Qualitative interpretation of XRD

Random powder XRD for the 50-2 μm fractions (Appendix A.1, Figure A.1) indicates the presence of quartz, feldspars, mica, chlorite and kaolinite, in addition to small reflections associated to calcite, anatase and amphibole. The phases present in the 50-2 μm model are consistent with the analyses of Rivard et al. (2016) for samples from 1904 and 2012 from the Morrow Plots, and although these authors did not report the presence of amphibole or calcite older Champaign county soils surveys do report their presence

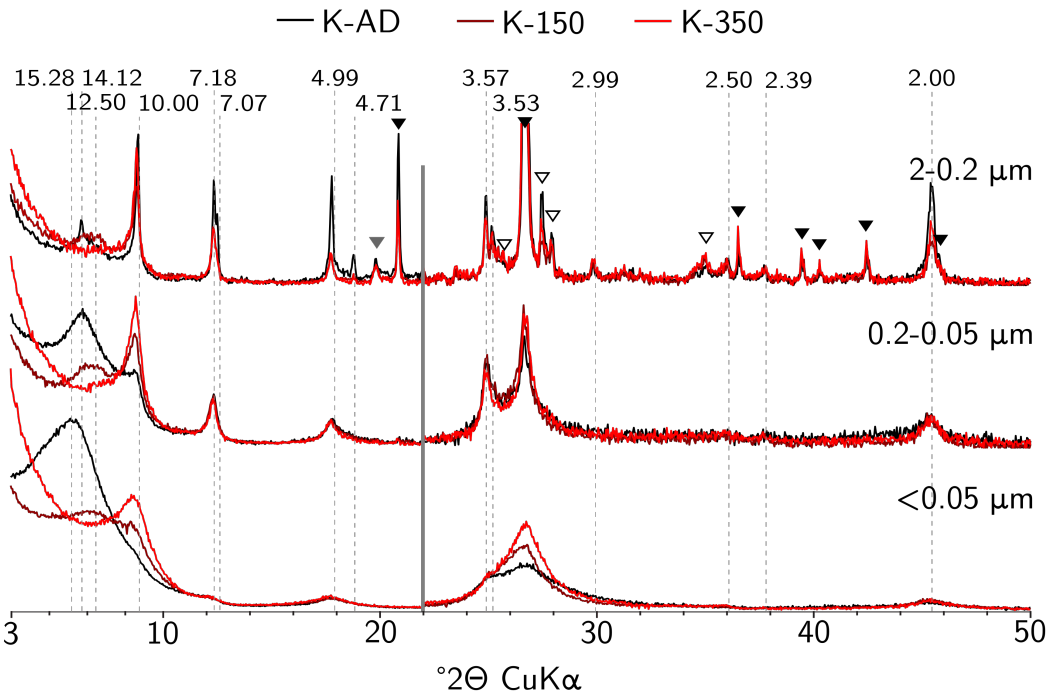

Figure 3.3: Comparison of experimental XRD profiles for Ca-AD, K-150 and K-350 samples for the three subfractions from 2014 RU subplot. AD samples are shown in solid black lines, K-150 in maroon and K-350 in red. Quartz reflections are indicated by solid black triangles, whilst open triangles those of feldspars and solid grey hkl reflections. Dotted grey lines indicate the positions of major reflections, with d-spacings provided in Å. The solid vertical grey bar represents an increase in intensity of the high-angle region by a factor of two.

(Willman et al., 1963; Fehrenbacher et al., 1967; Mount, 1982; Endres, 2002). Rivard et al. (2016) also noted the presence of illite/muscovite, kaolinite, chlorite, and expandable clay minerals which are present in the current sample. Results of XRD analysis of oriented slides are shown in Figure 3.2 for 2014 2-0.2, 0.2-0.05 and <0.05 μm subfractions Ca-AD and Ca-EG samples. Qualitative analysis of the profiles under the different treatments identifies the presence of quartz and feldspars, which are concentrated in the 2-0.2 μm subfractions (Figure 3.2, solid and open triangles respectively). Comparing the different sizes shows increasingly broad and asymmetric peaks as size decreases, an indication of decreasing CSD size and/or mixed-layering and the finest fractions have no sharp, well-defined reflections. The <0.05 μm subfraction also shows significant expansion on EG solvation and a large collapse in the K-150 state (Figure 3.3) which indicate a greater proportion of expandable 2:1 layers compared to the two other subfractions. Comparison of the XRD patterns for all the subfractions for the samples from 1904 to 2014 shows no systematic variation in either the position of the intensity of the reflections for individual

clay phases (representative data in Figure 3.4).

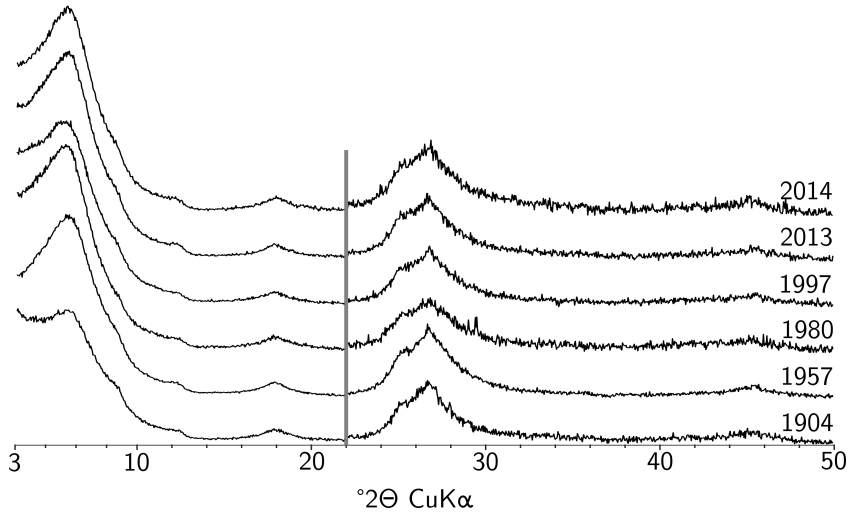

Figure 3.4: Comparison of experimental data obtained from 1904 (bottom) to 2014 (top). Note that very little variation in the shape or position of the 001 reflection with time, with the exception of the 1904 sample. The vertical grey bar represents an increase in intensity of the high-angle region by a factor of two.

Discrete illite can be identified through the presence of a rational 00l series at 9.98, 4.99 and 2.00 Å (contribution at 3.33 Å overlapped by that of quartz). In the 0.2-0.05 μm subfraction these reflections are shifted to 10.07 and 4.96 Å in the Ca-AD state and shift to 10.13 and 4.99 Å respectively on EG solvation. This indicates some interstratification with expandable layers. This phase is indicated by a shoulder centred on 10 Å in the <0.05 μm subfraction. Discrete chlorite and kaolinite can also be identified in the 0.2-2 μm subfraction due to their rational basal spacing series of 14.12, 7.07, 3.53 and 2.39 Å and 7.16, 3.58 and 2.39 Å, respectively; these reflections remain unchanged on EG solvation. The presence of at least one mixed-layer can be identified from the shifts in the peak position of the broad 001 reflection from 13.60 to 16.67 Å in the 2-0.2 μm subfraction. This is represented by a shoulder in the 0.2-0.05 μm subfraction. Mixed-layers are also responsible for the reflection at 15.28 Å (EG 18.5 Å) in the <0.05 μm subfraction in addition to the subtle shoulder at 20.3 Å which appears in the Ca-AD state. Reflections at 7.25 and 3.52 Å suggest the presence of a kaolinite-illite (KI) phase as described by Hubert et al. (2012) and Viennet et al. (2015) in the two finest fractions. Progressive collapse of the 001 reflection on K-saturation and heating indicates the presence of layers with chloritic nature as the brucite-like interlayer sheet prevents full collapse of the layer-to-layer space. It also suggests differing layer-type composition between mixed-

layers, as it may reflect variations in smectite dehydration behaviour or differences in the proportion of layers with chloritic nature. However the nature of the mixed-layers cannot be ascertained and simulation of the complete XRD profile is necessary to obtain this information.

XRD profile simulation

Quantitative phase analysis of 50-2 μm fractions showed they are dominated by quartz (∼65-70%), with significant contribution from albite and microcline (10-12 and 10-13% respectively), minor amounts of mica, chlorite and kaolinite (1-5%) and trace amounts of amphibole, anatase, calcite and hornblende (<1% each). This mineralogy remained very stable from 1904-2014, notwithstanding some slight heterogeneity between different years. For <2 μm subfractions, a comparison between experimental and calculated results is shown in **??** and details of the complete structural models are reported in Table 3.2. Up to seven different mixed-layers were necessary to obtain an adequate description of the sample, in addition to the four discrete phases of illite, chlorite, kaolinite and smectite. The quantitative results of modelling the 2014 2-0.2, 0.2-0.05 and <0.05 μm subfractions in Ca-AD and Ca-EG states are reported in Table 3.3. For modelling the <0.05 μm subfraction, an illite-S_2-S_1-chlorite (ISSCh) was required to account for the shoulder at 10.04 Å in the AD treatment. W_a, which expresses the proportion of the first layer-type in a given mixed-layer (in this case illite), was set at ∼90 (phase notation ISSCh 90). The presence of both S_2 and Ch layer-types was necessary to properly replicate the position of this shoulder. An additional ISSCh phase with W_a ∼50-60 (ISSCh 50) contributes to the breadth of the 001 reflection towards 10 Å and significantly to reflections at 4.90 and 3.38 Å. An ISSCh mixed-layer dominated by smectite layers takes into account the maxima at 15.30 Å and the low broad shoulder centred at 3.10 Å for the AD treatment. The position of the 001 reflection in the AD sample and the shift to 18.50 Å on EG solvation is indicative of a pure smectite but a small proportion of chlorite layers were introduced due to the non-complete collapse of K-150 samples. This mixed-layer also contains ∼5% illite layers (ISSCh 5). A further mixed-layer, consisting of ISSCh layers with W_a ∼35 (ISSCh 35) was needed to completely account for the shape of the 001 reflection, and also provides a significant contribution to the broad reflection centred on 8.50 Å in the EG state and to the reflection at ∼3.38 Å for both AD and EG treatments. Most of these mixed-layers contained a portion of chloritic layers, owing to the incomplete collapse of the 001 reflection to between 12.15 and 14.10 Å following K-150 treatment. A pure smectite phase,

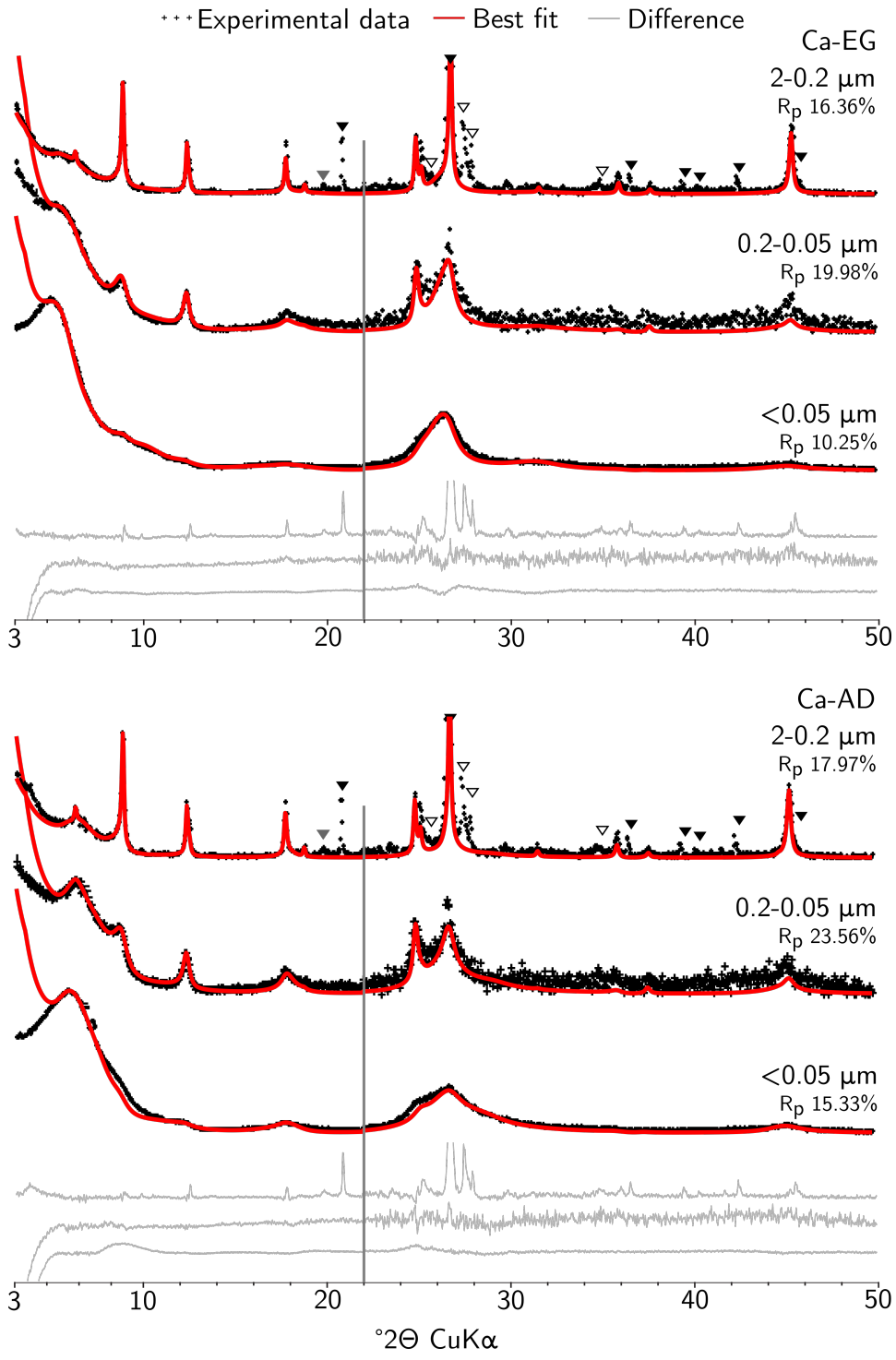

Figure 3.5: Comparison of experimental and calculated XRD profiles for the 2-0.2, 0.2-0.05 and <0.05 μm subfractions of the 2014 sample. Quartz reflections are indicated by solid black triangles, those of feldpsars by open triangles and solid grey triangles indicate *hk* reflections, which are not modelled. The vertical grey bar represents an increase in intensity of the high-angle region by a factor of two.

with extremely low CDS and completely expanded to two interlayer planes of glycol was necessary to explain the shoulder at 20.30 Å. A probable KI ($W_K = 80$) was introduced to explain the two reflections at 7.25 and 3.52 Å. To reproduce the apparent irrationality of the spacing, partial segregation was imposed between the two layer-types (KI R1 notation).

Table 3.2: Structural parameters for the different phases obtained from full-profile fitting of 2014 <2 μm subfractions using Sybilla. I/S/S/Ch represents the proportion of illite, smectite S_1, smectite S_2 and chlorite layers, and I/Ch the proportion of illite and chlorite layers, in the mixed-layers. These mixed layers are randomly interstratified (Reichweite value R0). The KI R1 mixed-layer exhibits a tendency to partial segregation which is defined by the parameter P_{II}, which represents the probability of finding two adjacent layers of the given type (in this case illite). CSD size is given as N, the average number of layers per crystal.

		Subfraction					
		2-0.2 μm		0.2-0.05 μm		<0.05 μm	
		Treatment					
Contribution		AD	EG	AD	EG	AD	EG
Illite	N	36		-	-	-	-
ISSCh 90	I/S/S/Ch	92/3/0/5		94/2/0/4	94/1/1/4	89/4/3/4	89/7/0/4
	N	27		12		10	9
ISSCh 80	I/S/S/Ch	75/5/10/10		80/4/2/14	78/5/3/14	-	-
	N	23		18	18	-	-
ISSCh 50	I/S/S/Ch	50/20/5/25	50/18/7/25	56/8/11/25	52/13/10/25	60/6/12/22	54/12/12/22
	N	19	19	9	9	7	7
ISSCh 35	I/S/S/Ch	35/36/9/20		30/38/12/20	30/35/15/20	40/20/14/26	30/38/6/26
	N	17		7	7	4	4
ISSCh 5	I/S/S/Ch	0/80/0/20		0/70/10/20	0/73/7/20	5/66/17/12	0/85/3/12
	N	7		6	5	4	3
Kaolinite	N	47		28		-	-
KI R1	K/I			80 20			
	P_{II}			0.4			
	N	47		28		19	
ICh 6	I/Ch	1/99		3/97		-	-
	N	27		13		-	-
Smectite S_2	N	-	-	-	-	2	

For 0.2-0.05 μm subfractions, very similar mixed-layer contributions were used with augmented CSD sizes and an additional ISSCh mixed-layer was introduced with W_a ~80 (ISSCh 80). This reproduced the additional broadening around the 10 Å reflection in experimental data which was inadequately reproduced by the mixed-layers of the initial <0.05 μm subfraction model. Discrete kaolinite was also introduced as the 0.2-0.05 subfraction presents a rational series at 7.16, 3.58 and 2.39 Å. Finally, due to the presence of shoulders at 4.76 and 3.51 Å an illite-chlorite mixed-layer, with few illite layers (ICh, W_a ~6) was introduced. For the 2-0.2 μm subfraction, discrete illite and chlorite were also introduced to account for the rational peak series previously described. The relative proportions of each contribution are reported in Table 3.3. Given the constraint of the two treatments the structure model can be treated with reasonable confidence. Note however there is some misfit on either side of the 001 reflection at 10.00 Å and again 3.53 Å in Ca-AD <0.05 μm subfractions for all samples which suggests the presence of additional heterogeneity as the region could not be reproduced with the current model.

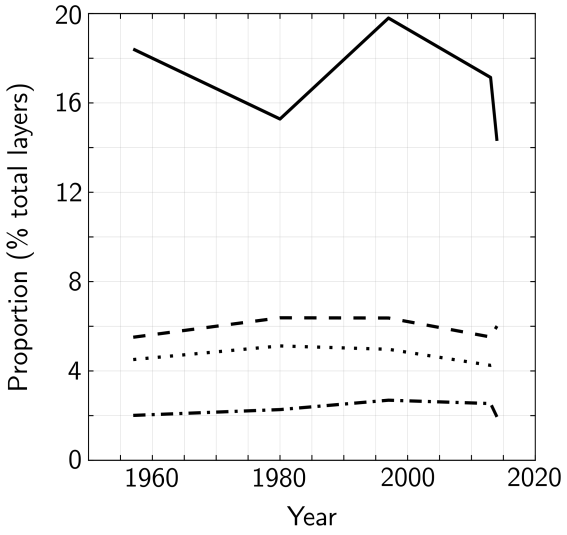

Figure 3.6: Total proportion of layers of a given type in complete <2 μm fractions, calculated from the sum of modelling results for 2-0.2, 0.2-0.05 and <0.05 μm subfractions. Note the strong variation in illitic content for 1980 and 2014 is due to large variations in the mass percent of 2-0.2 μm fractions which primarily affect the proportion of discrete illite. The values reported here are normalised to the total % of the <2 μm fraction in the sample.

These phases, with few modifications to layer-type proportions and CSD sizes, were used to model all the <2 μm subfractions from 1904-2014 and the calculated phase

Table 3.3: Results of quantitative phase analysis of the proportions of the contributions under either AD or EG treatments for the three <2 μm subfractions for the 2014 sample.

	Subfraction					
	2-0.2 μm		0.2-0.05 μm		<0.05 μm	
	Treatment					
Contribution	AD	EG	AD	EG	AD	EG
Illite	44	40	-	-	-	-
ISSCh 90	16	14	17	15	13	10
ISSCh 80	9	7	22	18	-	-
ISSCh 50	14	20	40	42	39	40
ISSCh 35	4	7	9	13	38	39
ISSCh 5	0	0	0	1	3	5
Kaolinite	7	7	8	8	-	-
KI R1	3	3	4	3	5	5
Chlorite	3	3	1	1	-	-
Smectite	-	-	-	-	2	2

proportions (Appendix A.4, Figure A.2) exhibit several interesting features. The phase proportions in <2 μm subfractions show considerable, but not systematic, variation over the time period. In particular the 2-0.2 μm subfraction of 1980 which contains almost 50% less discrete illite than the other 2-0.2 μm subfractions obtained between 1957 and 2014. The decrease is compensated for with an increase in ISSCh 35 and ISSCh 50 relative to other 2-0.2 μm subfractions. The 1904 2-0.2 μm subfraction also has a lower amount of discrete illite and an elevated amount of ISSCh 35. Interestingly, when comparing the phase proportions obtained for <0.05 and 0.2-0.05 μm subfractions the 1980 samples also show slight variations in phase proportions relative to its position in the sample series although these effects are subtle. The amounts of discrete chlorite, kaolinite and KI phases do not show any significant changes within 2-0.2 μm subfractions (supplementary data). While 0.2-0.05 μm subfractions demonstrate a decrease in discrete illite content between 1957 and 2014, this change is very small and accompanied by a concurrent increase in the proportion of the ISSCh 90 fraction and the contribution of both phases seems to be stable over the study period. The tendency for the <0.05 μm subfraction is for a decrease in the proportion of ISSCh 90 and increasing proportions of ISSCh 50 and ISSCh 35, but again this effect is very subtle. The results of modelling on the proportions of the various phases also confirms the qualitative assessment of decreasing expandable mixed-layers with increasing size and discrete illite dominating the 2-0.2 μm subfractions. This is coupled with an increase in the CSD sizes of the different phases with increasing size.

3.4 Discussion

Validity of the proposed structural model

A satisfactory replication of experimental XRD data was achieved, save for areas between 8-10 and 24-26 °2Θ in AD conditions for <0.05 μm subfractions, and between 24-26 °2Θ for the same subfractions under EG treatment (quality of fit based on visual assessment, R_p values, and agreement between AD and EG states). Additionally, the model was able to produce a similar quality of fit for all the subfractions modelled (Appendix A.5, Figures A.3 to A.24). Full-profile modelling of experimental data from different <2 μm subfractions allowed to obtain compositional information on mixed-layers present in the sample. This highlighted a complex mineral assemblage with the coexistence of mixed-layers with similar composition. The presence of such similar phases rather than those suggested by the peak decomposition method is validated by the use of the multi-specimen method. Fitting the structural model to XRD data obtained from different treatments (Ca-AD/EG) is necessary to assess the sensitivity of the model to the presence and composition of mixed-layers. Qualitative interpretation of XRD data in unable to obtain this information, as qualitative assessment is limited to the identification of well-defined reflections which tend to be from discrete and/or well-crystallised clay mineral phases and <0.05 μm contributions are completely overlooked. As these results show, the <0.05 μm subfraction is dominated by mixed-layers with small CSD sizes which are not detected by analysis based on <2 μm fractions due to their broad, diffuse reflections although they account for 35-45% of the <2 μm sample mass. The comparison not only of AD and EG data, but also with K-150 treatment provides additional information on the presence of chloritic layers. Thus in general, the fitting of XRD data obtained by sequential fractionation allows to conclusively identify the presence of mixed-layers and to place constraints on their composition, information that is unobtainable when considering the complete <2 μm fraction.

The sensitivity of the model to the presence and composition of mixed-layers was also assessed (Figure 3.7). In particular, the necessity of both ISSCh 35 and 50 can be assessed by substitution with a phase of intermediate composition and CSD size between the two used in the best-fit model of the <0.05 μm subfraction. This substitution increases the misfit in the 8-10 °2Θ range and does not allow to replicate the breadth of the 001 reflection. Misfit in the region of 24-26 °2Θ is also increased (Figure 3.7a,b). Similarly, when chlorite layers are replaced by smectite ones in ISSCh 80, not only is the fit of the

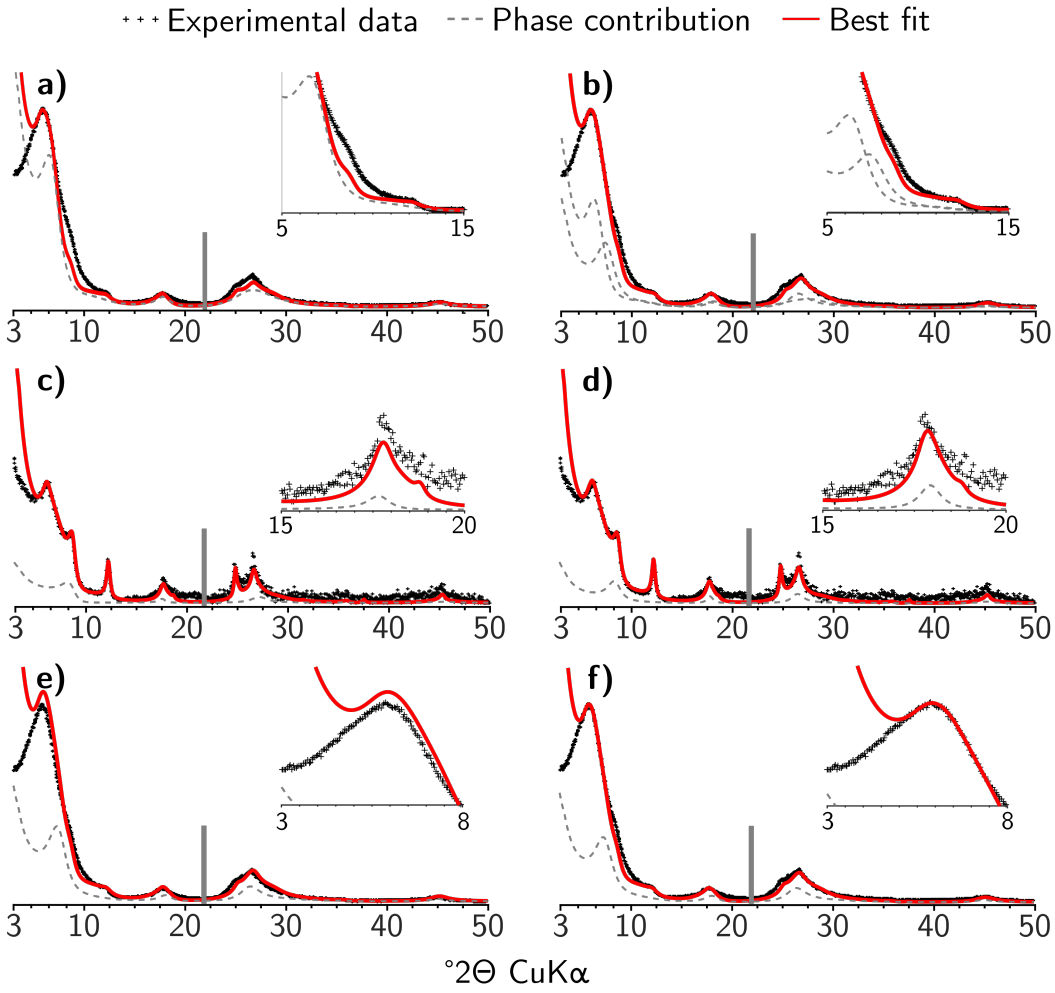

Figure 3.7: Sensitivity of calculated XRD patterns to the mineralogical composition. Experimental (sample 2014) and calculated XRD patterns are shown as solid black and red lines, respectively. Optimal fits are shown in the right-hand-side column. Calculated patterns in the left-hand-side column illustrate a) the effect on the 001 reflection of replacing the ISSC 30 and ISSC 50 phases with one of intermediate nature proportion; c) the impact of the chlorite layers in the ISSC 80 contribution; and e) the effect of variation in octahedral occupancy in the brucite sheet in the chlorite layers in ISSCh 50. Zoomed regions highlight areas with significant misfit compared to the best-fit.

illite 001 reflection degraded in AD conditions, but the 15-20 °2Θ reflection is affected by broadening and positional shift to lower angles compared to the best fit (Figure 3.7c). The presence of chlorite layers is necessary to shift the latter reflection toward higher angles and better reproduce the profile of this diffraction maximum (Figure 3.7c,d). Furthermore, the model is sensitive to the interlayer occupancy of brucite sheets in chlorite layers, as when this occupancy of chlorite layers in ISSCh 50 was decreased to 4.9 from 5.4

(a variation of 10% change), misfit in the intensity of the 001 maxima is observed, in addition to slight increase of misfit in the 7-10 Å region (Figure 3.7e,f). In the present case, comparison of XRD data obtained not only for Ca-AD and Ca-EG treatments, but also for K-150 treatment provides additional information on the presence of chlorite layers in complex ISSCh.

Comparison with previous assessment of the mineralogy of the Morrow Plots

Clay mineralogy of the Morrow Plots was previously characterised by Velde and Peck (2002) to investigate the influence of cultivation on the weathering of soil clay minerals. The study, performed using the peak decomposition method, proposed a structural model based on comparisons of AD and EG samples. To replicate AD data the authors used four different mineral phases: two R0 mixed-layer illite-smectite, one rich in smectite (smectite-IS, $W_a < 50$) and the other rich in illite (illite-IS, $W_a = 60$), and two phases considered as well- and poorly-crystallised mica/illite. The authors were not able to reproduce experimental data in the EG state using the same phases, as the description of the 001 reflection was reduced to a single IS contribution. In the present study, the full-profile technique resolved the 001 reflection into the contributions from different ISSCh mixed-layers, and permitted refinement of the composition of independent phases to include chlorite layers which were not present in the previous model. The full-profile method was also able to progress beyond the description of well- and poorly-crystallised illite to identify illite-dominated mixed-layers with the presence of few chlorite or smectite layers (ISSCh 80 and 90). Furthermore, the full-profile model was also able to quantify the contributions of kaolinite and KI required by the subtle intensity variation of higher-angle maxima. Whilst the general observation of a clay mineralogy with abundant 2:1 layers was consistent between the two techniques, it is clear that the full-profile fitting, multi-specimen methodology provides a more comprehensive and complete picture of the nature of the soil clay mineral assemblage, and in particular on the nature of the mixed-layers. Added complexity comes from the incorporation of XRD data of K-150 samples.

Evolution of clay mineralogy over time

Despite the small size of the subplots ($\sim$50m^2), there is considerable variation in the proportions of different mineral phases between each year. Furthermore, the granulometric

results for 1904 samples show significantly different proportions of 2 mm-50 μm fraction in addition to the altered proportions of <2 μm subfractions. This trend is highlighted when all subplots are considered, not solely RU samples (data not shown here). This suggests that the sample was subject to grinding before being received, thus the following discussion concerns primarily those samples from 1957-2014.

The proportion of the total <2 μm fraction remained stable over time, as levels were 31% in 1957 and 2013, with slight variations in other years, i.e. 29% in 1980 and 2014, but up to 37% in 1997. These values are slightly elevated in comparison to those reported by Odell et al. (1984), who reported <2 μm proportions of 24.5 and 26.5%, however these values are taken from subplots subject to different crop rotations or fertilisation regimes within the Morrow Plots experiment than the subplot included in the current study. The more comprehensive dispersion and extraction methodology used in the present study may also account for the better recovery reported here. Given this stability with time and consistency with previous studies, preferential leaching of clay phases has not occurred to a significant extent at the Morrow Plots over time despite the presence of drainage tiles between plots.

The results of XRD profile modelling reveal that there has been no significant augmentation in the quantity of chloritic or hydroxy-interlayer minerals over time, although acidification of the rhizosphere has been linked to the formation of such phases (Turpault et al., 2008; Ranger et al., 1991; Robert et al., 1987; Righi, 1993). However DeTurk (1939) quoted a pH of surface soils in unfertilised subplots of 5.0, while more recently Aref and Wander (1998) found an average pH value of 5.5 for RU subplots averaged over the experimental phase 1969-1995 which indicate the pH has remained stable, or even slightly increasing over time. Additionally, a pH of 5.5 is slightly elevated when compared to the pH 2-5 range which is frequently reported as typical for aluminisation of clay minerals (Robert et al., 1987), which may account for the absence of such effects here. Despite 60 years of continued cropping, no specific plant-related effects such as the transformation of illite-like layers due to plant uptake of potassium were observed in the clay subfractions even after sustained cropping (Dissing-Nielsen and Möberg, 1984; Tributh et al., 1987; Hinsinger et al., 1993; Hinsinger and Jaillard, 1993; Barré et al., 2008a). This is similar to the qualitative analysis of Singh and Goulding (1997) of XRD data for samples from the Rothamsted field experiment in the UK. It is also consistent with the results of Velde and Peck (2002) for RU samples from the Morrow Plots. Whilst

variations in peak position and profile in XRD data for the current study were observed, these variations were not reproduced as differences in mineral composition following quantitative modelling using the full-profile method. This suggests that the influence of the corn-oats-hay crop rotation as a pedogenetic factor is not important over the period studied for the mineral assemblage identified using full-profile XRD modelling.

Table 3.4: Measured vs. calculated CEC values for 2014 <2 μm fraction. Values are calculated from the measured CEC of the subfraction multiplied by the percent mass of the subfraction.

Sample	Subfraction	CEC (meas., ceq_c/kg^{-1})	Mass % subfraction	CEC (calc., ceq_c/kg^{-1})
2014 RU	<2 μm	55.2	-	57.8
	2-0.2 μm	22.13	30.7	-
	0.2-0.05 μm	58.6	25.6	-
	<0.05 μm	82.2	43.8	-

Cultivation effects on soil composition

Despite no significant mineralogical variation being observed in the samples presented here, the CEC of the <2 μm fractions increased from 1957 to 2014. This change occurred in conjunction with a slight decrease in the C/N ratio, however this can account for only a small part of the observed change in CEC. Therefore, it appears this augmentation is consistent with the observed increase in the proportion of the <0.05 μm subfraction from 31% of the total <2 μm fraction in 1957 to 42% for 2013-2014. This is also consistent with the CEC calculated from the basis of the CEC and the mass percent of the three subfractions which produces a value of 58 ceq_c/kg^{-1} in place of the 55 ceq_c/kg^{-1} which was measured for the total <2 μm fraction for the 2014 sample (**??**). There are only small differences in composition between the phases present in the <0.05 μm and the two coarser subfractions which indicates that this redistribution is taking place by congruent dissolution processes rather than alteration or transformation of the phases present in 2-0.2 and 0.2-0.05 μm subfractions. Given that the RU subplots receive no external fertiliser inputs, they are reliant on minerals to meet their nutritional needs and as such dissolution may be favoured not only by the uptake of potassium, but of silicon and other mineral nutrients (Fe, Mg, Mn) by crops (Boyle and Voigt, 1973; Marschner, 1995; Hinsinger, 1998; Meunier, 2003). While not considered an essential nutrient for plants, improved bioavailability of silicon has been linked to improved yields in some soils, and cereal crops can accumulate up to several percent of silicon in their tissues which is in favour of a dissolution mech-

anism (Lewin and Reimann, 1969; Lanning et al., 1980; Epstein, 1999; Blecker et al., 2006).

3.5 Conclusion

The present study successfully used quantitative phase analysis of XRD profiles of samples from non-fertilised corn-oats-hay rotation subplots of the Morrow Plots experimental fields. Rietveld refinement of silt fractions confirmed that the mineralogy of this fraction was stable over the duration of the study. Full-profile fitting of <2 μm subfractions identified up to eleven different phases which make up the clay mineral assemblage of the Aquic Argiudoll soil of the Morrow Plots. These phases included discrete illite, kaolinite, chlorite, smectite, a partially segregated kaolinite-illite phase, and five mixed-layer illite-smectite-chlorite phases of which three were illite-rich and the remainder smectite-rich. The use of the multi-specimen approach and comparison of Ca-AD, Ca-EG and K-150 samples provided additional compositional constraint by identifying the presence of chlorite layers. As a result, chlorite layers were included in the ISSCh mixed-layers. The mineral assemblage identified through full-profile fitting is significantly increased in complexity in both the number and the nature of the clay phases than the previous assessment of the clay mineralogy performed by Velde and Peck (2002) using peak decomposition methods. This detailed information obtained proves the value of the full-profile fitting methodology when evaluating the clay mineralogy of soil samples.

This mineralogical characterisation allowed the investigation of the evolution of the individual phases in the different subfractions. In particular, this showed that this mineral assemblage was not significantly affected by plant growth and potassium uptake for the period 1904-2014, as there were no significant signs of mineral formation or transformation, such as increases in the proportion of chlorite nature which have been previously noted in a number of different soil environments (Bain and Griffen, 2002; Bortoluzzi et al., 2008; Calvaruso et al., 2009; Collignon et al., 2012; Viennet et al., 2015). The mineralogy of phases remained consistent between different <2 μm subfractions, where only small variations in layer-composition were noted, and also remained unchanged over time. The granulometric variation observed, of an increase in the proportion of <0.05 μm subfraction at the expense of 2-0.2 and 0.2-0.05 μm subfractions, was accompanied by an increase in the cation exchange capacity. These changes are attributed to preferential dissolution of the coarser clay fractions to provide plant nutrients, while the <0.05 μm fraction was

perhaps protected by association with soil organic matter. Further data on C levels in subfractions is required to confirm this hypthesis. This dissolution takes place without significant modification of the clay mineralogy related to potassium extraction from the clay mineral structure. The results indicate that overall the mineralogy of the Plots displays remarkable stability with time, and may provide insight into the behaviour of other temperate agricultural soil clay mineral assemblages.

II

Mineralogical impacts of different agronomic practices in subplots of the Morrow Plots

Mineralogical differences in a temperate cultivated soil arising from different agronomic practices and plant potassium uptake

4.1 Introduction

Together with nitrogen and phosphorus, potassium,is an essential plant nutrient, with roles in photosynthesis, water regulation and disease resistance of plants (Marschner, 1995; Mengel et al., 2001). In soil potassium is bound in different forms, with 95-99% of potassium being contained in the crystal structure of potassium-feldspars and micas such as muscovite and biotite (Sparks, 1987). Under natural conditions, release of this structural potassium is strongly dependent on the nature of the soil parent material and the rate of climate-induced weathering (Mengel et al., 2001; Velde and Barré, 2009). Remaining potassium is found in the pools of non-exchangeable (1-5%), exchangeable potassium (1-2%) and in the soil solution (0.1-0.2%) (Sparks, 1987). Whilst exchangeable and solution potassium are freely available for plant uptake, release of non-exchangeable potassium which is fixed in the interlayer spaces of 2:1 clay minerals requires depletion of exchangeable and solution potassium and can lead to measurable changes in clay mineral structure (Walker, 1950; Mortland et al., 1956; Tributh et al., 1987; Marschner, 1995; Hinsinger, 1998). The extent of this release depends strongly on the nature and size of the mineral species, and requires an extremely low concentration of potassium in the soil solution which are seldom encountered in cultivated soils (Reitemeier, 1951; Mortland, 1958; Arnold and Close, 1961; Reed and Scott, 1962; Scott and Reed, 1962b; Scott and Smith, 1966; Hinsinger, 1998).

Nevertheless, the ability of plants to extract non-exchangeable potassium has been observed, and rapid changes have been noted in the rhizosphere of plant roots in laboratory experiments, such as the vermiculitisation of micaceous minerals following plant growth on clay substrate (Hinsinger et al., 1992, 1993; Niebes et al., 1993; Barré et al., 2007a, 2008a). Conversely, Adamo et al. (2016) reported illitisation in the rhizosphere of maize compared to bulk soil after 40 days growth on fertilised and unfertilised soil samples, but illitisation was no longer present after 130 days. Similar illitisation in the rhizosphere has been reported elsewhere (Turpault et al., 2008; Calvaruso et al., 2009; Mouas-Bourbia et al., 2015). The extent of such extraction by plants is strongly dependent on species type, proximity to plant roots and soil solution chemistry, and on the nature of the clay mineral assemblage (Scott and Reed, 1962a; Boyle and Voigt, 1973; Schenk and Barber, 1980; Kraffczyk et al., 1984; Barber and Mackay, 1986; Marschner, 1995; Rengel and Damon, 2008). Further studies have shown other plant-related effects occurring over weeks or seasons, such as the aluminisation or dealuminisation of interlayer spaces of 2:1 clay minerals in a range of soils under acidic conditions, showing plant induced mineralogical changes are not limited to potassium extraction (Hatton et al., 1987; Ranger et al., 1991; Bain and Griffen, 2002; Bortoluzzi et al., 2008; Turpault et al., 2008; Calvaruso et al., 2009; Viennet et al., 2015). Seasonal variations are likely related to the effects of short-term fluctuations in temperature and soil moisture, and possibly on modification of these following parameters by the plant itself during its growth, which affect soil solution chemistry, pH, microbial metabolism, and potassium fixation/release equilibria, among other factors (Foth, 1991; Khan, 1991; Marschner, 1995; Mengel et al., 2001; Peoples et al., 2014).

Long term field experiments which were established in the 19^{th} and 20^{th} centuries offer a unique chance to investigate the effect of continuous plant growth on the evolution of clay minerals in the soils as a consequence of nutrient uptake. In studies of soils from the Broadbalk continuous wheat plot at Rothamsted Experimental Station in the UK (est. 1843), Singh and Goulding (1997) found an increase in average potassium content over the period from 1856 to 1987 of 1.01% to 1.20% and 1.10% in soils with and without potassium fertiliser application respectively. However they did not observe any changes in XRD data. Conversely, several authors have reported decreases in illite content and the formation of smectite and/or vermiculite in the clay minerals of other continuous agricultural field experiments of differing durations (30-135 years) (Möberg and Dissing-Nielsen, 1983; Dissing-Nielsen and Möberg, 1984; Tributh et al., 1987). However, these studies have been limited in their analysis of clay mineralogical changes to qualitative

assessment of XRD data, which is limited to a description of sharp, well-defined peaks which typically correspond to discrete minerals and as such qualitative descriptions cannot accurately identify the composition of mixed-layers. More recent studies have involved the use of the peak decomposition method and NEWMOD to interpret XRD profiles, whereby part of the XRD profile is decomposed into pseudo-Voigt functions to attempt to identify contributions from discrete and mixed-layers, and compositions of the mixed-layers are proposed (Reynolds Jr., 1985; Lanson, 1997). Several studies of this nature on soil clay minerals have linked changes in potassium content or potassium fertilisation to shifts in the position of diffraction maxima and the composition of mixed layers phases (Pernes-Debuyser et al., 2003; Barré et al., 2008a,b). Velde and Peck (2002) studied soils from the Morrow Plots using XRD peak decomposition and identified the presence of two illite-smectite mixed-layers in addition to well- and poorly-crystallised illite. From the increase in the proportion of smectite layers in the mixed-layer of the younger sample they inferred that significant mineralogical transformation had occurred in the soil of unfertilised plots under continuous corn culture between 1913 and 1996.

Nevertheless, despite improving the description of clay mineral phases to include mixed-layer composition, the peak decomposition method does not fit the full XRD profile and as such the information obtained cannot be interpreted in a quantitative manner. Peak-decomposition also does not take into account the influence of highly-disordered and mixed-layers with very small CSD sizes as broad diffuse reflections are routinely stripped as 'background'. Recently, a full-profile fitting method and multi-specimen technique has been used to characterise the clay mineral assemblages of a range of hydrothermal and diagenetic sequences (Drits et al., 1997b; Sakharov et al., 1999b,a; Lindgreen et al., 2000; McCarty et al., 2004; Inoue et al., 2005; Aplin et al., 2006). This approach has been adapted to soil samples and provides the opportunity to investigate the soil in a quantitative manner (Hubert et al., 2009, 2012; Viennet et al., 2015). This is particularly important in light of expected increases in fertilisation and competition for arable land resources, and the interest in CO_2 sequestration in cultivated soils (DeFries et al., 2010; Lambin and Meyfroidt, 2011; Mueller et al., 2012). It is evident that clearer description of soil clay mineral assemblages in agricultural soils is needed given the conflicting nature of results from studies based on qualitative analyses of XRD data which means the responses of soils to land-use changes or fertiliser inputs are not well understood. The aim of this study was to use full-profile XRD modelling to obtain a comprehensive compositional description the clay minerals of the Morrow Plots experimental fields and to compare

and contrast, quantitatively, the effects of 110 years of continuous plant-growth under different agronomic treatments on the status and potassium content of clay minerals in the soil.

4.2 Materials and methods

Sample collection, particle size distribution, chemical analyses and analysis of XRD patterns were performed as described in Chapter 2. The results described and discussed in the following sections were collected from CF, CU, RF and RU subplots.

4.3 Results

Particle size analysis

Results of size-fractionation, averaged over all subplots for a given year and normalised to 100%, are presented in Figure 4.1a. Recovery was 94.9% of the starting weight on average for all samples. For the years 1957 to 2014, the 2000-50 μm fraction represents 7% ($\pm$ 2%), the 50-2 μm fraction 64% and the <2 μm fraction 29%. However for 1904 samples these values are 4, 62, and 33 % respectively. Overall, no variation was observed between subplots for 2000-50, 50-2 and <2 μm fractions as a result of the different crop rotations or fertilisation treatments. The proportions of the 2-0.2, 0.2-0.05 and <0.05 μm subfractions are also significantly different from 1904 compared to other years, suggesting light grinding of the sample before it was stored. When looking at the average for all subplots in a given year for <2 μm subfractions (Figure 4.1b-d), there is a tendency for the <0.05 μm subfraction to increase from $\sim$9% of total sample mass in 1957 to close to $\sim$13% in 2013-2014 (Figure 4.1d). At the same time the mass of 0.2-0.05 μm subfraction decreases by 2 % and 2-0.2 μm subfractions decrease very slightly (1-2 mass %) (Figure 4.1b,c). There is considerable variation in granulometric results between subplots in a given year, and also significant variation when considering a single subplot in different years (Appendix A.3). As a result of this variation, plots were assessed on the basis of the treatment received. Conversely slight differences can be observed between the proportions of 2-0.2 μm subfractions of C and R subplots, where C subplots contain systematically slightly less mass than the corresponding R subplots (Figure 4.1b). The inverse is observed for <0.05 μm subfractions of C and R subplots, where C tends to

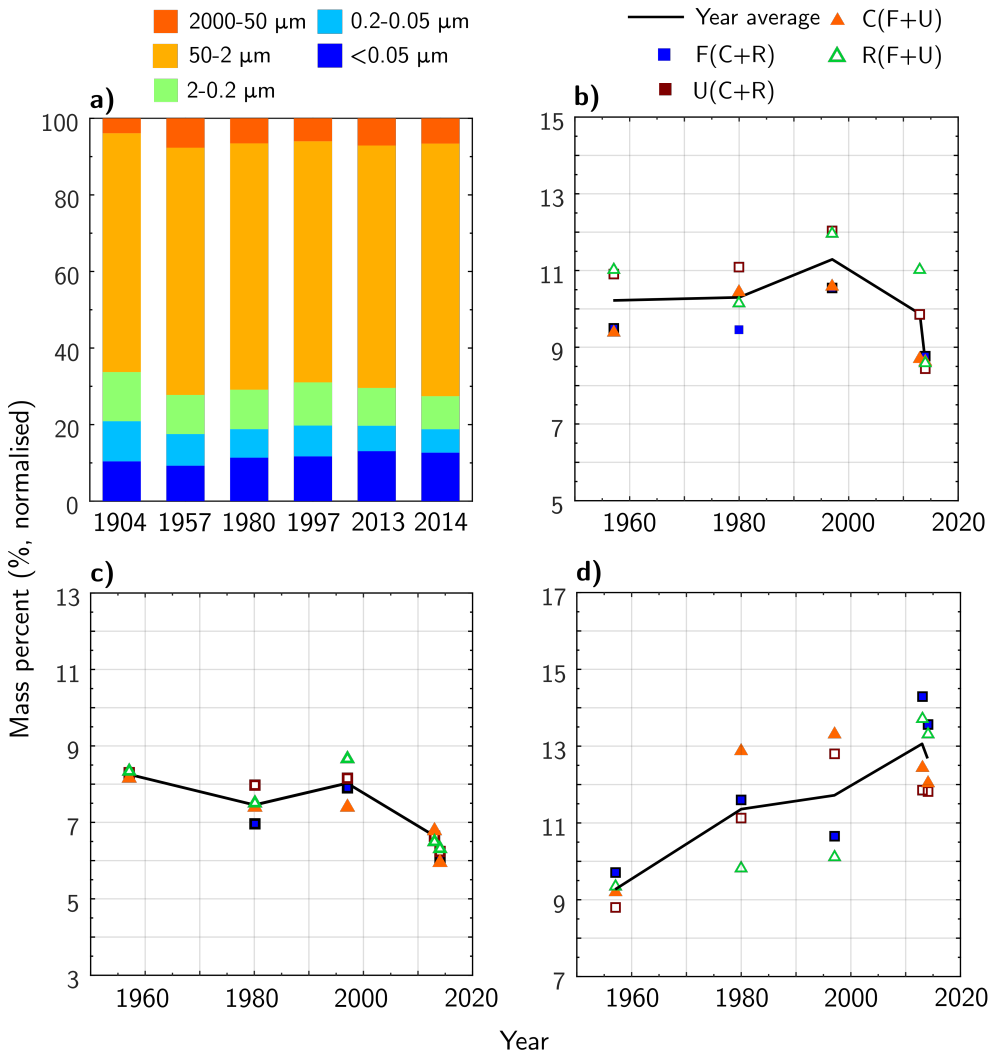

Figure 4.1: Results of sequential fractions for a) yearly averages over all subplots; and differences between C, F, R or U treatments highlighted for b) 2-0.2, c) 0.2-0.05 and d) <0.05 μm subfractions. Solid black lines represent the yearly average, while closed triangles and squares are C and F treatments respectively, open triangles R subplots and open squares U subplots.

have greater <0.05 μm mass than respective R subplots. However these differences are statistically insignificant over the period studied as they fall within one standard deviation.

Chemical analyses

The CEC measured in 1904 is essentially similar between the CU and RU subplots, and remains constant between 1904 and 1957. From 1957 the CEC of both subplots increased

Table 4.1: CEC and elemental composition of selected subplots of the Morrow Plots soil samples. The low value of Ca is due to Na-saturation of samples prior to analysis.

Sample	Fraction	CEC	C	N	C/N	K_2O	Na_2O	MgO	CaO
		ceq_c/kg^{-1}	%				%		
1904 CU	<2	47.8	6.29	0.66	9.53	2.11	0.21	1.82	0.07
1904 RU	<2	45.5	6.47	0.58	11.25	2.15	0.25	1.78	0.08
1957 CF	<2	47.9	4.41	0.49	9.09	2.13	0.17	1.97	0.06
1957 RU	<2	47.9	6.18	0.57	10.93	2.18	0.22	1.78	0.07
2014 CF	<2	55.3	4.24	0.49	8.73	1.98	0.17	2.01	-
	2-0.2	14.0							
	0.2-0.05	51.3							
	<0.05	81.2							
2014 RU	<2	55.2	5.79	0.60	9.65	1.83	0.15	1.91	-
	2-0.2	22.1							
	0.2-0.05	58.6							
	<0.05	82.2							

significantly from 48 to 55 ceq_c/kg^{-1} in 2014, an increase of 15%. CEC increases with decreasing size for <2 μm subfractions measured in 2014, and <0.05 subfractions CF and RU subplots are fairly similar at 81/82 ceq_c/kg^{-1} respectively, 0.2-0.05 and 2-0.2 μm subfractions show RU subplots have a CEC $\sim$8 ceq_c/kg^{-1} greater the CF subplots. The elemental analyses are consistent with a soil dominated by phyllosilicate minerals, with high levels of SiO_2 (43-46%) and Al_2O_3 (17-19%). potassium levels were similar in both subplots in 1904, and did not vary between 1904 and 1957. Levels are similar to those reported for clay fractions from a variety of soils (Doll et al., 1965; Singh and Goulding, 1997). Whilst potassium decreased in both RU and CF subplots since 1957, the rate of decrease of RU subplots is faster than that of CF subplots. In 1904, the C/N ratio of the RU subplot (11.25) was greater than the CF subplot (9.53), and the value for both subplots has decreased since in line with loss of carbon. The rate of decrease in carbon has slowed in CF subplots since the measurement in 1957 and the introduction of fertilisation, whilst carbon levels continue to decrease at a similar rate post-1957 in unfertilised RU subplots.

XRD qualitative analysis and XRD profile simulation

Random powder XRD of 50-2 μm fractions and subsequent modelling found the 50-2 μm fraction is dominated by quartz (65-70%) and feldspars (albite 10-13% and microcline 10-12%) (Figure 4.2, Appendix A.4). Mica, kaolinite and chlorite also contribute in small amount to this fraction ($\sim$5, 1 and 1.5% respectively), and trace amounts of calcite, anatase, and amphibole were also identified (<1% contribution each). There is no systematic variation in mineralogy of 50-2 μm fractions from subplot to subplot or from year-to-year, with the exception of those of 1904 which had less mica and chlorite, presumably in relation to grinding of the sample.

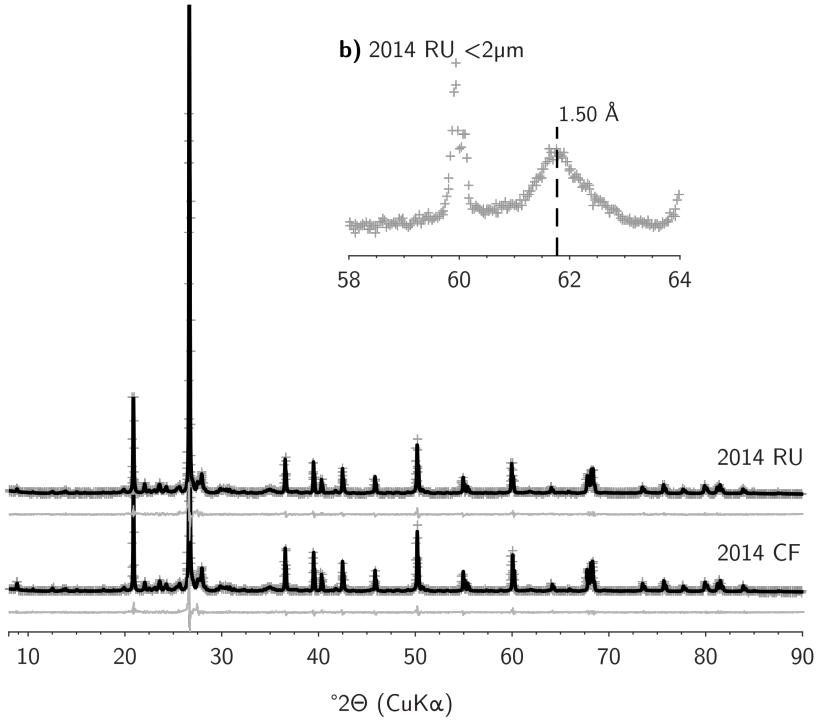

Figure 4.2: Examples of Rietveld refinement fit for 2014 CF and RU subplots. Experimental data is represented by grey crosses, while solid black lines indicate the calculated intensity. Difference plots are solid grey lines underneath. Inset b) shows the position of the 060 reflection for the random powder <2 μm fraction.

Full-profile fitting of 2-0.2, 0.2-0.05 and <0.05 μm subfractions for CF, CU, RF and RU subplots from 1904, 1957, 1980, 1997, 2013 and 2014 was carried out following the structural model presented in Section 2.3.6. Examples of the fit for 2014 CF and RU samples are shown in Section 4.3.3 (all samples Appendix A.5). Experimental XRD traces showed little variation in either peak position or intensity between the same subfraction

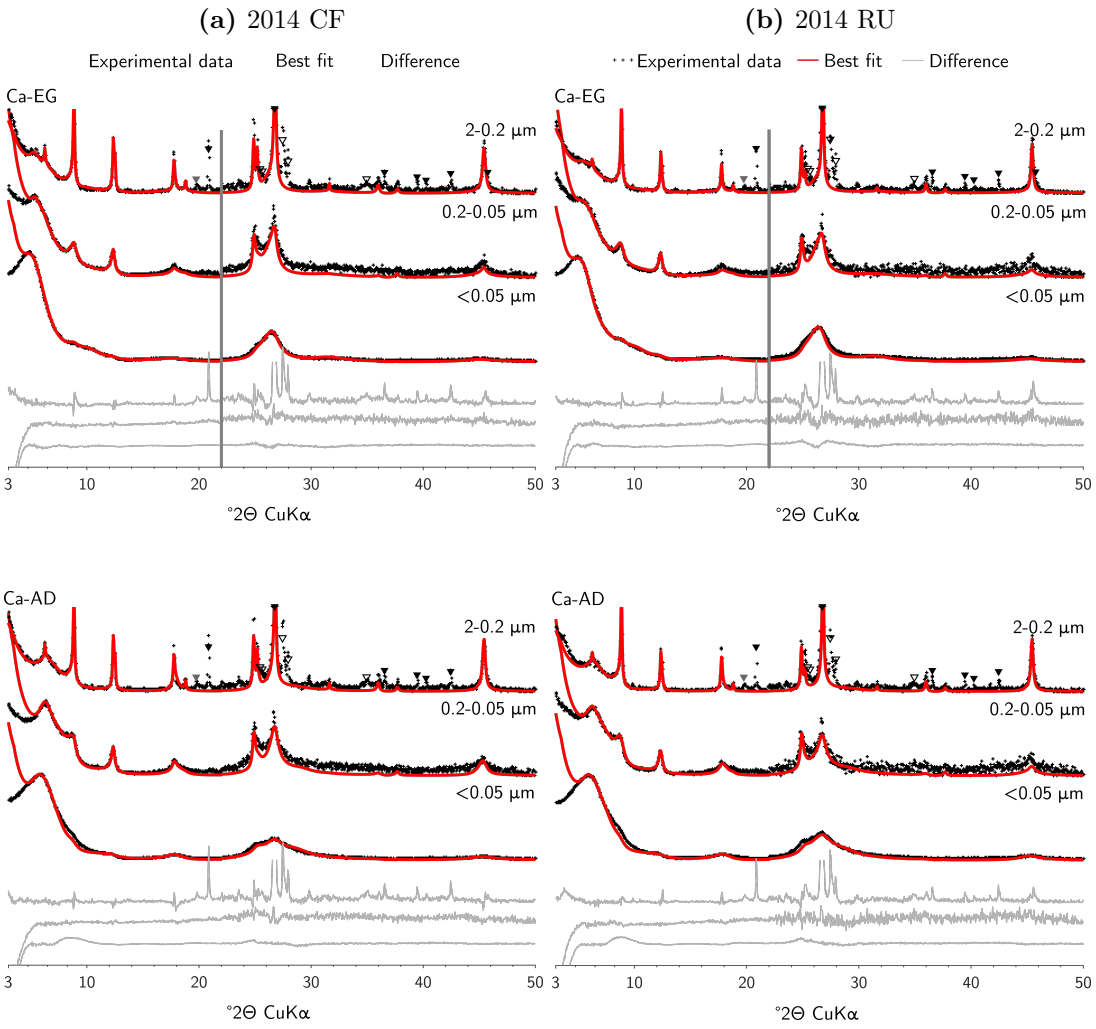

Figure 4.3: Examples of full-profile fitting in both AD and EG conditions for a) 2014 RU and b) 2014 CF subplots, for 2-0.2, 0.2-0.05 and <0.05 μm subfractions. Solid black lines represent the fitted profile, grey crosses experimental data, and grey lines at the bottom plot the difference between calculated and measured data. Quartz, feldspar, and *hk* contributions are marked by solid black, open and solid grey triangles respectively, and were not taken into account during the modelling procedure. Quartz intensity has been cut at 26.6 for clarity. Solid grey bars at 22 °2Θ indicate modification of intensity by a factor of two for the higher angle region to the right.

from different subplots or year, and results of the full-profile fitting reflect this, as very little mineralogical difference was noted. The model used required up to eleven different phases to describe the three <2 μm subfractions. It inlcuded discrete illite, kaolinite, chlorite and smectite, and a KI R1 phase. Six mixed-layers were included, five with the layer-composition illite-smectite-smectite-chlorite (ISSCh), and one illite-chlorite (ICh). Mixed-layers are denoted by the proportion of illite layers, W_a, and as such include: ISSCh

90, ISSCh 80, ISSCh 50, ISSCh 35, ISSCh 5, and ICh 6. Phase composition varies only slightly between different subfractions, e.g. for 2014 CF subplot ISSCh 50 has the layer composition 52/19/7/22 (CSD 7) in <0.05 μm subfraction which changes only slightly to 45/7/13/25 in 2-0.2 μm fractions (EG treatment) (full structural details Appendix A.4). This is typical of the evolution in content of layer-type composition between <0.05 and 2-0.2 μm subfractions for all subplots and phases. ISSCh tended to include some smectite layers with zero planes of water in the Ca-AD state (S0), and the content of these layers tended to decrease for 2-0.2 μm subfractions compared to finer fractions whilst illite-like layers decreased for ISSCh 50, 35 and 0 but increased in ISSCh 90 and 80. This variation is not greater than the sensitivity of the technique (Hubert et al., 2009), as it accounts for <5 % of layers within each mixed-layer. Furthermore, the composition of ISSCh 50 for 1904 CU and 1957 CF <0.05 μm subfractions is 55/14/9/22 (CSD 9) and 52/17/9/22 (CSD 7) respectively, which is again a very slight compositional difference when compared with the same phase in 2014 CF <0.05 μm subfractions which implies little mineralogical variation with time. Further, when comparing between different subplots, in the same year compositional differences are again small, in the range of 1-5 layers, indicating the impact of different agronomic treatments is limited.

When looking at the data on the basis of the total number of layers of a given nature (illite/smectite/chlorite/kaolinite), calculated from the proportion of the layer-type within a ML phase ($W_{a/b/c/d}$) multiplied by the amount of the contribution (%) in the subfraction, certain trends appear. The proportion of illite, smectite and chlorite layers in <0.05 μm subfractions all increase from 1957 to 2014, while the amount of kaolinite is stable (Figure 4.4a). There is a concurrent decrease in the number of illite, smectite and chlorite layers in 0.2-0.05 μm subfractions with time, while kaolinite layers in this fraction is stable (Figure 4.4b). The proportion of illite layers in 2-0.2 μm subfractions varies considerably, making it difficult to discern a clear trend, however the proportion of illite layers would appear to be stable or marginally decreasing with time, whilst smectite layers also show a marginal decrease and chlorite and kaolinite layers are stable. Nonetheless these apparent trends in 2-0.2 μm subfractions are very subtle given the time period studied (60 years) and not statistically significant. Figure 4.4d shows the changes in layer proportions for the complete <2 μm fraction, where despite some annual variation the overall composition of the Morrow Plots has not changed during 60 years.

A more detailed analysis of the impact of the different treatments provides further

information. In <0.05 μm subfractions C subplots have systematically more illite layers than R subplots, whilst in 2-0.2 and 0.2-0.05 μm subfractions C subplots have systematically fewer illite layers when compared to R subplots. Furthermore, <0.05 subfractions also have more smectite and chlorite layers than the R subplots, while no such difference is evident in the coarser clay fractions. Differences between F and U subplots are not systematic, save for the proportion of illite layers in 2-0.2 μm subfractions where F subplots contain consistently fewer illite layers than U subplots. However, it is important to note that the scale of these trends is very small and not statistically significant for time period and the mineral assemblage investigated.

4.4 Discussion

Variability of results

The granulometric results show significant variability between subplots in a given year. In addition, this variation is not consistent on a year-to-year-basis. This implies that there is considerable heterogeneity in the Morrow Plots despite their small size, and there are no detectable systematic impacts of either crop rotation or fertilisation treatment. Variation between sampling dates must be taken into consideration, as the exact timing of sampling post-harvest for historic samples is not certain. Planting dates in the plots have also varied by as much as 147 days during the Morrow Plots experiment, regardless of species, which suggests that harvest and therefore sampling is also subject to this variation (Aref and Wander, 1998). Given that numerous studies have related changes in soil properties over periods as short as two weeks, this may play a role in the observed variability, although analysis for potassium in particular showed no residual change over a period of four years on plots both with and without fertilisation history (Weaver and Forcella, 1979; Haines and Cleveland, 1981; Khan, 1991; Marschner, 1995; Mengel et al., 2001; Turpault et al., 2008; Collignon et al., 2012; Peoples et al., 2014). Furthermore, analysis of yield and climate data of the Morrow Plots from 1888 to 1996 carried out by Aref and Wander (1998) revealed that yield was positively correlated not only with the temperature and precipitation of the preceding November and December, and of the preceding year, indicating that climatic fluctuations can have relatively long-lasting impacts which may explain a portion of the difference between 2013 and 2014 despite their small separation in time. Climatic variation also affects the distribution of plant roots in soils, and therefore the location of nutrient uptake (Marschner, 1995; Mengel et al., 2001), and this variation on a year-to-year basis may be significant, due to the

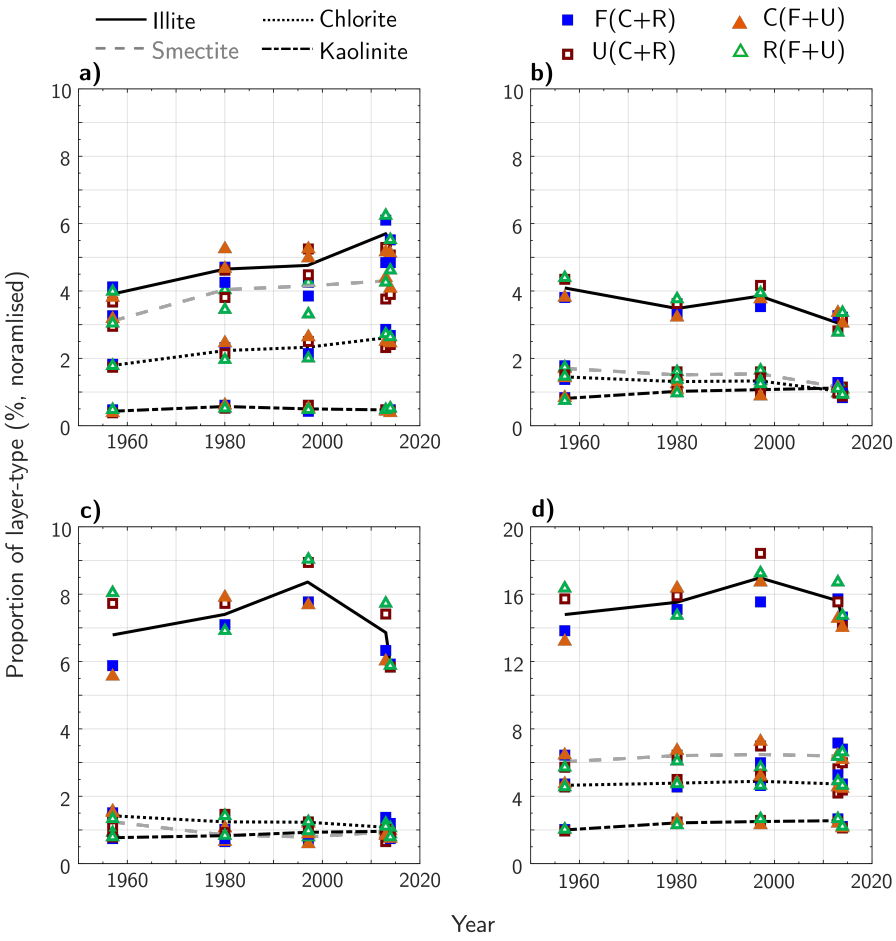

Figure 4.4: Proportion of illitic, smectitic, chloritic and kaolinite layers in each of a) <0.05, b) 0.2-0.05, c) 2-0.2, and d) <2 μm subfractions. Yearly averages are represented by lines, while solid squares represent F subplots, outlined squares U subplots, solid triangles C subplots, and outlined triangles R subplots. Smectite has been represented in grey to better highlight difference between illite and smectite treatment contributions. Note the y-axis scale in d) is twice that of the other plots. Note the temporal variation is easy to see, as illite, chlorite and smectite layers increase in a) <0.05 μm subfractions whilst decreasing in b) 0.2-0.05 μm subfractions and to a lesser extent in c) 2-0.2 μm subfractions while d) the overall value for <2 μm fractions is unchanged.

impact of wetting and drying cycles on potassium fixation and release (Khan, 1991; Sparks and Carski, 1985; Sparks, 1987; Hanway and Scott, 1957, 1959). The impact of fertilisation treatments is also a factor to consider. Khan et al. (2014) suggested that KCl fertilisation may have negative effects in some circumstances, and while L-NPK fertilisation increased the average yields in the F subplots, yield stability decreased with greater rates of fertiliser application (Aref and Wander, 1998), reflecting variation in the availability of plant nutrients in the short term which may be linked to temporary

changes in soil structure and mineralogy.

The results of the investigation of RU subplots as presented in Part I is upheld here when considering all different subplots and treatments. Whilst the results are in agreement with (Velde and Peck, 2002) for R subplots, the results for C subplots are in contradiction as the authors found a decrease in illite-nature of clay mineral phases in the C subplots based on analysis of the XRD using peak decomposition methods. However the model proposed by the authors was not consistent in the number of phases used to describe samples in both AD and EG-solvated states. Furthermore, the use of the peak decomposition method, whilst providing more information than qualitative assessment alone, does not take the entire XRD profile into account and this may be responsible for the observed differences. The subtle variations in the shape and position of the 001 reflections in XRD profiles noted by Velde and Peck were also observed for some samples in the current study, however these were not systematic and did not resolve into quantitative differences in mineralogy following full-profile fitting.

Clay mineral evolution

Following more than 150 years of continuous cultivation, mineralogical differences in the Morrow Plots are limited to a statistically insignificant increase of illite and smectite layers in C treatments when compared to R treatments. This may reflect the fact that soil potassium reserves are greater than the plough layers, and a significant portion plant nutrition can be obtained from subsoil (Marschner, 1995; Khan et al., 2014). Furthermore, whilst Adamo et al. (2016) described differences between rhizosphere and bulk soil as a result of corn cultivation after 40 days, they were not persistent longer than a growth cycle (130 days). The similarity between fertilised and non-fertilised treatments may reflect the fact that while fertilised subplots had greater potassium input over the period 1957-2014, they were also planted at a higher density – 20,000 plants ha^{-1} in CU and 30,000 plant ha^{-1} in RU subplots versus 40,000 plants ha^{-1} in CF and RF from 1957 to 1977, followed by 60,000 plants ha^{-1} in CF and RF subplots for 1978-2013 (Odell et al., 1984). This represents a potassium demand of up to twice as much as that of unfertilised subplots. Furthermore, yield increases have been observed in unfertilised subplots following the introduction of hybrid crops in 1967, an indication that there are significant potassium reserves remaining in the soil (Aref and Wander, 1998).

The augmentation of the mass of <0.05 μm subfractions of all subplots regardless of agronomic treatment between 1957 and 2014 is accompanied by an increase of CEC over the same period which is consistent with the CEC of the <2 μm subfractions for

2014 samples (Table 4.1) suggesting the increase is due to the increased proportion of expandable mixed-layers in the <0.05 μm subfraction. Despite the lower C/N ratio of CF subplots, the difference is not sufficient to explain the difference between the CECs of CF and RU subplots. Neither can differences in the CEC of between 2014 CF and RU subplots be explained on the basis of differences in mineralogical composition, as the mineral assemblage in both subplots is essentially identical. This change in particle size distribution is attributed to dissolution of the mineral structure to extract potassium for plant nutrition, as the potassium content of the plots decreases with time. This is in agreement with the negative potassium balances reported by Khan et al. (2014) for the period 1955-2005 for U subplots of the Morrow Plots, however positive potassium balances were calculated for F subplots and a decrease in total potassium is observed here, a seemingly contradictory result. The apparent selectivity for 0.2-0.05 μm subfractions over <0.05 μm subfractions and to a lesser extent 2-0.2 μm subfractions may be explained by minor compositional differences between phases in 2-0.2 and 0.2-0.05 μm subfractions and the protection of <0.05 μm particles by SOM and sesquioxides which are preferentially associated with this fractionm however further study is required to confirm this hypothesis (von Lützow et al., 2006; Barré et al., 2014; Singh et al., 2017).

Mechanism of transformation

Release of potassium from micaceous minerals can occur by potassium exchange or by dissolution. The preference of one mechanism over another is strongly dependent on the concentration of elements in the soil solution, the nature of the mineral and the proximity to plant roots (Arnold and Close, 1961; Scott and Reed, 1962b; Mengel and Rahmatullah, 1994; Marschner, 1995; Mengel et al., 2001). The release of potassium from trioctahedral micas due to plant growth has previously been reported, with Hinsinger et al. (1992, 1993) reporting release of potassium and magnesium in the rhizosphere of rape, accompanied by vermiculitisation of phlogopite, which suggests an exchange mechanism operating to provide potassium nutrition for plants. Similar results were reported by Barré et al. (2007a, 2008b) for potassium release from a natural soil clay assemblages which was reversible on potassium saturation. Naderizadeh et al. (2010) and Norouzi and Khademi (2010) compared the release of potassium from both biotite and phlogopite against that from a muscovite under alfalfa growth and found modifications of XRD data consistent with release of potassium from biotite and phlogopite interlayers whilst no modification was observed in the XRD data of muscovite. These authors also found the potassium content of alfalfa grown on phlogopite and biotite

was correlated to the potassium released from the clay minerals, while the alfalfa grown on muscovite displayed deficiency symptoms and the potassium content was similar to that of a quartz sand control, concluding that release of potassium from muscovite was insignificant and insufficient to meet plant nutritional needs. Vetterlein et al. (2013) found that a natural soil was unaffected by plant uptake following almost 100 days of growth, while under the same conditions modification was detected in the same soil modified with <20 μm particles of a reference illite (IMt–2, Clay Minerals Society Repository).

Further to this, laboratory studies on the release of fixed potassium from interlayer spaces of 50-20 μm mica particles found that the rate of release of potassium is 20 times faster from biotite than muscovite, and this rate was increased further to 63-123 times faster in the presence of common plant exudates (Feigenbaum et al., 1981; Song and Huang, 1988). The extent of release from trioctahedral minerals was also greater, as Scott and Smith (1966) reported that biotite was capable of releasing 30 % of interlayer potassium if solution potassium concentration was maintained at 10 ppm and 100 % was released at 7 ppm, while no exchange of potassium was observed for muscovite or <2 μm illite at the same 7 ppm potassium concentrations. Such concentrations are not typically obtained in agricultural soils although levels as low as 1 ppm have been obtained in the rhizosphere close to plant roots in laboratory studies (Woodhouse et al., 1978; Jungk et al., 1982; Kuchenbuch and Jungk, 1982; Hinsinger, 1998). These results suggest that release of interlayer-K by exchange mechanisms may only be important for trioctahedral micaceous clay minerals. As the soils of the Morrow Plots are typified by dioctahedral clay minerals (inset Figure 4.2), it seems that release of interlayer potassium would be disfavoured mechanism and plant nutrient needs are met through dissolution of soil clay minerals as discerned in Part I. Several different mechanisms have been proposed for the favourability of dissolution rather than extraction mechanism in dioctahedral minerals. Bassett (1960) suggested the orientation of hydroxyl ions around tetrahedral vacancies inhibits release, however Robert and Barshad (1972); Feigenbaum et al. (1981) suggest that the presence of iron (and/or manganese) in octahedral sites may aid the release of potassium by oxidation processes which reduce charge imbalance during the process of potassium extraction. Importantly, Robert and Barshad (1972) stress that the tetrahedral charge of dioctahedral micas could prevent the expansion of interlayer space which is crucial to the mica to smectite/vermiculite transformation (Mortland, 1958; Mengel et al., 2001). Additionally, Scott and Reed (1962b) and Feigenbaum and Shainberg (1975) showed that the rate and total amount of potassium released from <2 μm illite particles

is disfavoured when compared to <20 μm muscovite particles indicating that potassium extraction by exchange is disfavoured for clay-sized particles and that dissolution would be the mechanism favoured by plants to obtain potassium.

4.5 Conclusions

The full-profile XRD fitting approach was successfully applied to soil samples from mthe Morrow Plots experiment fields, an Aquic Argiudoll. A rich and complex <2 um mineralogy was identified, consisting of eleven different phases including discrete illite, kaolinite, chlorite, smectite, KI R1, and five different illite-smectite-smectite-chlorite mixed-layers, three of which were illite-rich and two which were smectite-rich. All the ISSCh phases contained a portion of chlorite layers, in line with the identification of chlorite layers by comparison of K-150 and Ca-AD/Ca-EG XRD diffractograms. The number and nature of the mixed-layers identified here is much more complex than in the previous description of the Morrow Plots mineralogy obtained by the peak decomposition method ((Velde and Peck, 2002)).

The results of quantitative phase analysis did not show any significant variation in either the abundance or the layer-composition of the mineral assemblage between different subplots with different agronomic treatments. The mineral assemblage also showed no signs of alteration or formation of new phases over time, regardless of the agronomic treatment. Observed mineralogical differences were restricted to a greater number of illite and smectite layers in C subplots than in R subplots, but this difference was insignifcant, particularly over the time-period studied. This indicates that the mineralogy of the Morrow Plots is very stable over time despite the influence of plant growth and potassium uptake. Lack of differnce between fertilised and non-fertilised subplots may be attributed to the higher seeding rates of fertilised plots which represents a significantly higher potassium demand.

Granulometry of the subplots varied considerably on a yearly basis which suggests significant heterogeneity even on a relatively small scale, and there was no systematic variation identified on the basis of the agronomic treatment. Significant differences between 2013 and 2014 samples indicates the exact timing of planting and sampling can have an effect on very short timescales. The plots showed an evolution of granulometry over time, with the proprtion of <0.05 um subfraction increasing while the proportion of 2-0.2 and 0.2-0.05 um subfractions decreased. This is attributed to the dissolution

of clay minerals in the coarser subfractions due to plant uptake of nutrients. Lack of sinificant change in the composition of mixed-layers between subfractions indicates that this dissolution is congruent and preferential extraction of potassium layers does not take place. This behaviour is consistent with laboratory studies which showed that dioctahedral illite/micas, which dominate the Morrow Plots, are highly resistant to potassium extraction from the interlayer space, requiring soil solution concentrations of potassium which are not often encountered in agricultural soils save in the rhizosphere (Hinsinger, 1998; Jungk et al., 1982). Globally, the mineralogy of the Morrow Plots was stable over time and between different agronomic treatments. This may have implications for future efforts to improve fertiliser use efficiency, and may prove useful in predicting the responses of other temperate soil mineral assemblages to fertilisation treatments or land use changes.

Overall conclusions and perspectives

5.1 General Discussion

Mineral assemblage and evolution of the Morrow Plots

One of the challenges of studying clay minerals is the conclusive identification of the complete mineral assemblage. This difficulty arises from the large size range of clay particles, and their disordered, mixed-layer nature. This study has shown that, while time consuming, full-profile fitting of XRD profiles is a particularly useful tool to identify the composition of complex soil clay minerals. Sequential fractionation is an important tool to unmask the contributions of mixed-layer phases in the smaller size fractions, whose presense is often masked by the sharp, intense refelctions which arise from discrete and/or well-crystallised phases in the complete <2 um fraction. Using the multi-specimen approach and comparing XRD data obtained from the same sample saturated with different cations and in different solvation states allowed to identify the presence of chlorite layers, and this added important compositional constraints on the layer-composition of the mixed-layers.

The complete mineralogical assemblage of soil from the Morrow Plots, an Aquic Argiudoll, was assessed using quantitative phase analysis of XRD data. Initially applied to unfertilised corn-oats-hay rotation subplots, this technique improved the description of the mineral assemblage from the previous assessment which was performed using the peak-decomposition method. The improved description increased the total number of contributions identified from four to eleven, and complete compositional information of the mixed-layers was obtained. The previous description included two mixed-layer

illite-smectite phases, which were described as either illite- or smectite-rich, and two discrete illite phases, one well-crystallised and one poorly crystallised. The current model replaced these descriptions with discrete illite, chlorite, kaolinite and smectite and a partially segregated kaolinite-illite phase, in addition to six illite-smectite-smectite-chlorite mixed-layers. This represents a significant increase in complexity of the mineral assemblage, which is in line with other studies of soil clay mineralogy using full-profile fitting, however this is the first time this method has been applied to an agricultural soil (Hubert et al., 2009; Viennet et al., 2015). The proposed model was successfully expanded to include XRD data from additional subplots of the Morrow Plotswhich were subject to different crop rotations and agronomic treatments.

No significant differences were observed between the mineralogy of the different subplots subject to different agronomic regimes. Neither was any significant alteration or formation of clay minerals observed over time as a result of continuous agriculture. This suggests that the impact of plant growth and potassium uptake, and potassium removal by crop export, on clay minerals in the mineral assemblage identified here, is not important on the 110-year time-scale investigated in the present study. Aluminisation of the interlayer space of 2:1 layers, previously reported in <2 um fractions of other soils, was not evident in the samples analysed here and is explained by a pH slightly above that where aluminisation would be expected to take place (Robert et al., 1987; Viennet et al., 2015; Turpault et al., 2008). Compositional similarity of phases between 2-0.2, 0.2-0.05 and <0.05 um fractions is an indication that alteration of the clay minerals is not occurring. Overall, the mineralogy of both <2 um and 50-2 um fractions was very stable over the period studied.

The evolution observed in the Morrow Plotswas essentially limited to granulometric changes where the proportion of the <0.05 um subfraction increased and the proportion of 2-0.2 and 0.2-0.05 um subfractions decreased. Given that the layer-composition of the mixed-layers is relatively consistent between the different subfractions dissolution seems to be the preferred mechanism for such an evolution. Protection of <0.05 um subfractions is attributed to association with organic matter. Dissolution as the primary mechanism of soil formation and evolution is further related to the dioctahedral nature of the clay minerals of the MP. Whilst a number of pot experiments have reported the release of potassium from fixed 2:1 layer minerals, these studies have been performed on trioctahedral minerals such as biotite and phlogopite (Hinsinger et al., 1992; Barré et al.,

2008a). In the case of dioctehdral micas or illite, no such changes have been reported (Naderizadeh et al., 2010; Norouzi and Khademi, 2010). This lends credence to the theory of plant nutrient uptake by dissolution which would explain the granulometric evolution, in addition to possible changes in sampling method with time (and sample storage). This is supported by a number of laboratory experiments, which showed the extraction of potassium from the interlayer space of dioctahedral micas is strongly disfavoured, particularly for smaller particles (Robert and Barshad, 1972; Mortland and Lawton, 1961; Scott and Reed, 1962a; Scott and Smith, 1966; Reed and Scott, 1962). The concentration of potassium in the soil solution required to observe extraction from dioctahedral minerals is extremely low and unlikely to be observed in the natural soil studied here (Hinsinger, 1998; Scott and Smith, 1966).

Validity of the proposed structural model

The proposed model was able to to give a good approximation of experimental data, for all the samples and subplots investigated in this study. Two main regions of misfit between 8-10 and 24-26 °2Θ in AD conditions for <0.05 μm subfractions exist, while in EG conditions only the misfit in the region of 24-26 °2Θ persisted. The presence of contributions of mixed-layers with similar compositions was justified through the multi-specimen approach as in Figure 3.7. The presence of chlorite layers in mixed-layers is also validated by the multi-specimen approach with the inclusion of K-150 samples in addition to Ca-AD and Ca-EG treatments. Sensitivity of mixed-layers to the presence of even 5% chlorite layers in the layer-composition was also demonstrated (Figure 3.7). The use of the sequential fractionation method and multi-specimen approach has allowed a more detailed description of the mineralogy than previous peak-decomposition methods, although both techniques include contributions from similar illite-rich mixed-layers. Specifically, the modelling of <0.05 μm subfractions isolates contributions that are not always evident in complete <2 μm fractions, and allows to determine compositional constraints.

5.2 Perspectives

Improved constraints

Although the model proposed in this thesis has improved the description of the mineral assemblage of the Morrow Plots compared to qualitative or peak-description methods, misfit still exists between experimental data and best-fit obtained with the current model.

This shows that the current model could benefit from additional constraints, which maybe be possible with the addition of electron microscopy to determine morphologies and elemental analyses, or other techniques such as infra-red spectroscopy. This may also provide insight into the difference in CEC between subfractions of the two subplots analysed for 2014, which the proposed mineral assemblage is unable to do. Electron microscopy may also be able to provide evidence to support the theory of particle-size evolution by dissolution. Furthermore, it would be interesting to determine whether the mineralogy in the rhizosphere differs from that of the bulk soil as analysed here. Samples were taken from 2014 which preserved the soil/root structure so X-ray absorption near-edge spectroscopy could provide an interesting complement to this study.

A further step to improving the constraints of the model is the application of the current model to complete <2 μm fractions and of the data obtained from K-150 samples. In particular the fitting of K-150 fractions would give a more definite distinction between the contributions of the 001 reflection and highlight any compositional differences. Ideally, the same phases used for the modelling of the <2 μm subfractions can be used for the <2 μm fraction. If significant compositional differences are found, this would suggest a way to improve the constraints and refine the model.

Broadening of scope

Another aspect which could increase the scope of this study would be the inclusion of samples from subplots of the Morrow Plots experimental fields which have been undergoing manure treatment. Manure fertilisation, alone or in conjunction with mineral fertilisers, has been linked to higher SOM content and higher exchangeable potassium values than for mineral fertiliser treatments alone (Pernes-Debuyser et al., 2003; Zhang et al., 2015; Guo et al., 2016). Given the suggested link between SOM and some of the granulometric evolution described in the current study, it would be interesting to see if a higher SOM content affects such evolution. The influence of an increased level of exchangeable potassium may also alter the mechanism of plant nutrient uptake, so mineralogical differences arising from such treatment may be greater than those demonstrated here. Additionally, the manure treatment was begun on subplots in 1904, so the effect of an additional 50 years of fertilisation may increase the magnitude of differences between subplots under the different treatments. Also of interest would be to add samples from the adjacent grass border. Although not a null-plot which is commonly included in experiments of this nature, it may provide an interesting comparison between a soil

which has been subject to high potassium demand and export due to continuous cropping versus a soil with low potassium demand and little to no removal of potassium by cropping.

Inclusion of additional experiments

There is additional interest in performing the same quantitative mineralogical analysis on samples from other agricultural experiments, as several studies using qualitative analysis of XRD data have reported changes in the mineralogical assemblage (Tributh et al., 1987; Dissing-Nielsen and Möberg, 1984; Möberg and Dissing-Nielsen, 1983). As these changes involve micaceous layers in particular, the inclusion of sequential fractionation and full-profile fitting would provide confirmation of these observations. The interest in such a study lies in determining if the behaviour detected here is consistent across soils of different origins and climates and under different agronomic regimes. This can be extended to studies involving crops with higher potassium demande, such as sugar beet and potatoes. Such studies could be linked to eventual improvements in fertilisation regimes which is important to consider in light of the debated nature of soil and yield responses to potassium fertilisation and the likelihood of increasing fertiliser demand in agriculture around the world (Khan et al., 2014; UNFAO, 2017).

Bibliography

Adamo, P., Barré, P., Cozzolino, V., Di Meo, V., and Velde, B. (2016). Short term clay mineral release and re-capture of potassium in a Zea mays field experiment. *Geoderma*, 264:54–60.

Al-Harahsheh, A. M. and Al-Itawi, H. I. (2005). Salts Production from Dead Sea by using Different Technological Methods: Prospective Outlook. *Journal of Applied Sciences*, 5(8):1334–1339.

Aplin, A. C., Matenaar, I. F., McCarty, D. K., and van der Pluijm, B. A. (2006). Influence of mechanical compaction and clay mineral diagenesis on the microfabric and pore-scale properties of deep-water Gulf of Mexico mudstones. *Clays and Clay Minerals*, 54(4):500–514.

Aref, S. and Wander, M. M. (1998). Long-Term Trends of Corn Yield and Soil Organic Matter in Different Crop Sequences and Soil Fertility Treatments on the Morrow Plots. *Advances in Agronomy*, 62:153–198.

Arnold, P. W. (1958). Potassium Uptake by Cation-Exchange Resins from Soils and Minerals. *Nature*, 182(4649):1821594a0.

Arnold, P. W. (1960). Nature and mode of weathering of soil-potassium reserves. *Journal of the Science of Food and Agriculture*, 11(6):285–292.

Arnold, P. W. and Close, B. M. (1961). Potassium-releasing power of soils from the Agdell rotation experiment assessed by glasshouse cropping. *The Journal of Agricultural Science*, 57(3):381–386.

Aylward, G. and Findlay, T. (2002). *SI Chemical Data*. John Wiley & Sons, Milton, Queensland, 5th edition.

Badraoui, M., Bloom, P. R., and Delmaki, A. (1992). Mobilization of non-exchangeable K by ryegrass in five Moroccan soils with and without mica. *Plant and Soil*, 140(1):55–63.

Bain, D. C. and Griffen, D. T. (2002). Possible effects of land use on the clay mineralogy of a brown forest soil. *Clay Minerals*, 37(4):663–670.

Barber, S. A. and Mackay, A. D. (1986). Root growth and phosphorus and potassium uptake by two corn genotypes in the field. *Fertilizer Research*, 10:217–230.

Barker, A. and Pilbeam, D. (2015). *Handbook of Plant Nutrition, Second Edition*. Taylor & Francis.

Barré, P., Fernandez-Ugalde, O., Virto, I., Velde, B., and Chenu, C. (2014). Impact of phyllosilicate mineralogy on organic carbon stabilization in soils: Incomplete knowledge and exciting prospects. *Geoderma*, 235-236:382–395.

Barré, P., Montagnier, C., Chenu, C., Abbadie, L., and Velde, B. (2008a). Clay minerals as a soil potassium reservoir: Observation and quantification through X-ray diffraction. *Plant and Soil*, 302:213–220.

Barré, P., Velde, B., and Abbadie, L. (2007a). Dynamic role of "illite-like" clay minerals in temperate soils: Facts and hypotheses. *Biogeochemistry*, 82:77–88.

Barré, P., Velde, B., and Catel, N. (2007b). Soil-plant potassium transfer: Impact of plant activity on clay minerals as seen from X-ray diffraction. *Plant and Soil*, 292:137–146.

Barré, P., Velde, B., Fontaine, C., Catel, N., and Abbadie, L. (2008b). Which 2:1 clay minerals are involved in the soil potassium reservoir? Insights from potassium addition or removal experiments on three temperate grassland soil clay assemblages. *Geoderma*, 146:216–223.

Bassett, W. A. (1960). Role of hydroxyl orientation in mica alteration. *GSA Bulletin*, 71(4):449–456.

Batha, E. (2000). Death of a river. http://news.bbc.co.uk/2/hi/europe/642880.stm.

Bhadra, D. and Brandao, A. S. (1993). Urbanization, Agricultural Development, and Land Allocation. Technical report, The World Bank, Washington, USA.

Blecker, S. W., McCulley, R. L., Chadwick, O. A., and Kelly, E. F. (2006). Biologic cycling of silica across a grassland bioclimosequence. *Global Biogeochemical Cycles*, 20(3):GB3023.

Borchardt-Ott, W. (2012). *Crystallography: An Introduction*. Springer-Verlag, Berlin Heidelberg, 3 edition.

Bortoluzzi, E. C., Moterle, D. F., Rheinheimer, D. d. S., Casali, C. A., Melo, G. W., and Brunetto, G. (2012). Mineralogical changes caused by grape production in a regosol from subtropical Brazilian climate. *Journal of Soils and Sediments*, 12(6):854–862.

Bortoluzzi, E. C., Velde, B., Pernes, M., Dur, J. C., and Tessier, D. (2008). Vermiculite, with hydroxy-aluminium interlayer, and kaolinite formation in a subtropical sandy soil from south Brazil. *Clay Minerals*, 43(2):185–193.

Boyle, J. R. and Voigt, G. K. (1973). Biological weathering of silicate minerals. *Plant and Soil*, 38(1):191–201.

Brindley, G. W. and Brown, G., editors (1980). *Crystal Structures of Clay Minerals and Their X-Ray Identification*, volume 5. Mineralogical Society London.

Calvaruso, C., Mareschal, L., Turpault, M.-P., and Leclerc, E. (2009). Rapid Clay Weathering in the Rhizosphere of Norway Spruce and Oak in an Acid Forest Ecosystem. *Soil Science Society of America Journal*, 73(1):331–338.

Caner, L., Joussein, E., Salvador-Blanes, S., Hubert, F., Schlicht, J.-F., and Duigou, N. (2010). Short-time clay-mineral evolution in a soil chronosequence in Oléron Island (France). *Journal of Plant Nutrition and Soil Science*, 173(4):591–600. Caner2010.

Chenu, C. and Plante, A. F. (2006). Clay-sized organo-mineral complexes in a cultivation chronosequence: Revisiting the concept of the 'primary organo-mineral complex'. *European Journal of Soil Science*, 57(4):596–607.

Chute, J. H. and Quirk, J. P. (1967). Diffusion of Potassium from Mica-like Clay Minerals. *Nature*, 213(5081):2131156a0.

Claassen, N. and Jungk, A. (1982). Kaliumdynamik im wurzelnahen Boden in Beziehung zur Kaliumaufnahme von Maispflanzen. *Zeitschrift für Pflanzenernährung und Bodenkunde*, 145(6):513–525.

Collignon, C., Ranger, J., and Turpault, M. P. (2012). Seasonal dynamics of Al- and Fe-bearing secondary minerals in an acid forest soil: Influence of Norway spruce roots (Picea abies (L.) Karst.). *European Journal of Soil Science*, 63(5):592–602.

Cornu, S., Montagne, D., Hubert, F., Barre, P., and Caner, L. (2012). Evidence of short-term clay evolution in soils under human impact. *Comptes Rendus Geoscience*, 344:747–757.

DeFries, R. S., Rudel, T., Uriarte, M., and Hansen, M. (2010). Deforestation driven by urban population growth and agricultural trade in the twenty-first century. *Nature Geoscience*, 3(3):ngeo756.

DeTurk, E. (1939). Changes in the soil of the Morrow plots which have accompanied long-continued cropping. *Soil Science Society of America Journal*, 3(C):83–85. Deturk1939.

Dissing-Nielsen, J. and Möberg, J. P. (1984). The Influence of K-Depletion on Mineralogical Changes in Pedons from Two Field Experiments and in Soils from Four Pot Experiments. *Acta Agriculturae Scandinavica*, 34(3):391–399.

Doebelin, N. and Kleeberg, R. (2015). Profex: A graphical user interface for the Rietveld refinement program BGMN. *Journal of Applied Crystallography*, 48(5):1573–1580.

Dohrmann, R. and Kaufhold, S. (2009). Three New, Quick CEC Methods for Determining the Amounts of Exchangeable Calcium Cations in Calcareous Clays. *Clays and Clay Minerals*, 57(3):338–352.

Doll, E. C., Mortland, M. M., Lawton, K., and Ellis, B. G. (1965). Release of Potassium from Soil Fractions During Cropping. *Soil Science Society of America Journal*, 29(6):699–702.

Döös, B. R. (2002). Population growth and loss of arable land. *Global Environmental Change*, 12(4):303–311.

Drits, V., Srodon, J., and Eberl, D. (1997a). XRD measurement of mean crystallite thickness of illite and illite/smectite: Reappraisal of the Kubler index and the Scherrer equation. *Clays and clay minerals*, 45(3):461–475.

Drits, V. A., Sakharov, B. A., Lindgreen, H., and Salyn, A. (1997b). Sequential structure transformation of illite-smectite-vermiculite during diagenesis of Upper Jurassic shales from the North Sea and Denmark. *Clay Minerals*, 32(3):351–371.

Drits, V. A. and Tchoubar, C. (1990). *X-Ray Diffraction by Disordered Lamellar Structures*. Springer, Berlin, Heidelberg.

Endres, T. J. (2002). Soil survey of Champaign County, Illinois.

Epstein, E. (1999). Silicon. *Annual Review of Plant Physiology and Plant Molecular Biology*, 50(1):641–664.

Fageria, N. K. (1983). Ionic interactions in rice plants from dilute solutions. *Plant and Soil*, 70(3):309–316.

Fehrenbacher, J. B., Walker, G. O., and Wascher, H. L. (1967). Soils of Illinois. *University of Illinois Agricultural Experiment Station Bulletin*, (725).

Feigenbaum, S., Edelstein, R., and Shainberg, I. (1981). Release Rate of Potassium and Structural Cations from Micas to Ion Exchangers in Dilute Solutions. *Soil Science Society of America Journal*, 45(3):501–506.

Feigenbaum, S. and Shainberg, I. (1975). Dissolution of Illite—A Possible Mechanism of Potassium Release. *Soil Science Society of America Journal*, 39(5):985–990.

Ferrage, E., Lanson, B., Malikova, N., Plançon, A., Sakharov, B. A., and Drits, V. A. (2005a). New Insights on the Distribution of Interlayer Water in Bi-Hydrated Smectite from X-ray Diffraction Profile Modeling of 00l Reflections. *Chemistry of Materials*, 17(13):3499–3512.

Ferrage, E., Lanson, B., Sakharov, B. A., and Drits, V. A. (2005b). Investigation of smectite hydration properties by modeling experimental X-ray diffraction patterns: Part I. Montmorillonite hydration properties. *American Mineralogist*, 90:1358–1374.

Foth, H. D. (1991). *Fundamentals of Soil Science*. Wiley, 8th edition.

Fox, R. L. and Lipps, R. C. (1960). Distribution and activity of roots in relation to soil properties. *Transactions 7th int. Congr. Soil Sci.*, 3:260–267.

Gaines, G. L. (1957). The Ion-exchange Properties of Muscovite Mica. *The Journal of Physical Chemistry*, 61(10):1408–1413.

Guggenheim, S. and Martin, R. T. (1995). Definition of clay and clay mineral; joint report of the AIPEA and CMS nomenclature committees. *Clay Minerals*, 30(3):257–259.

Guo, L., Wu, G., Li, Y., Li, C., Liu, W., Meng, J., Liu, H., Yu, X., and Jiang, G. (2016). Effects of cattle manure compost combined with chemical fertilizer on topsoil organic matter, bulk density and earthworm activity in a wheat–maize rotation system in Eastern China. *Soil and Tillage Research*, 156:140–147.

Haines, S. G. and Cleveland, G. (1981). Seasonal Variation in Properties of Five Forest Soils in Southwest Georgia. *Soil Science Society of America Journal*, 45(1):139–143.

Halka, M. and Nordstrom, B. (2010). *Alkali and Alkaline Earth Metals*. Periodic Table of the Elements. Facts on File.

Hanway, J. J. and Scott, A. D. (1957). Soil Potassium-Moisture Relations: II. Profile Distribution of Exchangeable K in Iowa Soils as Influenced by Drying and Rewetting. *Soil Science Society of America Journal*, 21(5):501–504.

Hanway, J. J. and Scott, A. D. (1959). Soil Potassium-Moisture Relations: III. Determining the Increase in Exchangeable Soil Potassium on Drying Soils. *Soil Science Society of America Journal*, 23(1):22–24.

Hatton, A., Ranger, J., Robert, M., Nys, C., and Bonnaud, P. (1987). Weathering of a mica introduced into four acidic forest soils. *Journal of Soil Science*, 38(2):179–190.

Hilgard, E. W. (1921). *Soils: Their Formation, Properties, Composition, and Relations to Climate and Plant Growth in the Humid and Arid Regions*. Macmillan.

Hinsinger, P. (1998). How Do Plant Roots Acquire Mineral Nutrients? Chemical Processes Involved in the Rhizosphere. *Advances in Agronomy*, 64:225–265.

Hinsinger, P., Bengough, A. G., Vetterlein, D., and Young, I. (2009). Rhizosphere : Biophysics, biogeochemistry and ecological relevance. *Plant Soil*, 321:117–152.

Hinsinger, P., Elsass, F., Jaillard, B., and Robert, M. (1993). Root-induced irreversible transformation of a trioctahedral mica in the rhizosphere of rape. *Journal of Soil Science*, 44:535–545.

Hinsinger, P. and Jaillard, B. (1993). Root-induced release of interlayer potassium and vermiculitization of phlogopite as related to potassium depletion in the rhizosphere of ryegrass. *Journal of Soil Science*, 44:525–534.

Hinsinger, P., Jaillard, B., and Dufey, J. E. (1992). Rapid Weathering of a Trioctahedral Mica by the Roots of Ryegrass. *Soil Science Society of Americal Journal*, 56(3):977–982.

Huang, P. M., Li, Y., and Sumner, M. E. (2011). *Handbook of Soil Sciences: Resource Management and Environmental Impacts, Second Edition*. CRC Press.

Hubert, F., Caner, L., Meunier, A., and Ferrage, E. (2012). Unraveling complex <2 mm clay mineralogy from soils using X-ray diffraction profile modeling on particle-size sub-fractions: Implications for soil pedogenesis and reactivity. *American Mineralogist*, 97:384–398.

Hubert, F., Caner, L., Meunier, A., and Lanson, B. (2009). Advances in characterization of soil clay mineralogy using X-ray diffraction: From decomposition to profile fitting. *European Journal of Soil Science*, 60(6):1093–1105.

Huggett, R. J. (1998). Soil chronosequences, soil development, and soil evolution: A critical review. *CATENA*, 32(3):155–172.

Inoue, A., Lanson, B., Marques-Fernandes, M., Sakharov, B. A., Murakami, T., Meunier, A., and Beaufort, D. (2005). Illite-smectite mixed-layer minerals in the hydrothermal alteration of volcanic rocks: I. One-dimensional XRD structure analysis and characterization of component layers. *Clays and Clay Minerals*, 53(5):423–439.

IPI (2010). International Potash Institute: K in cereal crops. https://www.ipipotash.org/en/.

Jackson, M. L. (1958). *Soil Chemical Analysis*. Verlag: Prentice Hall, Inc., Englewood Cliffs, New Jersey, USA.

Jasinski, S. M. (2017a). 2015 Minerals Yearbook: Potash. Technical report, USGS.

Jasinski, S. M. (2017b). Potash. Technical report, USGS.

Jenny, H. (1994). *Factors of Soil Formation: A System of Quantitative Pedology*. Courier Corporation.

Joffe, J. S. (1936). *Pedology*. Rutgers University Press.

Jungk, A., Claassen, N., and Kuchenbuch, R. (1982). Potassium depletion of the soil-root interface in relation to soil parameters and root properties. In *Plant Nutrition*, volume 1, pages 250–255, Warwick University, England. Commonwealth Agricultural Bureaux.

Kesler, S. (1994). *Mineral Resources, Economics, and the Environment*. Macmillan.

Khan, S., Mulvaney, R., and Ellsworth, T. (2014). The potassium paradox: Implications for soil fertility, crop production and human health. *Renewable Agriculture and Food Systems*, 29(1):3–27.

Khan, S. A. (1991). *Soil K Level in Relation to K Treatment, Season of Year and Soil Moisture Level*. PhD, University of Illinois, Urbana-Champaign.

Khan, T. B. (2013). *Impact of Cropping Practices on Clay Mineralogy*. Master's thesis, Université Joseph Fourier, Grenoble.

Koch, K. and Mengel, K. (1974). The influence of the level of potassium supply to young tobacco plants (Nicotiana tabacum L.) on short-term uptake and utilisation of nitrate nitrogen (15N). *Journal of the Science of Food and Agriculture*, 25(5):465–471.

Kraffczyk, I., Trolldenier, G., and Beringer, H. (1984). Soluble root exudates of maize: Influence of potassium supply and rhizosphere microorganisms. *Soil Biology and Biochemistry*, 16(4):315–322.

Kuchenbuch, R. and Jungk, A. (1982). A method for determining concentration profiles at the soil-root interface by thin slicing rhizospheric soil. *Plant and Soil*, 68(3):391–394.

Kutílek, M. and Nielsen, D. R. (2015). *Soil: The Skin of Planet Earth*. Springer, Dordrecht.

Laird, D. A., Barak, P., Nater, E. A., and Dowdy, R. H. (1991). Chemistry of Smectitic and Illitic Phases in Interstratified Soil Smectite. *Soil Science Society of America Journal*, 55(5):1499–1504.

Lambin, E. F. and Meyfroidt, P. (2011). Global land use change, economic globalization, and the looming land scarcity. *Proceedings of the National Academy of Sciences*, 108(9):3465–3472.

Lanning, F. C., Hopkins, T. L., and Loera, J. C. (1980). Silica and Ash Content and Depositional Patterns in Tissues of Mature Zea mays L. Plants. *Annals of Botany*, 45(5):549–554.

Lanson, B. (1997). Decomposition of Experimental X-ray Diffraction Patterns (Profile Fitting): A Convenient Way to Study Clay Minerals. *Clays and Clay Minerals*, 45(2):132–146.

Lewin, J. and Reimann, B. E. F. (1969). Silicon and Plant Growth. *Annual Review of Plant Physiology*, 20(1):289–304.

Li, D.-c., Velde, B., Li, F.-m., Zhang, G.-l., Zhao, M.-s., and Huang, L.-m. (2011). Impact of Long-Term Alfalfa Cropping on Soil Potassium Content and Clay Minerals in a Semi-Arid Loess Soil in China. *Pedosphere*, 21(4):522–531.

Lindgreen, H., Drits, V. A., Sakharov, B. A., Salyn, A. L., Wrang, P., and Dainyak, L. G. (2000). Illite-smectite structural changes during metamorphism in black Cambrian Alum shales from the Baltic area. *American Mineralogist*, 85(9):1223–1238.

MacLean, A. J. and Brydon, J. E. (1963). Release and fixation of potassium in different size fractions of some Canadian soils as related to their mineralogy. *Canadian Journal of Soil Science*, 43(1):123–134.

Marschner, H., editor (1995). *Mineral Nutrition of Higher Plants*. Academic Press, London.

Martin, R. T. (1960). Adsorbed water on clay: A review. *Clays and Clay Minerals*, 9(1):28–70.

McCarty, D. K., Drits, V. A., Sakharov, B., Zviagina, B. B., Ruffell, A., and Wach, G. (2004). Heterogeneous mixed-layer clays from the Cretaceous Greensand, Isle of Wight, southern England. *Clays and Clay Minerals*, 52(5):552–575.

Mengel, K., Kirkby, E. A., Kosegarten, H., and Appel, T., editors (2001). *Principles of Plant Nutrition*. Springer Netherlands, Dordrecht.

Mengel, K. and Rahmatullah (1994). Exploitation of potassium by various crop species from primary minerals in soils rich in micas. *Biology and Fertility of Soils*, 17:75–79.

Méring, J. (1949). L'interférence des rayons X dans les systèmes à stratification désordonée. *Acta Crystallographica*, 2(6):371–377.

Meunier, A. (2005). *Clays*. Springer, Berlin, Heidelberg.

Meunier, J.-D. (2003). Le rôle des plantes dans le transfert du silicium à la surface des continents. *Comptes Rendus Geoscience*, 335(16):1199–1206.

Möberg, J. P. and Dissing-Nielsen, J. (1983). Mineralogical Changes in Soils Used for Potassium-depletion Experiments for Some Years in Pots and in the Field. *Acta Agriculturae Scandinavica*, 33(1):21–27.

Moore, D. M. and Reynolds, R. C. (1997). *X-Ray Diffraction and the Identification and Analysis of Clay Minerals*. Oxford University Press Oxford, New York, USA, 2 edition.

Mortland, M. M. (1958). Kinetics of Potassium Release from Biotite. *Soil Science Society of America Journal*, 22(6):503–508.

Mortland, M. M. and Lawton, K. (1961). Relationships Between Particle Size and Potassium Release From Biotite and Its Analogues. *Soil Science Society of America Journal*, 25(6):473–476.

Mortland, M. M., Lawton, K., and Uehara, G. (1956). Alteration of biotite to vermiculite by plant growth. *Soil Science*, 82(6):477.

Mouas-Bourbia, S., Barre, P., Boudiaf-Nait Kaci, M., Mouffok, M., Rebbouh, M., Kessouri, L., Ouahab, H., Derridj, A., and Velde, B. (2015). Influence of Olea europea L. and Ficus Carrica L. fine root activity on the K biodisponibility and clay mineralogy of the rhizosphere. *Eurasian Journal of Soil Science*, 4(4):220–226.

Mount, H. R. (1982). Soil survey of Champaign County, Illinois.

MRCC (2018). Cli-MATE: Midwestern Regional Climate Centre Application Tools Environment (cli-MATE). http://mrcc.isws.illinois.edu/CLIMATE/.

Mueller, N. D., Gerber, J. S., Johnston, M., Ray, D. K., Ramankutty, N., and Foley, J. A. (2012). Closing yield gaps through nutrient and water management. *Nature*, 490(7419):254–257.

Naderizadeh, Z., Khademi, H., and Arocena, J. M. (2010). Organic matter induced mineralogical changes in clay-sized phlogopite and muscovite in alfalfa rhizosphere. *Geoderma*, 159(3):296–303.

Niebes, J.-F., Dufey, J. E., Jaillard, B., and Hinsinger, P. (1993). Release of nonexchangeable potassium from different size fractions of two highly K-fertilized soils in the rhizosphere of rape (Brassica napus cv Drakkar). *Plant and Soil*, 155/156:403–406.

Nielsson (1986). *Manual of Fertilizer Processing*, volume 5 of *Fertilizer Science and Technology*. Marcel Dekker, Inc., New York.

Norouzi, S. and Khademi, H. (2010). Ability of alfalfa (Medicago sativa) to take up potassium from different micaceous minerals and consequent vermiculitization. *Plant and Soil*, 328(1-2):83–93.

Norse, D. (1992). A New Strategy for Feeding a Crowded Planet. *Environment: Science and Policy for Sustainable Development*, 34(5):6–39.

Odell, R. T., Melsted, S. W., and Walker, W. M. (1984). Changes in organic carbon and nitrogen of Morrow Plot soils under different treatments, 1904-1973. *Soil Science*, 137(3):160.

Orsini, L. and Remy, J. (1976). Utilisation du chlorure de cobaltihexamine pour la détermination simultanée de la capacité d'échange et des bases échangeables des sols. *Sci. Sol*, 4:269–275.

Parsons, P. and Dixon, G. (2013). *The Periodic Table: A Field Guide to the Elements*. Quercus.

Peoples, M. B., Richardson, A. E., Simpson, R. J., and Fillery, I. R. P. (2014). Soil: Nutrient Cycling. In Alfen, N. K. V., editor, *Encyclopedia of Agriculture and Food Systems*, pages 197–210. Academic Press, Oxford.

Pernes-Debuyser, A., Pernes, M., Velde, B., and Tessier, D. (2003). Soil Mineralogy Evolution in the Inra 42 Plots Experiment (Versailles, France). *Clays and Clay Minerals*, 51(5):577–584.

Ramann, E. (1928). *The Evolution and Classification of Soils*. W. Heffer.

Ranger, J., Robert, M., Nys, C., Blet-Charaudeau, C., Bonnaud, P., and Gelhaye, D. (1991). An in Situ Experimental Study of Forest Soil Functioning using the Mineral Bag Technique. In Berthelin, J., editor, *Developments in Geochemistry*, volume 6 of *Diversity of Environmental Biogeochemistry*, pages 519–536. Elsevier.

Reed, M. G. and Scott, A. D. (1962). Kinetics of Potassium Release from Biotite and Muscovite in Sodium Tetraphenylboron Solutions. *Soil Science Society of America Journal*, 26(5):437–440.

Reitemeier, R. F. (1951). Soil Potassium. In Norman, A. G., editor, *Advances in Agronomy*, volume 3, pages 113–164. Academic Press.

Rengel, Z. and Damon, P. M. (2008). Crops and genotypes differ in efficiency of potassium uptake and use. *Physiologia Plantarum*, 133(4):624–636.

Reynolds Jr., R. (1985). *NEWMOD: A Computer Program for the Calculation of the One-Dimensional X-Ray Diffraction Patterns of Mixed-Layered Clays*. Hanover, New Hampshire, USA.

Righi, D. (1982). Relations entre l'illuviation de matiere organique, l'activité de la microfaune et les structures d'horizons B de sols podzolisés du Pleateau de Millevaches. *Pédologie*, 32(1):19–37.

Righi, D. (1993). Characterization of Hydroxy-Interlayered Vermiculite and Illite/Smectite Interstratified Minerals from the Weathering of Chlorite in a Cryorthod. *Clays and Clay Minerals*, 41(4):484–495.

Righi, D. and Chauvel, A. (1987). *Podzols et podzolisation*. AFES ; INRA, Plaisir (FRA) ; Paris.

Rivard, C., Lanson, B., and Cotte, M. (2016). Phosphorus speciation and micro-scale spatial distribution in North-American temperate agricultural soils from micro X-ray fluorescence and X-ray absorption near-edge spectroscopy. *Plant and Soil*, 401(1):7–22.

Robert, M. and Barshad, I. (1972). Transformation expérimentale des micas en vermiculites ou smectites. Propriétés des smectites de transformation. *Bulletin du Groupe français des argiles*, 24(2):137–151.

Robert, M., Razzaghe, M. H., and Ranger, J. (1987). Role du facteur biochimique dans la podzolisation. In *Podzols et podzolisation*, Comptes rendus de la table ronde internationale. AFES ; INRA, Plaisir (FRA) ; Paris.

Sakharov, B. A., Lindgreen, H., Salyn, A., and Drits, V. A. (1999a). Determination of illite-smectite structures using multispecimen X-ray diffraction profile fitting. *Clays and Clay minerals*, 47(5):555–566.

Sakharov, B. A., Lindgreen, H., Salyn, A. L., and Drits, V. A. (1999b). Mixed-layer kaolinite-illite-vermiculite in North Sea shales. *Clay Minerals*, 34(2):333–344.

Schenk, M. K. and Barber, S. A. (1980). Potassium and phosphorus uptake by corn genotypes grown in the field as influenced by root characteristics. *Plant and Soil*, 54:65–76.

Scott, A. and Smith, S. (1966). Susceptibility of interlayer potassium in micas to exchange with sodium. In *Proceedings of the Clays and Clay Minerals: Proceedings of the Fourteenth National Conference, Berkeley, California*, page 69.

Scott, A. D. and Reed, M. G. (1962a). Chemical Extraction of Potassium from Soils and Micaceous Minerals With Solutions Containing Sodium Tetraphenylboron: II. Biotite. *Soil Science Society of America Journal*, 26(1):41–45.

Scott, A. D. and Reed, M. G. (1962b). Chemical Extraction of Potassium from Soils and Micaceous Minerals With Solutions Containing Sodium Tetraphenylboron: III. Illite. *Soil Science Society of America Journal*, 26(1):45–48.

Simonsson, M., Hillier, S., and Öborn, I. (2009). Changes in clay minerals and potassium fixation capacity as a result of release and fixation of potassium in long-term fi eld experiments. *Geoderma*, 151:109–120.

Singh, B. and Goulding, K. W. T. (1997). Changes with time in the potassium content and phyllosilicates in the soil of the Broadbalk continuous wheat experiment at Rothamsted. *European Journal of Soil Science*, 48:651–659.

Singh, M., Sarkar, B., Sarkar, S., Churchman, J., Bolan, N., Mandal, S., Menon, M., Purakayastha, T. J., and Beerling, D. J. (2017). Stabilization of Soil Organic Carbon as Influenced by Clay Mineralogy. *Advances in Agronomy*.

Soil Survey Staff, U. (1999). *USDA Soil Taxonomy*. United States Department of Agriculture, 2nd edition.

Song, S. K. and Huang, P. M. (1988). Dynamics of Potassium Release from Potassium-Bearing Minerals as Influenced by Oxalic and Citric Acids. *Soil Science Society of America Journal*, 52(2):383–390.

Sparks, D. L. (1987). Potassium Dynamics in Soils. In *Advances in Soil Science*, Advances in Soil Science, pages 1–63. Springer, New York, NY.

Sparks, D. L. (2001). Dynamics of K in Soils and Their Role in Management of K Nutrition. In *Technical Sessions*, pages 79–101, New Delhi. International Potash Institute.

Sparks, D. L., editor (2003). *Environmental Soil Chemistry*. Academic Press, Burlington, second edition edition.

Sparks, D. L. and Carski, T. H. (1985). Kinetics of potassium exchange in heterogeneous systems. *Applied Clay Science*, 1(1):89–101.

Sposito, G. (2008). *The Chemistry of Soils*. Oxford University Press, New York, 2nd edition.

Sposito, G. and Anderson, D. M. (1975). Infrared Study of Exchangeable Cation Hydration in Montmorillonite. *Soil Science Society of America Journal*, 39(6):1095–1099.

Tachimoto, M., Fukutomi, M., Matsushiro, H., Kobayashi, M., and Takahashi, E. (1992). Role of putrescine in Lemna plants under potassium deficiency. *Soil Science and Plant Nutrition*, 38(2):307–313.

Tributh, H., v Boguslawski, E., v Lieres, A., Steffens, D., and Mengel, K. (1987). Effect of potassium removal by crops on transformation of illitic clay minerals. *Soil Science*, 143(6):404.

Turpault, M. P., Righi, D., and Utérano, C. (2008). Clay minerals: Precise markers of the spatial and temporal variability of the biogeochemical soil environment. *Geoderma*, 147(3):108–115.

UNFAO (2017). United Nations World Population Prospects: The 2017 Revision. Technical Report ESA/P/WP/248, Department of Economic and Social Affairs, United Nations.

Uralkali (2017). Geological Safety. http://www.uralkali.com/sustainability/geology/.

Velde, B. and Barré, P. (2009). *Soils, Plants and Clay Minerals*. Springer, Berlin, Heidelberg.

Velde, B., Goffé, B., and Hoellard, A. (2003). Evolution of clay minerals in a chronosequence of poldered sediments under the influence of a natural pasture development. *Clays and Clay Minerals*, 51(2):205–217.

Velde, B. and Meunier, A. (2008). *The Origin of Clay Minerals in Soils and Weathered Rocks*. Springer, Berlin, Heidelberg.

Velde, B. and Peck, T. (2002). Clay mineral changes in the Morrow Experimental Plots, University of Illinois. *Clays and Clay Minerals*, 50(3):364–370.

Vetterlein, D., Kühn, T., Kaiser, K., and Jahn, R. (2013). Illite transformation and potassium release upon changes in composition of the rhizophere soil solution. *Plant and Soil*, 371:267–279.

Viennet, J.-C., Hubert, F., Ferrage, E., Tertre, E., Legout, A., and Turpault, M.-P. (2015). Investigation of clay mineralogy in a temperate acidic soil of a forest using X-ray diffraction profile modeling: Beyond the HIS and HIV description. *Geoderma*, 241-242(Supplement C):75–86.

von Lützow, M., Kögel-Knabner, I., Ekschmitt, K., Matzner, E., Guggenberger, G., Marschner, B., and Flessa, H. (2006). Stabilization of organic matter in temperate soils: Mechanisms and their relevance under different soil conditions – a review. *European Journal of Soil Science*, 57(4):426–445.

Walker, G. F. (1950). Trioctahedral Minerals in the Soil-Clays of North-East Scotland. *Mineralogical Magazine*, 29(208):72–84.

Weaver, T. and Forcella, F. (1979). Seasonal Variation in Soil Nutrients Under Six Rocky Mountain Vegetation Types. *Soil Science Society of America Journal*, 43(3):589–593.

Wedepohl, H. K. (1995). The composition of the continental crust. *Geochimica et Cosmochimica Acta*, 59(7):1217–1232.

Wells, C. B. and Norrish, K. (1968). Accelerated rates of release of interlayer potassium from micas. In *Transactions of the 9th International Congress on Soil Science*.

Willman, H. B., Glass, H. D., and Frye, J. C. (1963). Mineralogy of glacial tills and their weathering profiles in Illinois : Part I. Glacial tills. *Illinois State Geological Survey Circular*, 347:1–55.

Woodhouse, P. J., Wild, A., and Clement, C. R. (1978). Rate of Uptake of Potassium by Three Crop Species in Relation to Growth. *Journal of Experimental Botany*, 29(4):885–894.

Zhang, W., Liu, K., Wang, J., Shao, X., Xu, M., Li, J., Wang, X., and Murphy, D. V. (2015). Relative contribution of maize and external manure amendment to soil carbon sequestration in a long-term intensive maize cropping system. *Scientific Reports*, 5:10791.

Supplementary information

A.1 RU Rietveld

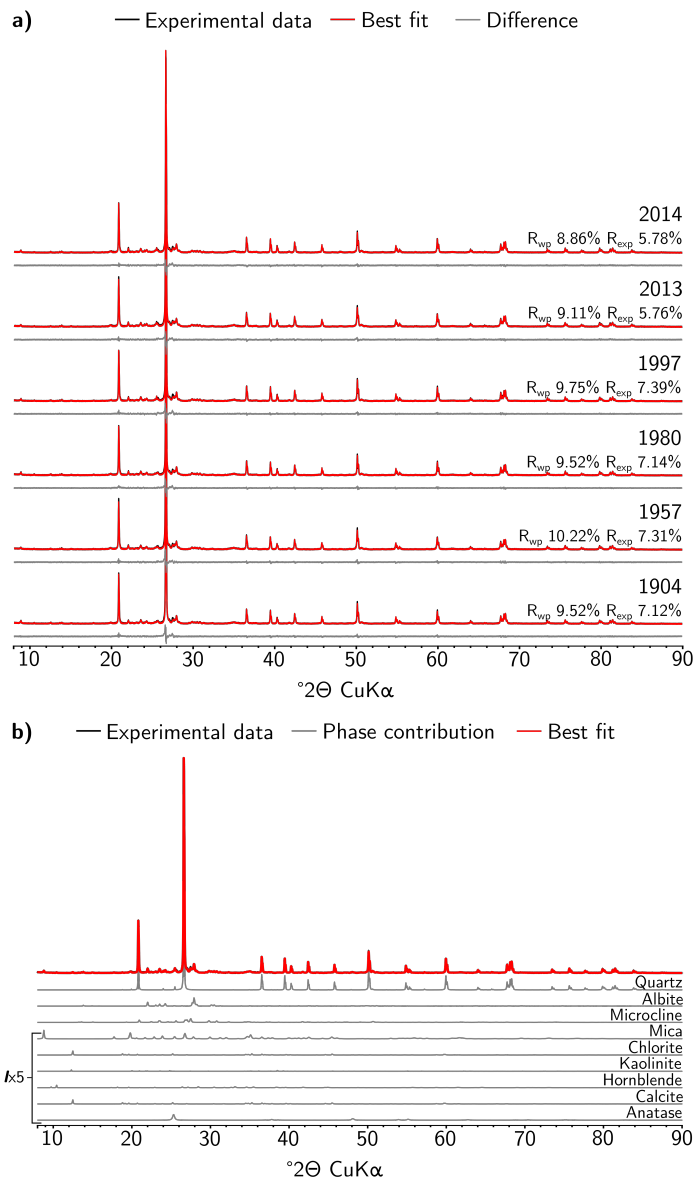

Figure A.1: Experimental XRD data of 50-2 μm fractions (grey crosses) and Rietveld results for a) 1904-2014 samples. Difference plots are shown in solid grey below each comparison plot. The mineralogy of all fractions is similar over the period studied. b) shows the contributions of each of the different mineral phases included in the refinement process.

A.2 RU phase analysis

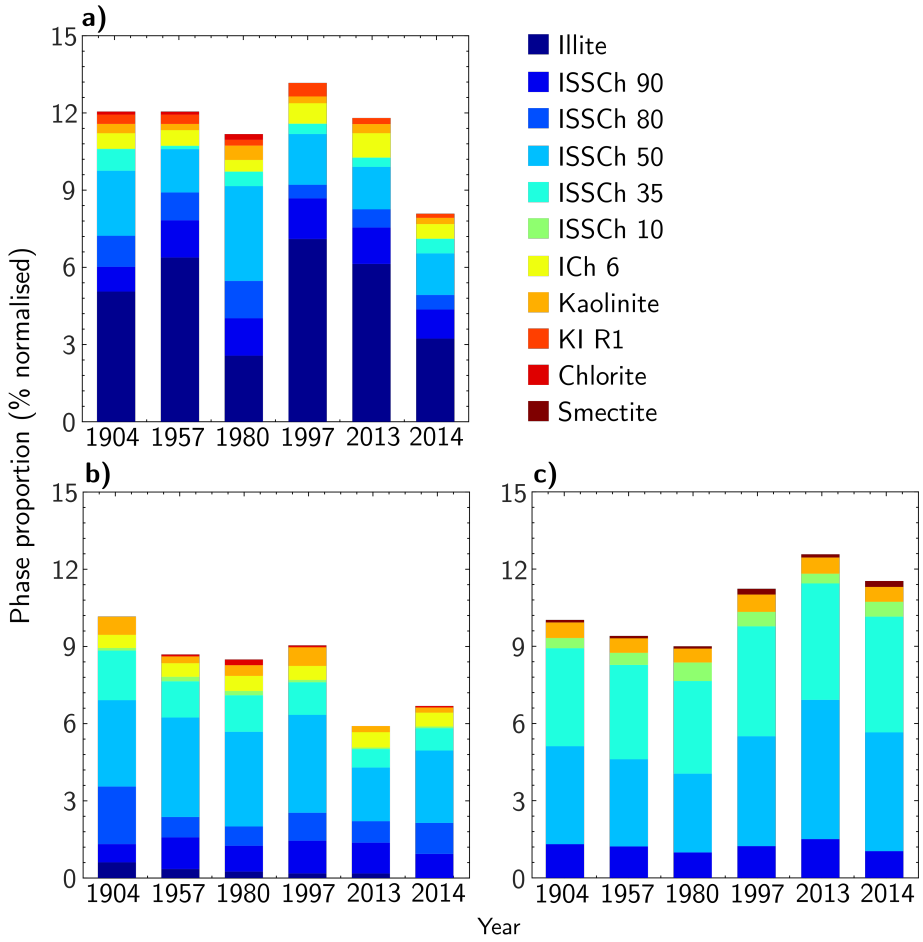

Figure A.2: Results of quantitative phase analysis on the evolution of phase proportions within the different fractions and subfractions of the 2014 RU sample. a) 2-0.2 μm, b) 0.2-0.05 μm, and c) <0.05 μm subfractions. The samples display no significant changes in mineralogical composition with time, although a size evolution is noted.

A.3 Particle size distribution

Table A.1: Results of size fractionation for all subplots and years 1904-2014

Sample	2000-50 μm	50-2 μm	<2 μm	2-0.2 μm	0.2-0.05 μm	<0.05 μm
1904 CU	4.2	60.9	34.9	13.5	10.7	10.7
1904 RU	3.5	63.9	32.6	12.2	10.3	10.1
1957 CF	6.9	65.1	28	9.1	8.6	10.3
1957 CU	7.8	66.6	25.6	9.7	7.7	8.2
1957 RF	8.1	65.1	26.9	9.9	7.8	9.2
1957 RU	7.9	61.6	30.6	12.2	8.9	9.5
1980 CF	6.8	63.3	29.9	9.9	7.4	12.6
1980 CU	4.8	63.6	31.6	11.0	7.5	13.2
1980 RF	7.6	66.2	26.2	9.1	6.6	10.6
1980 RU	6.9	64.3	28.8	11.3	8.5	9.1
1997 CF	6.4	63.1	30.5	10.4	7.7	12.4
1997 CU	4.7	63.2	32.2	10.8	7.1	14.3
1997 RF	7.1	65.2	27.7	10.7	8.1	8.9
1997 RU	5.9	60.4	33.8	13.3	9.2	11.3
2013 CF	6.2	64.0	29.8	9.6	6.3	13.8
2013 CU	7.8	66.2	26.1	7.8	7.3	11.0
2013 RF	5.2	63.0	31.9	10.2	7.0	14.7
2013 RU	9.2	60.1	30.6	11.9	6.1	12.7
2014 CF	7.5	65.7	26.8	8.5	6.2	12.1
2014 CU	6.8	66.8	26.4	8.8	5.7	12.0
2014 RF	3.8	66.3	29.9	9.0	5.9	15.0
2014 RU	8.3	65.1	26.6	8.2	6.8	11.6

A.4 Phase proportions

Table A.2: Results of quantitative phase analysis using the Rietveld method for 50-2 μm subfractions.

Sample	Albite	Anatase	Calcite	Chlorite	Hornblende	Kaolinite	Microcline	Mica	Quartz
1904 CU	10.3	0.4	0.3	1.5	0.8	1.3	10.8	3.8	71.2
1904 RU	11.1	0.3	0.4	1.7	0.6	1.1	12.0	4.8	68.3
1957 CF	11.2	0.3	0.3	2.1	0.5	1.4	11.1	5.3	68.1
1957 CU	11.0	0.5	0.2	1.6	0.5	0.9	12.2	5.4	68.1
1957 RF	10.4	0.6	0.2	1.9	0.5	1.0	11.7	5.2	69.0
1957 RU	11.6	0.6	0.2	1.9	0.9	1.2	12.2	4.9	67.1
1980 CF	11.0	0.3	0.3	2.0	0.7	1.6	11.1	4.7	68.7
1980 CU	10.0	0.4	0.2	2.4	0.6	1.5	10.9	6.7	67.6
1980 RF	10.8	0.5	0.2	2.0	0.6	1.2	10.1	5.4	69.5
1980 RU	10.4	0.5	0.3	2.0	0.8	1.2	11.8	6.0	67.5
1997 CF	10.4	0.3	0.3	2.0	0.6	1.3	10.3	6.3	68.9
1997 CU	10.0	0.5	0.2	1.7	0.7	1.2	10.6	6.5	69.1
1997 RF	10.1	0.6	0.3	1.7	0.5	1.3	11.4	5.6	69.2
1997 RU	10.4	0.8	0.3	1.8	0.7	1.1	11.6	5.4	68.8
2013 CF	12.2	1.0	0.3	2.1	0.5	1.3	10.8	5.0	67.8
2013 CU	12.0	1.3	0.4	1.2	0.7	1.1	10.9	5.7	68.0
2013 RF	10.9	0.3	0.3	2.0	0.7	1.6	10.4	4.3	69.8
2013 RU	10.0	0.8	0.2	1.7	0.5	0.8	11.3	5.4	69.9
2014 CF	12.0	1.3	0.4	1.7	0.5	1.4	10.4	5.5	68.1
2014 CU	13.2	1.4	0.2	1.8	0.5	1.4	11.0	4.6	67.2
2014 RF	9.6	1.0	0.3	2.0	0.7	0.8	10.6	5.9	70.1
2014 RU	11.1	1.0	0.3	1.7	0.5	0.7	11.4	5.5	68.8

Table A.3: Quantitative phase results from full-pattern modelling using the Sybilla programme for 2-0.2 μm subfractions. Values are provided for both AD and EG states.

Sample	Illite		ISSCh 90		ISSCh 80		ISSCh 50		ISSCh 35		ISSCh 5		Kaolinite		KI R1		Chlorite		ICh 6		SS	
	AD	EG	AD	EG	AD	EG	AD	EG	AD	EG	AD	EG	AD	EG	AD	EG	AD	EG	AD	EG	AD	EG
1904 RU	45	42	10	8	11	10	17	21	5	7	<1	<1	6	5	3	3	2	3	1	1		
1957 CF	19	19	13	11	15	12	28	30	11	14	1	2	6	5	4	4	3	3				
1957 CU	26	26	16	11	12	10	21	27	12	12	0	1	5	5	6	4	3	4		0		
1957 RF	35	31	10	9	20	17	19	22	4	7	<1	<1	5	5	4	3	2	4	1	2		
1957 RU	55	53	14	12	9	9	9	14	2	1	<1	<1	5	5	2	2	3	3	1	1		
1980 CF	52	51	9	8	13	12	12	15	2	3	0	<1	6	5	3	3	2	2	1	1		
1980 CU	49	47	12	11	13	12	10	14	2	2	<1	<1	7	7	3	2	4	4	1	1		
1980 RF	45	43	16	13	10	8	15	20	1	3	<1	<1	6	6	5	3	2	4				
1980 RU	26	23	12	13	15	13	29	33	5	5	<1	<1	6	4	2	5	3	2	2	2		
1997 CF	46	47	13	10	12	8	15	20	2	2	0	<1	6	7	3	2	2	3	1	1		
1997 CU	41	41	15	10	16	14	14	18	1	4	<1	<1	7	6	3	3	2	3	1	1		
1997 RF	46	46	14	10	11	9	14	18	2	3	0	<1	5	6	3	3	3	3	2	2		
1997 RU	57	54	13	12	6	4	11	15	2	3	<1	<1	5	6	2	2	4	4				
2013 CF	26	26	17	14	19	11	22	29	4	8	0	<1	7	6	2	4	2	2	1	0		
2013 CU	41	40	19	15	14	16	11	14	1	4	<1	<1	9	9	2	1	2	1	1	<1		
2013 RF	29	26	12	10	10	8	28	37	6	5	0	1	6	6	7	4	1	2	1	1		
2013 RU	56	52	14	12	7	6	9	14	1	3	<1	<1	8	8	3	3	2	2				
2014 CF	36	37	13	12	16	9	20	24	3	5	0	<1	8	7	<1	2	2	2	2	2		
2014 CU	34	31	15	15	18	16	17	20	2	5	<1	1	8	8	2	1	1	1	3	2		
2014 RF	32	30	12	13	11	10	21	27	6	7	<1	<1	7	7	8	2	2	3	1	1		
2014 RU	44	40	16	14	9	7	14	20	4	7	<1	<1	7	7	3	3	3	2				

Table A.4: Quantitative phase results from full-pattern modelling using the Sybilla programme for 0.2-0.05 μm subfractions. Values are provided for both AD and EG states.

Sample	Illite		ISSCh 90		ISSCh 80		ISSCh 50		ISSCh 35		ISSCh 5		Kaolinite		KI R1		Chlorite		ICh 6		SS	
	AD	EG	AD	EG	AD	EG	AD	EG	AD	EG	AD	EG	AD	EG	AD	EG	AD	EG	AD	EG	AD	EG
1904 CU	7	7	12	10	13	9	44	44	12	16	1	2	6	5	5	6			1	1		
1904 RU	7	6	9	7	23	22	35	33	14	19	1	1	5	5	6	7			1	0		
1957 CF	8	8	10	9	13	8	42	43	12	16	3	3	8	6	2	5			2	2		
1957 CU	3	1	8	7	15	13	42	40	19	23	1	3	5	6	5	6			2	1		
1957 RF	4	3	13	11	11	8	41	43	17	22	2	2	6	6	5	5			1	1		
1957 RU	6	4	18	14	11	9	41	44	11	16	1	2	7	6	4	3			1	2		
1980 CF	1	2	9	8	14	12	45	42	12	17	1	1	7	6	8	10			3	2		
1980 CU	1	2	11	9	12	10	36	35	16	21	3	3	9	7	9	10			3	3		
1980 RF	5	4	11	8	16	15	35	33	15	20	<1	2	7	7	10	10			1	1		
1980 RU	3	3	15	12	12	9	45	44	12	17	1	2	7	7	4	5			1	1		
1997 CF	1	1	12	9	12	10	42	42	17	21	1	2	8	7	6	7			1	1		
1997 CU	1	1	11	9	15	14	43	42	14	19	1	2	7	6	6	7			2	1		
1997 RF	4	3	14	12	15	13	36	33	14	17	1	2	7	7	8	12			1	1		
1997 RU	5	2	15	14	11	12	41	42	12	14	1	1	7	6	7	8			1	1		
2013 CF	2	2	18	14	13	15	38	37	9	11	<1	1	14	15	5	4			1	1		
2013 CU	1	1	13	11	17	16	42	39	10	15	<1	1	12	12	4	4			1	1		
2013 RF	2	2	14	13	15	13	36	35	10	14	<1	1	15	15	7	7			1	<1		
2013 RU	4	3	23	20	14	14	35	35	10	12	<1	1	9	10	5	4			<1	1		
2014 CF	2	1	19	16	19	17	33	35	11	14	<1	1	6	6	9	9			1	1		
2014 CU	1	1	18	16	16	13	34	35	9	13	<1	1	15	14	6	6			1	1		
2014 RF	2	1	19	20	22	20	26	27	10	11	<1	1	15	15	6	5			<1	<1		
2014 RU	0	0	17	14	22	18	40	42	8	13	<1	1	8	8	4	3			1	1		

Table A.5: Quantitative phase results from full-pattern modelling using the Sybilla programme for <0.05 μm subfractions. Values are provided for both AD and EG states.

Sample	Illite		ISSCh 90		ISSCh 80		ISSCh 50		ISSCh 35		ISSCh 5		Kaolinite		KI R1		Chlorite		ICh 6		SS	
	AD	EG	AD	EG	AD	EG	AD	EG	AD	EG	AD	EG	AD	EG	AD	EG	AD	EG	AD	EG	AD	EG
1904 CU			18	15			37	38	31	33	6	6			7	7					1	1
1904 RU			14	13			38	38	37	38	2	4			8	6					1	1
1957 CF			13	13			40	38	33	36	5	6			8	5					1	2
1957 CU			11	7			35	35	39	43	7	8			6	5					2	2
1957 RF			13	11			36	36	38	38	4	6			7	7					2	2
1957 RU			13	13			36	36	40	39	3	5			7	6					1	1
1980 CF			12	10			40	40	31	33	6	9			10	6					1	2
1980 CU			11	9			37	37	39	39	5	7			7	6					1	2
1980 RF			11	8			37	35	39	41	5	7			7	7					2	2
1980 RU			10	11			32	34	41	40	8	8			8	6					1	1
1997 CF			13	9			36	36	36	40	7	9			6	4					2	2
1997 CU			13	8			40	41	35	37	4	7	1	<1	6	5					1	2
1997 RF			15	11			36	38	37	38	5	6			6	6					1	1
1997 RU			12	11			35	38	37	38	6	5			8	6					2	2
2013 CF			12	10			38	38	41	41	3	5			5	4					1	2
2013 CU			13	10			37	40	38	39	4	5	1	1	5	4					2	1
2013 RF			12	9			39	42	39	39	5	5			4	4					1	1
2013 RU			12	12			44	43	36	36	2	3			5	5					1	1
2014 CF			13	9			30	32	43	44	7	9			6	4					1	2
2014 CU			11	9			40	40	42	42	2	4			4	4					1	1
2014 RF			12	10			35	36	41	42	5	6			5	5					2	1
2014 RU			13	9			39	40	38	39	3	5			5	5					2	2

A.5 Fitted XRD profiles

1904

Figure A.3: 1904 CU

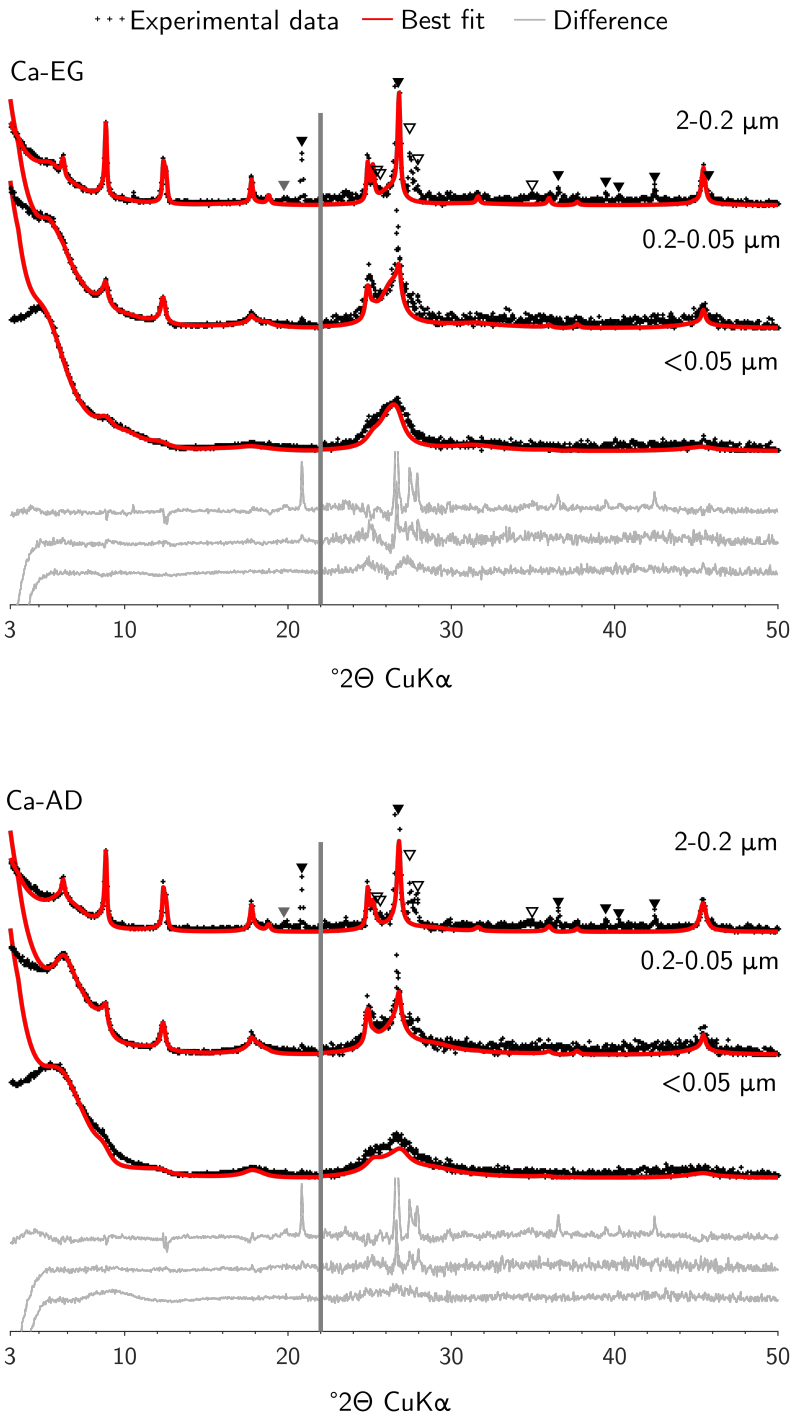

Figure A.4: 1904 RU

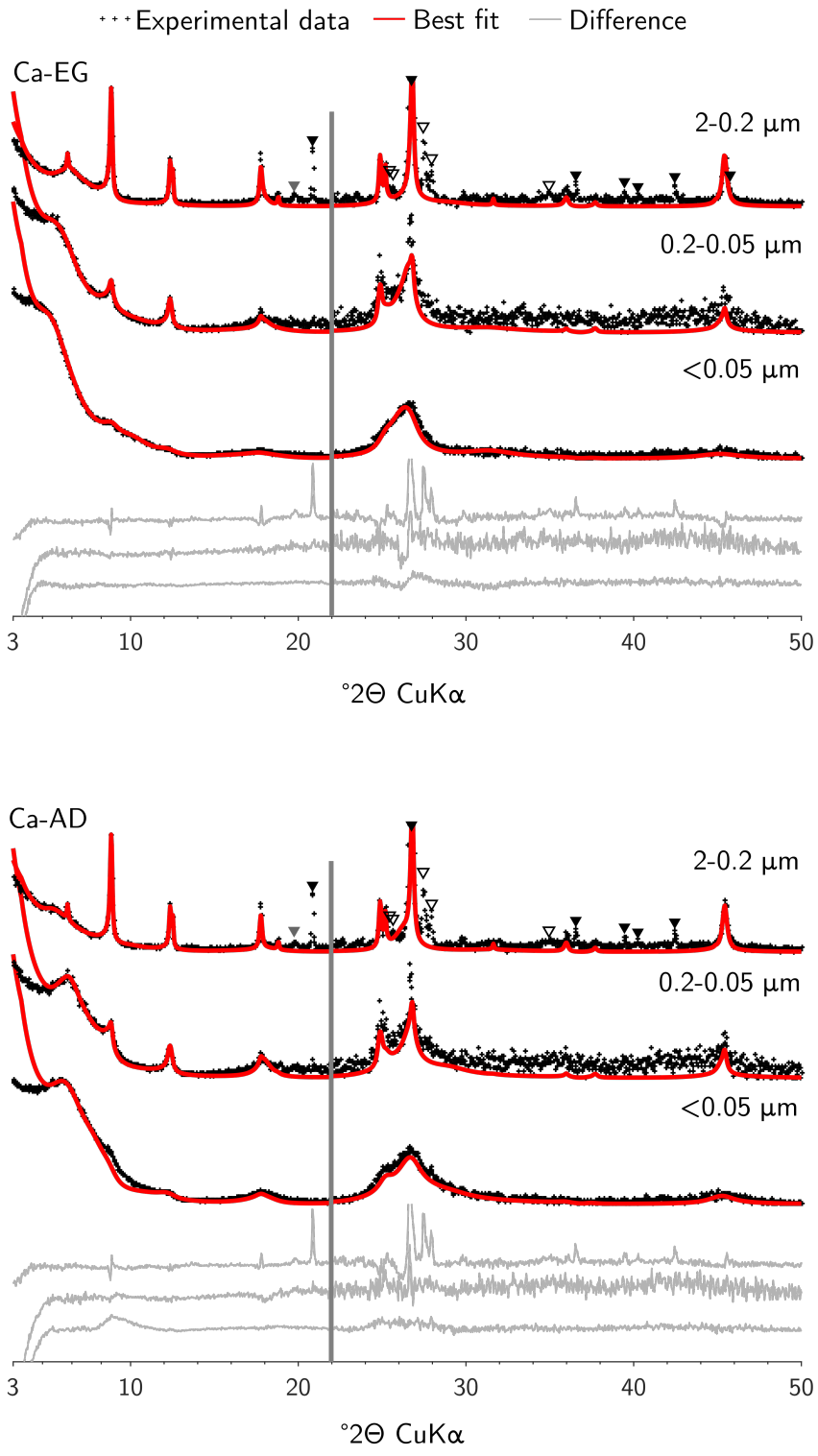

1957

Figure A.5: 1957 CF

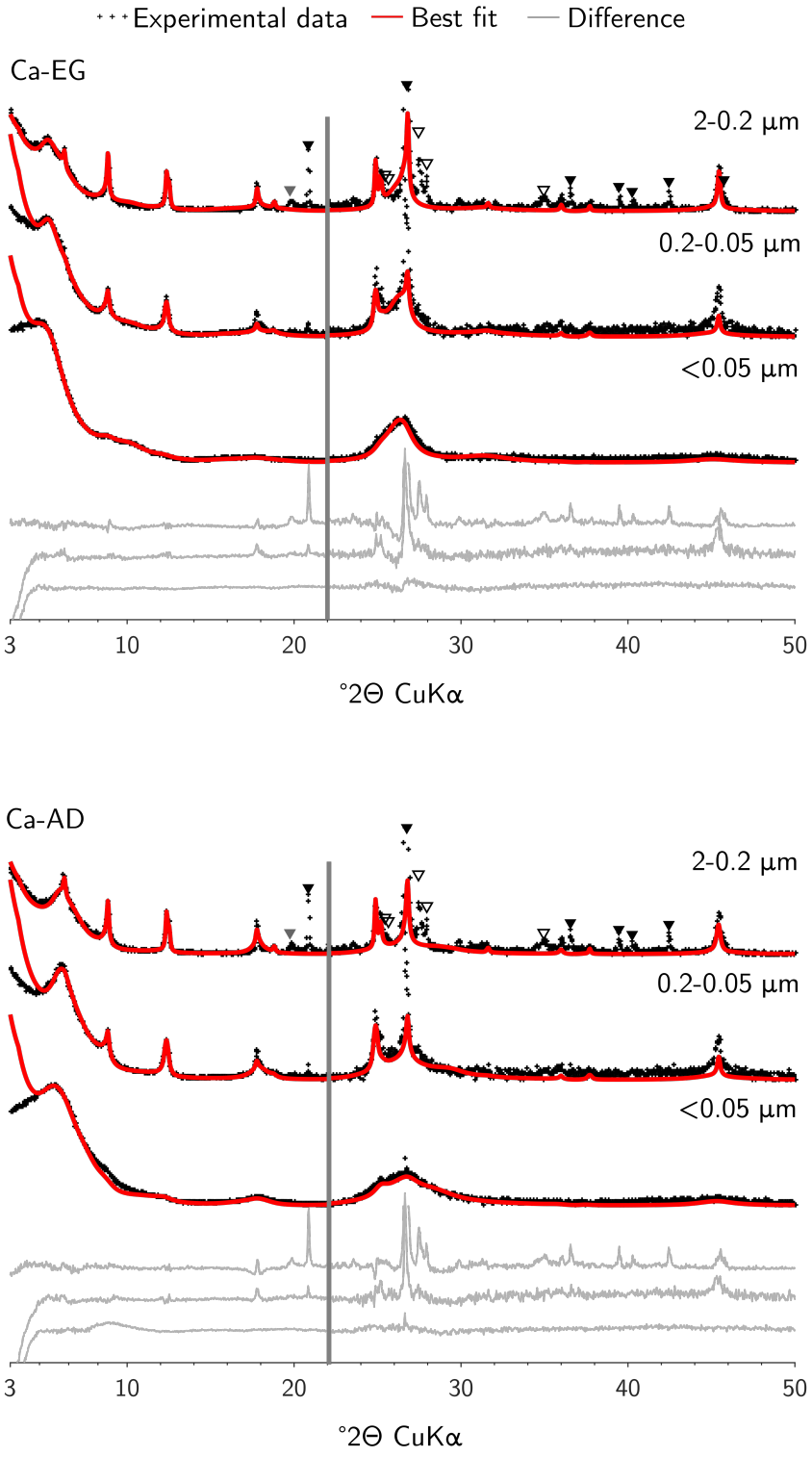

Figure A.6: 1957 CU

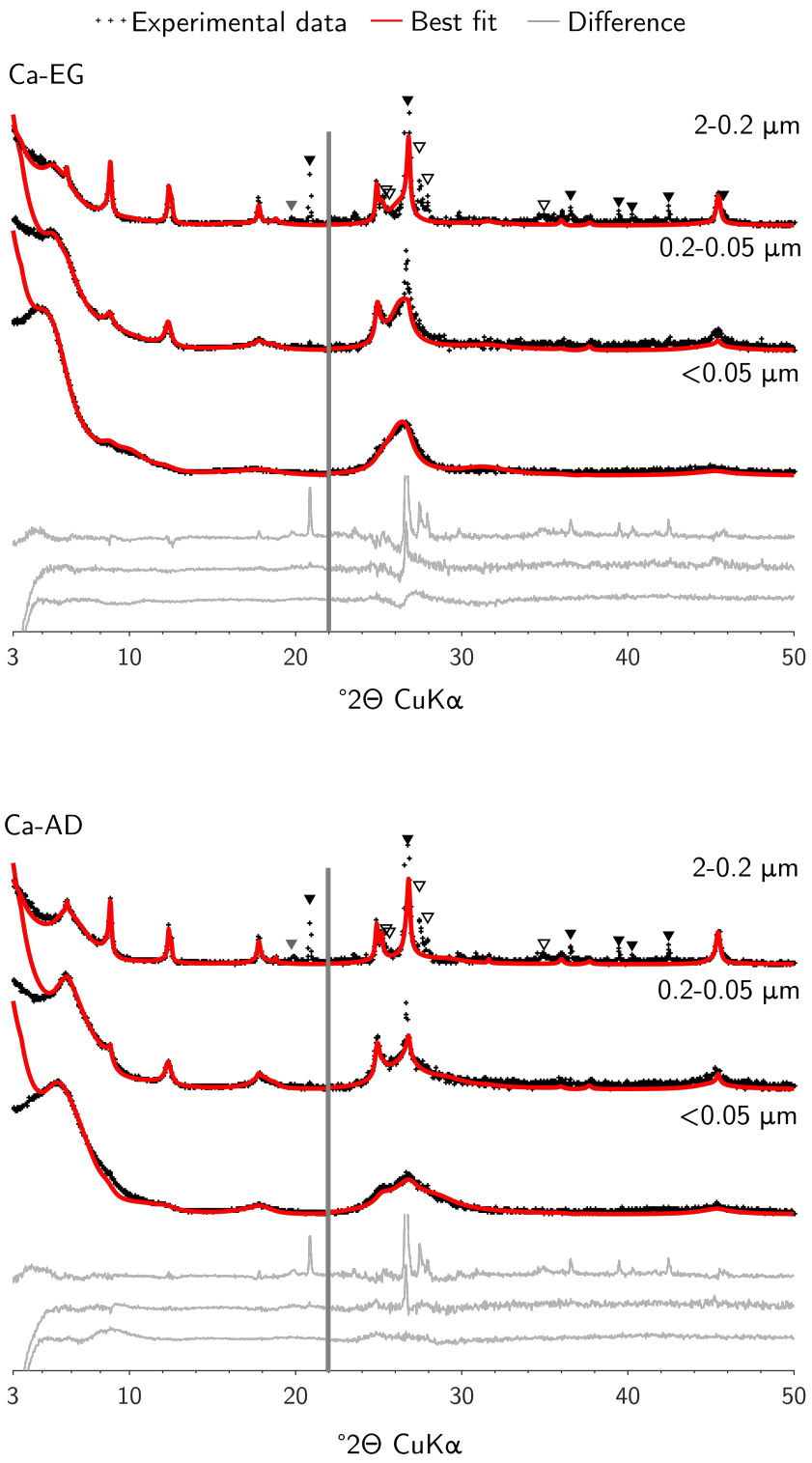

Figure A.7: 1957 RF

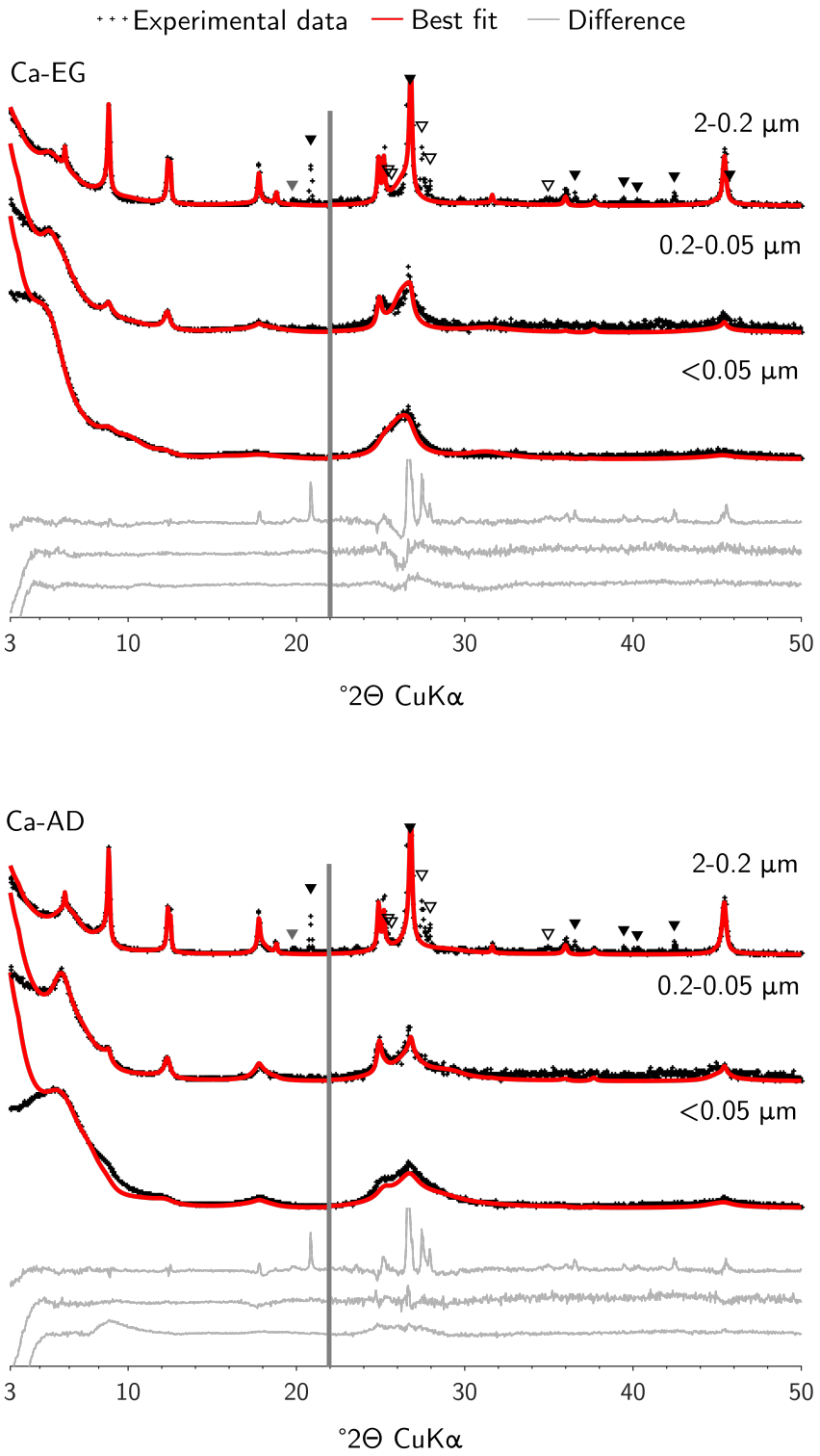

Figure A.8: 1957 RU

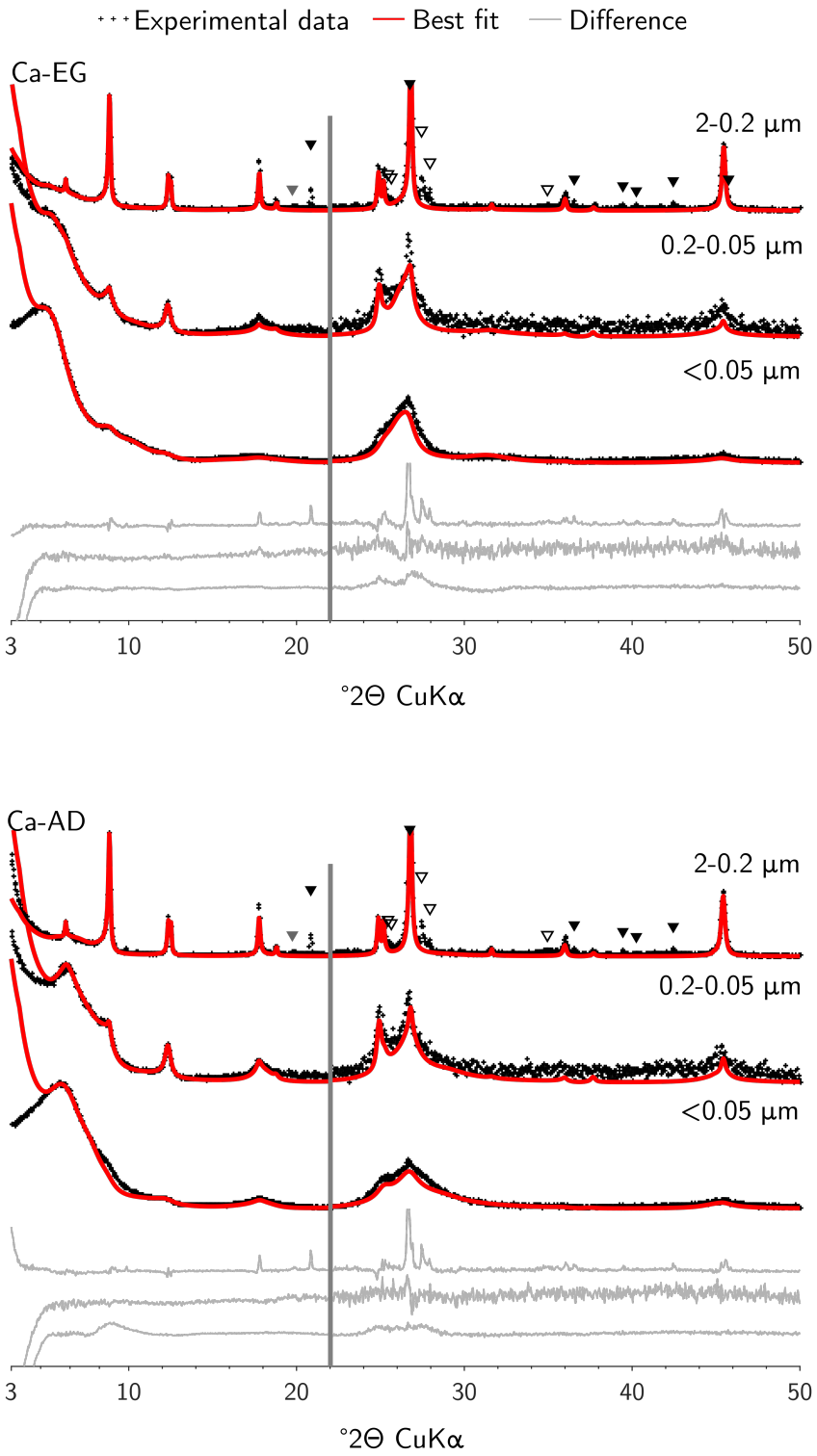

1980

Figure A.9: 1980 CF

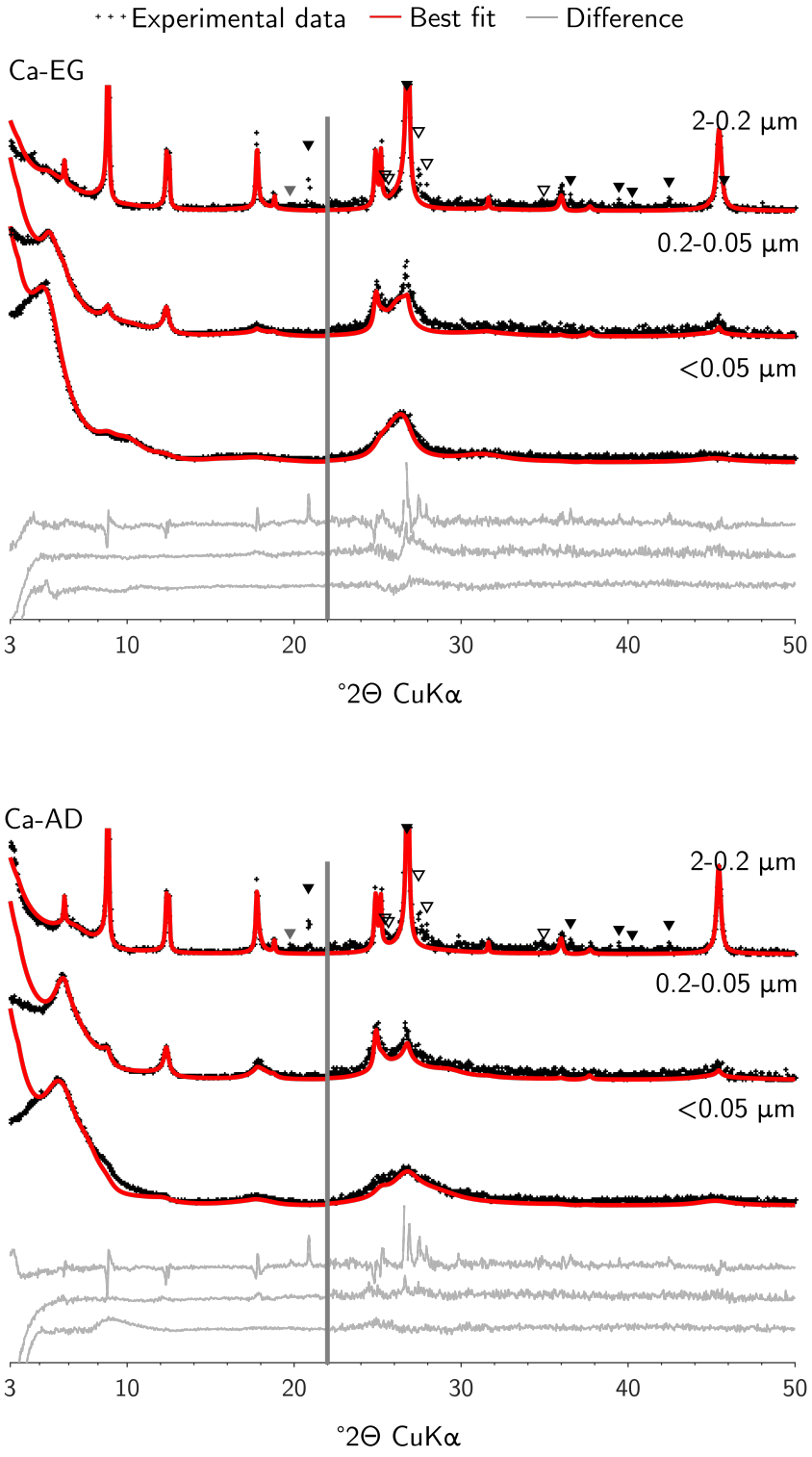

Figure A.10: 1980 CU

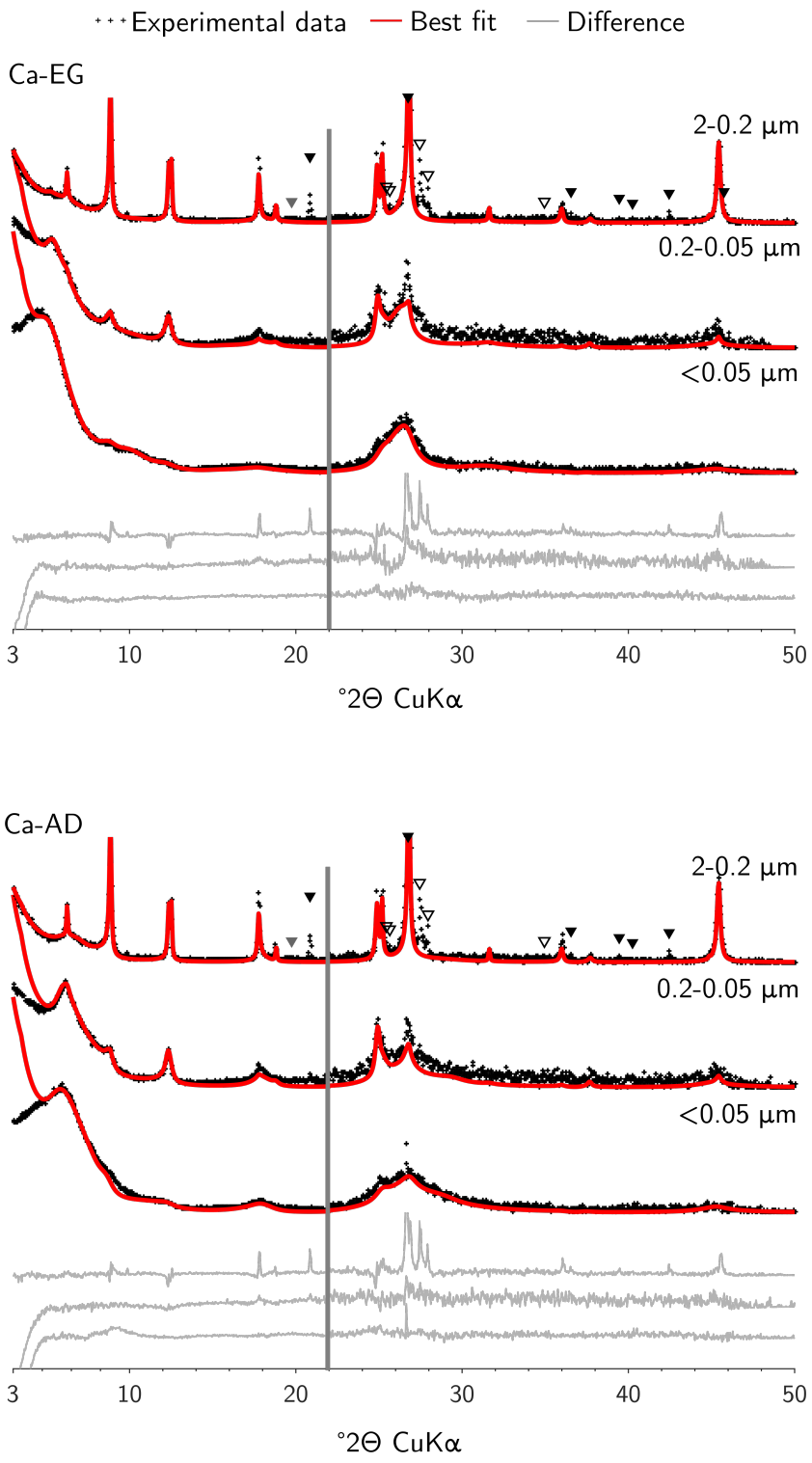

Figure A.11: 1980 RF

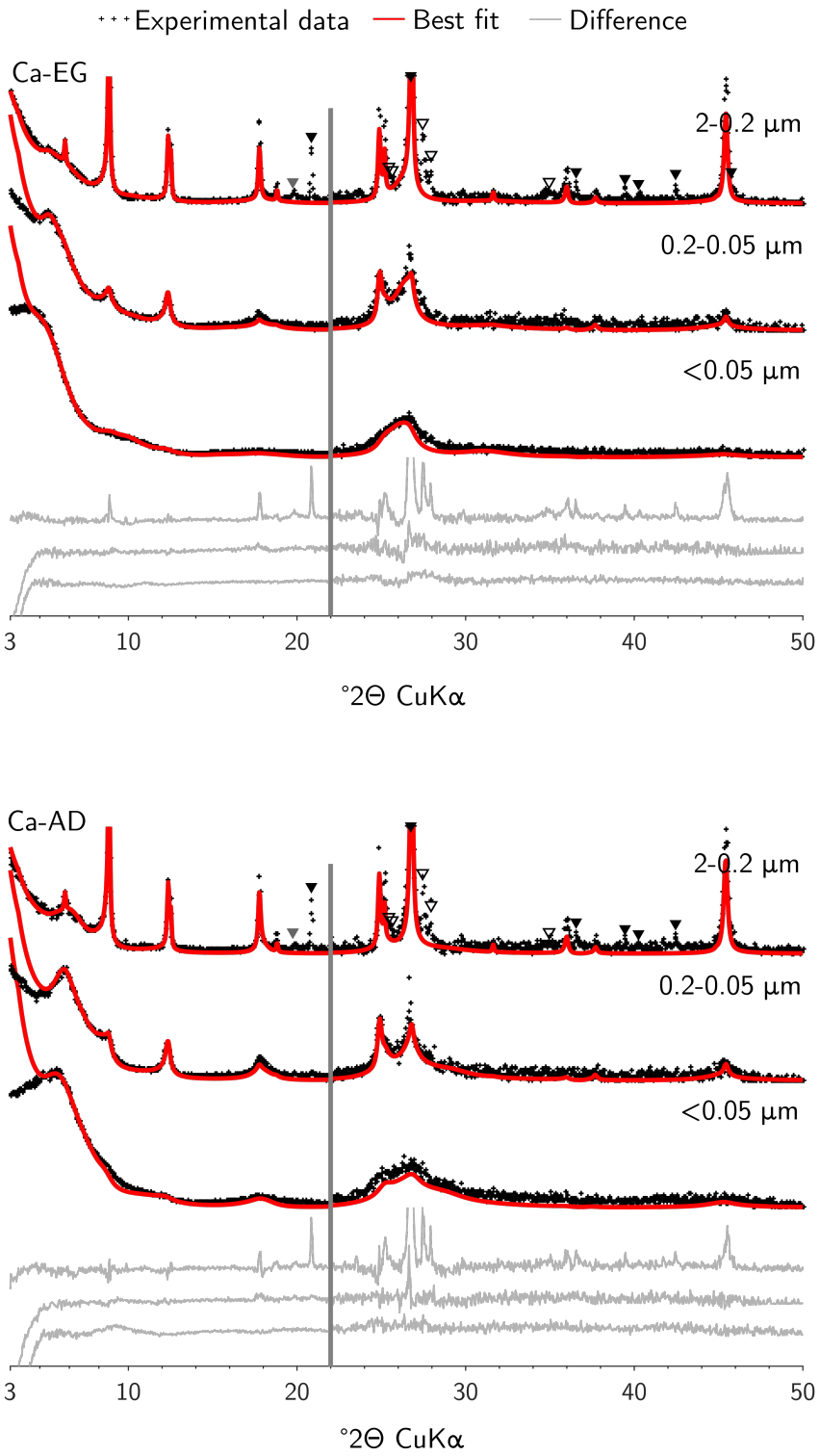

Figure A.12: 1980 RU

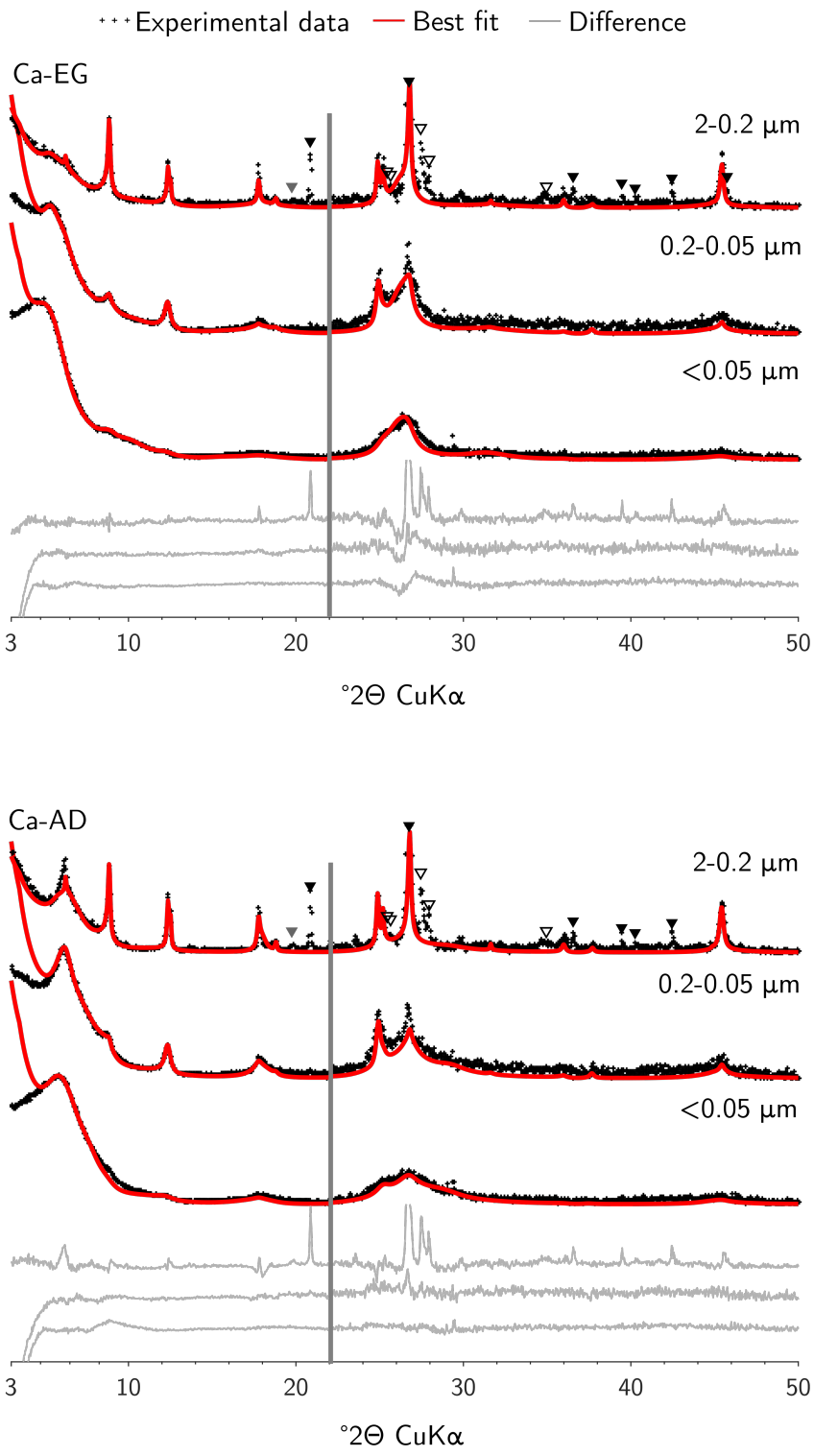

1997

Figure A.13: 1997 CF

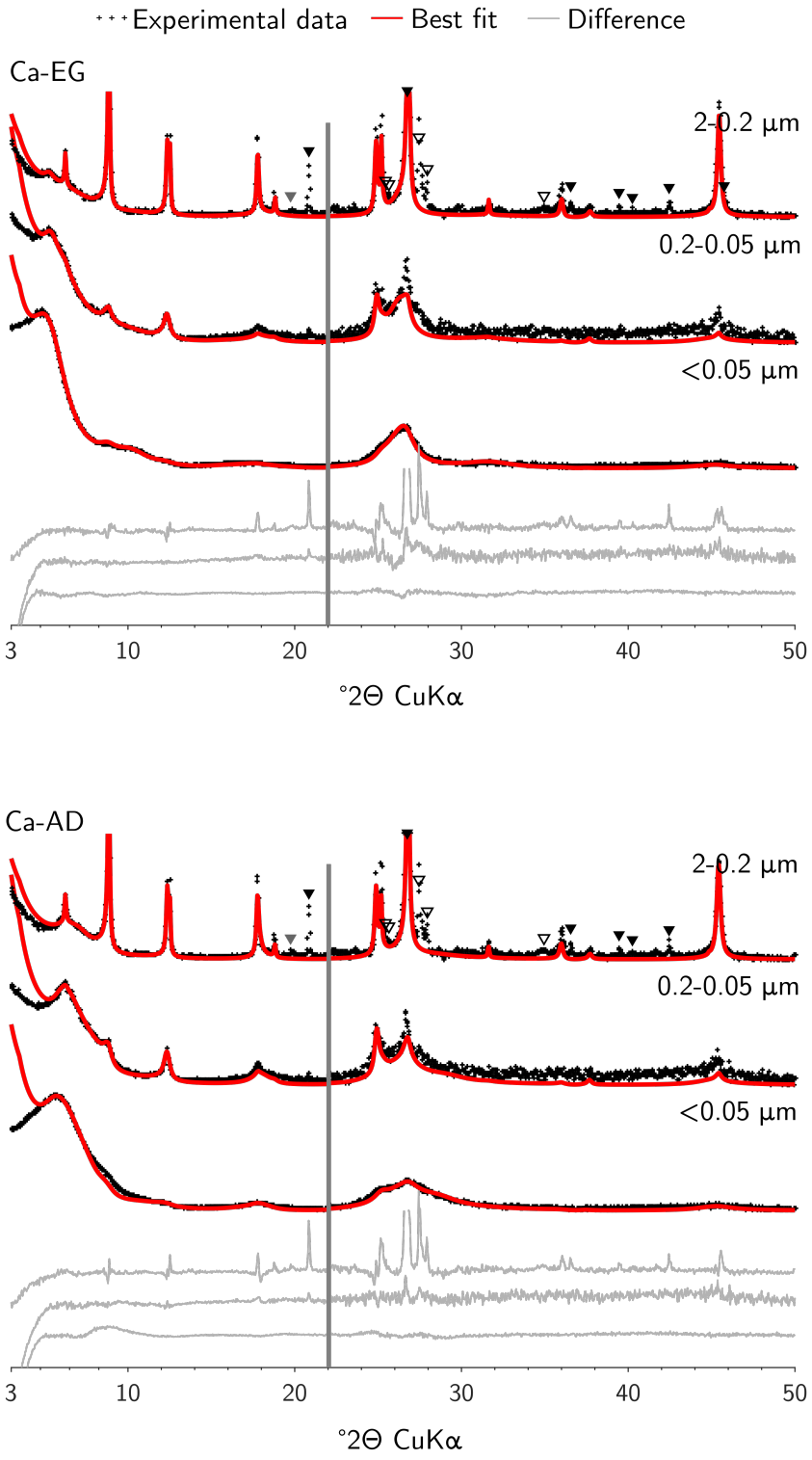

Figure A.14: 1997 CU

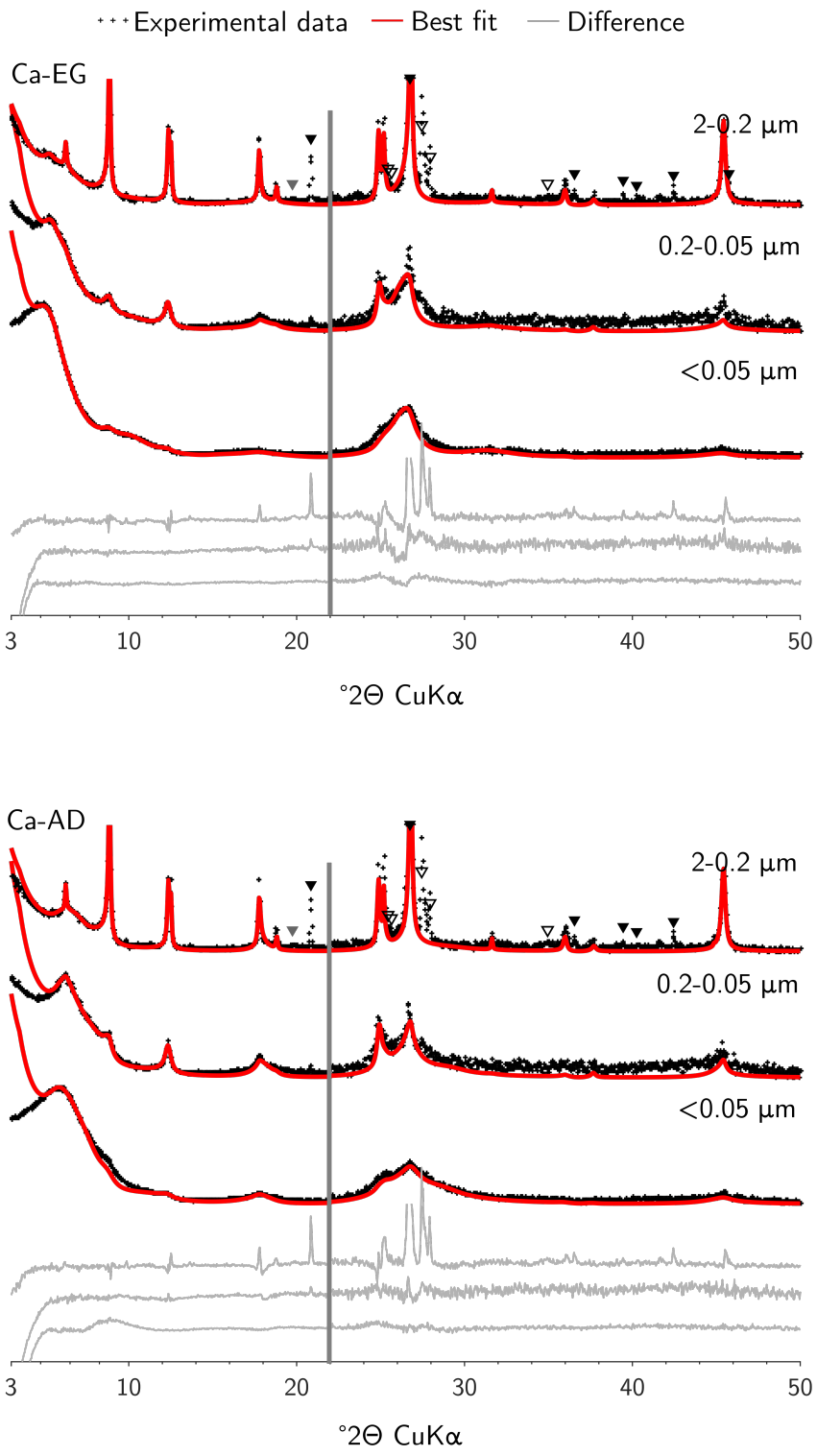

Figure A.15: 1997 RF

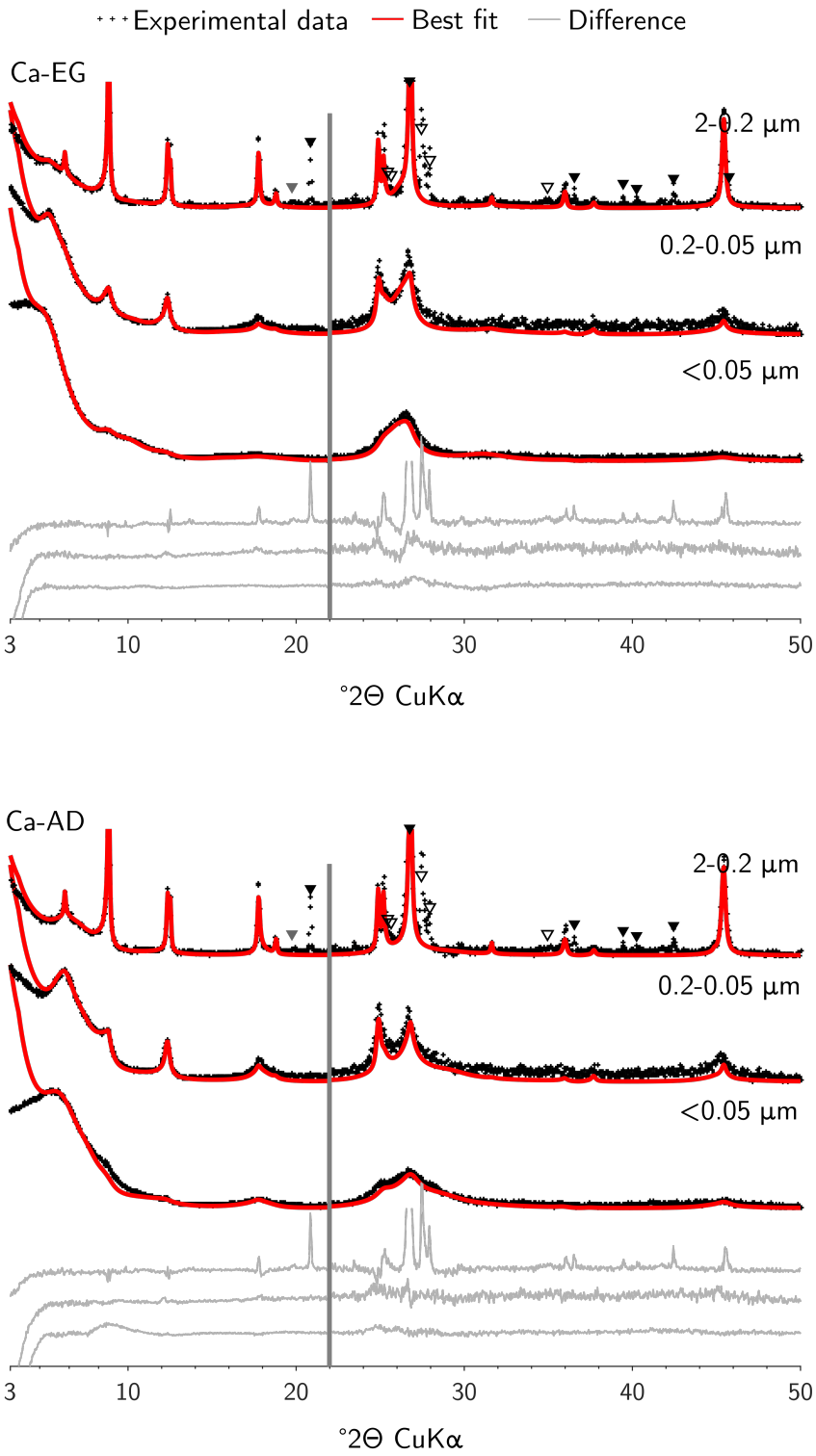

Figure A.16: 1997 RU

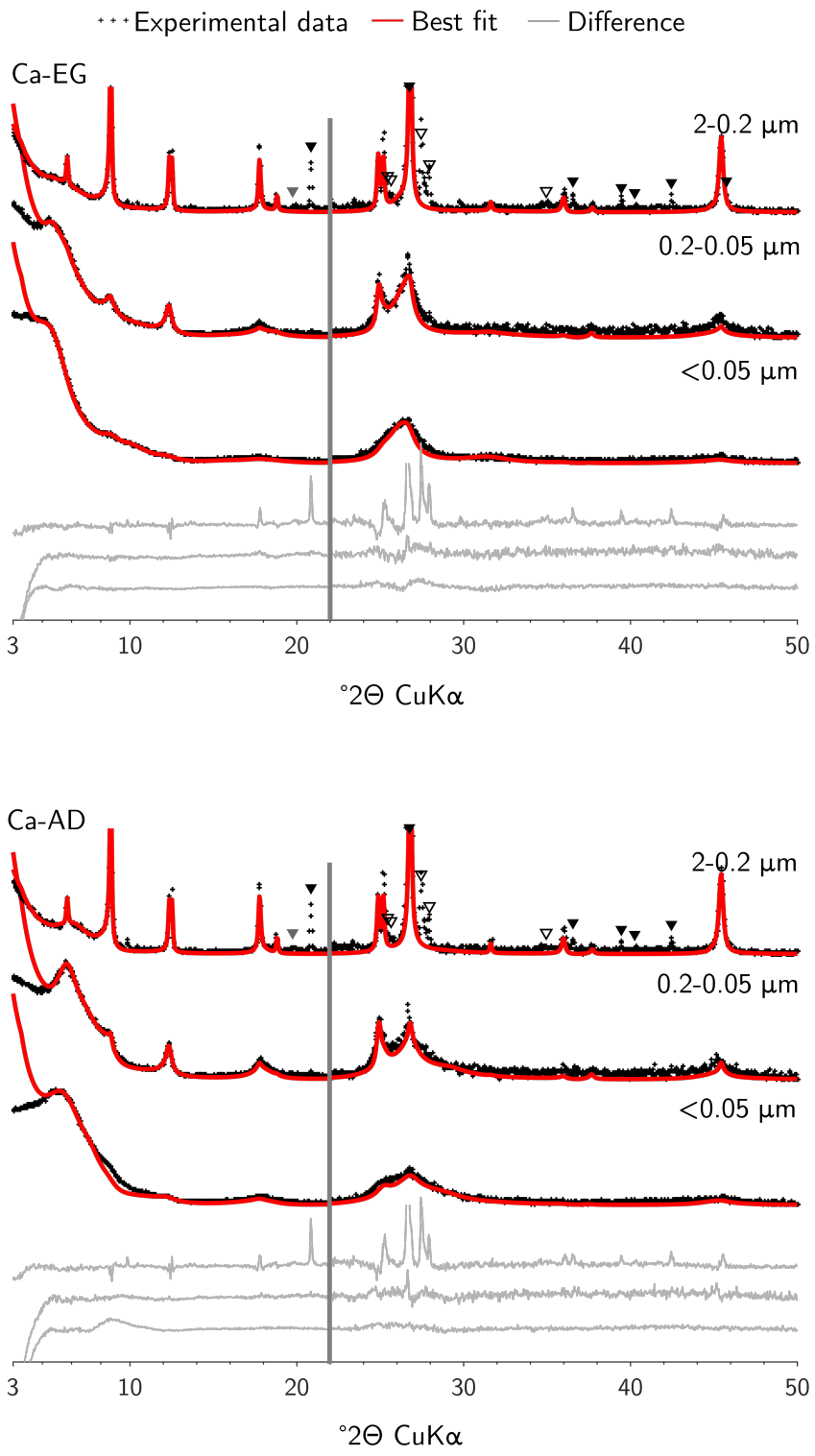

2013

Figure A.17: 2013 CF

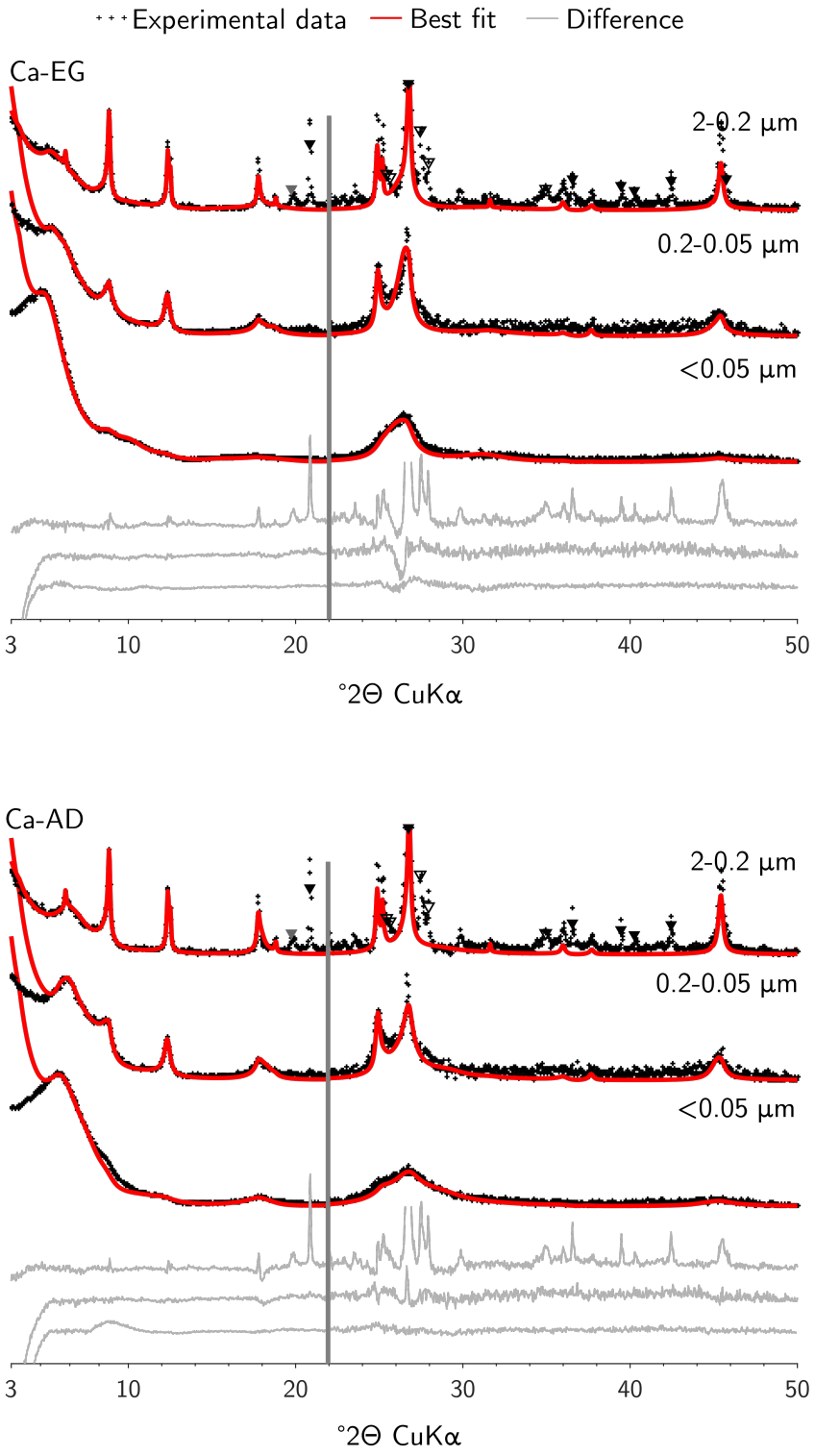

Figure A.18: 2013 CU

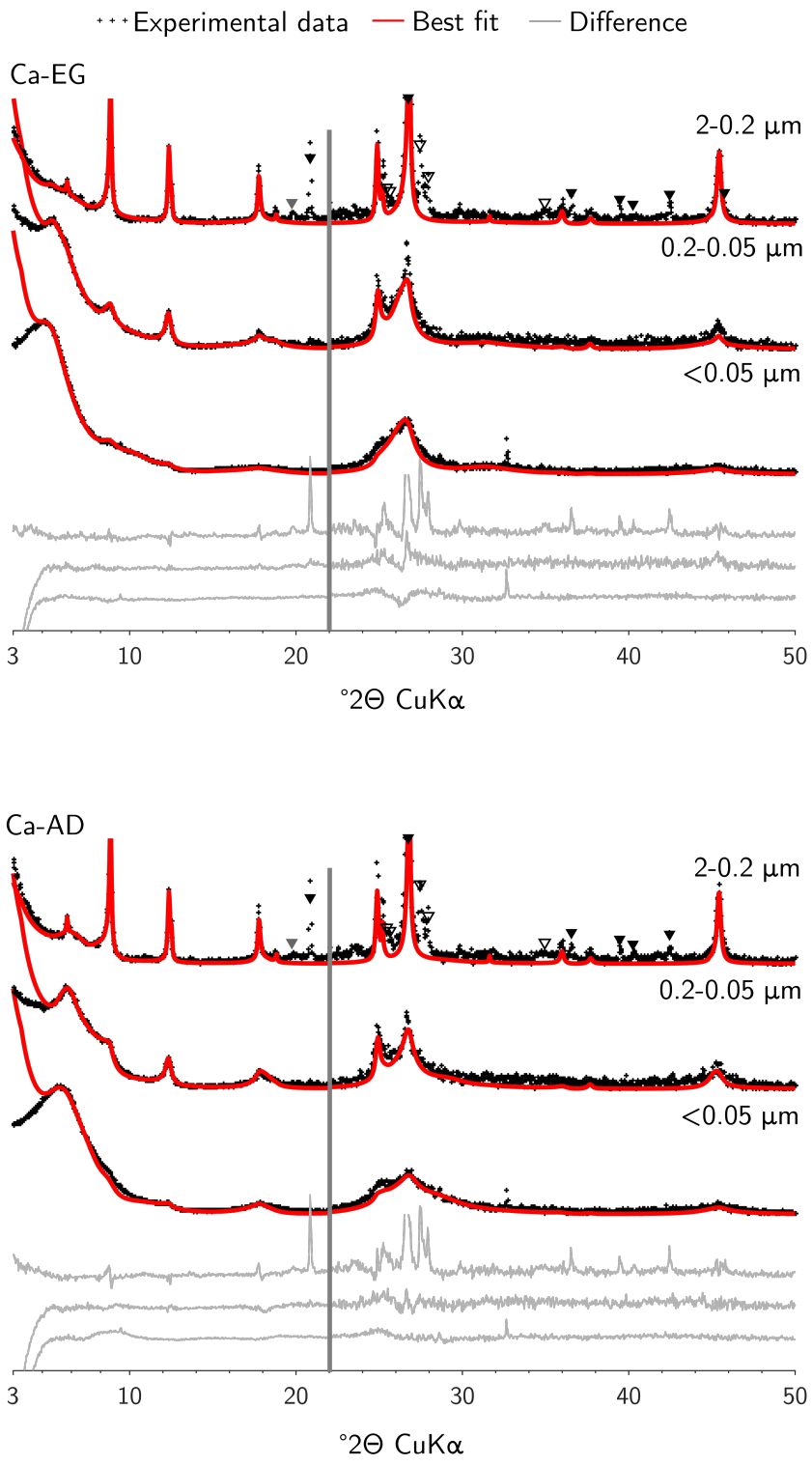

Figure A.19: 2013 RF

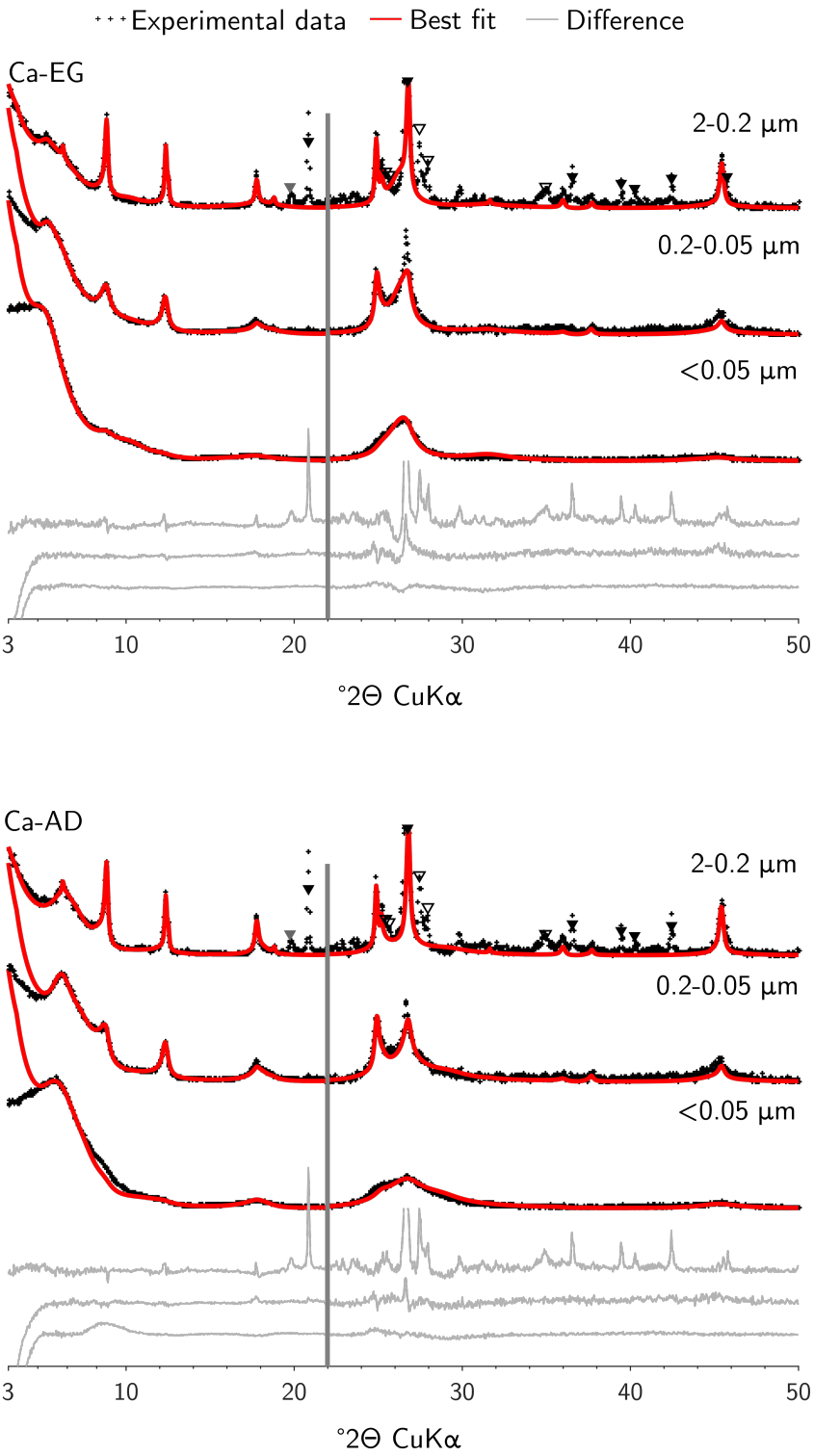

Figure A.20: 2013 RU

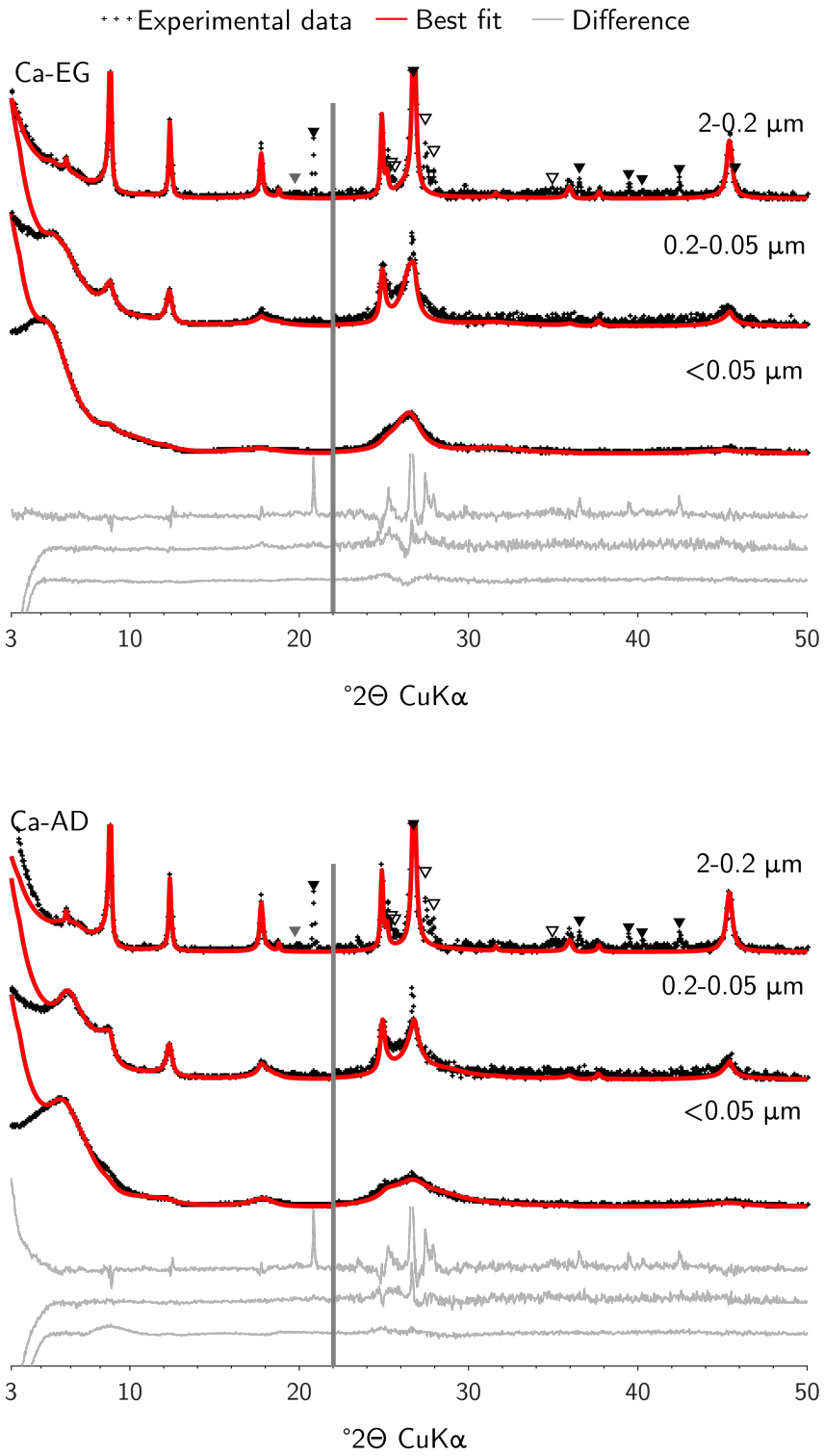

2014

Figure A.21: 2014 CF

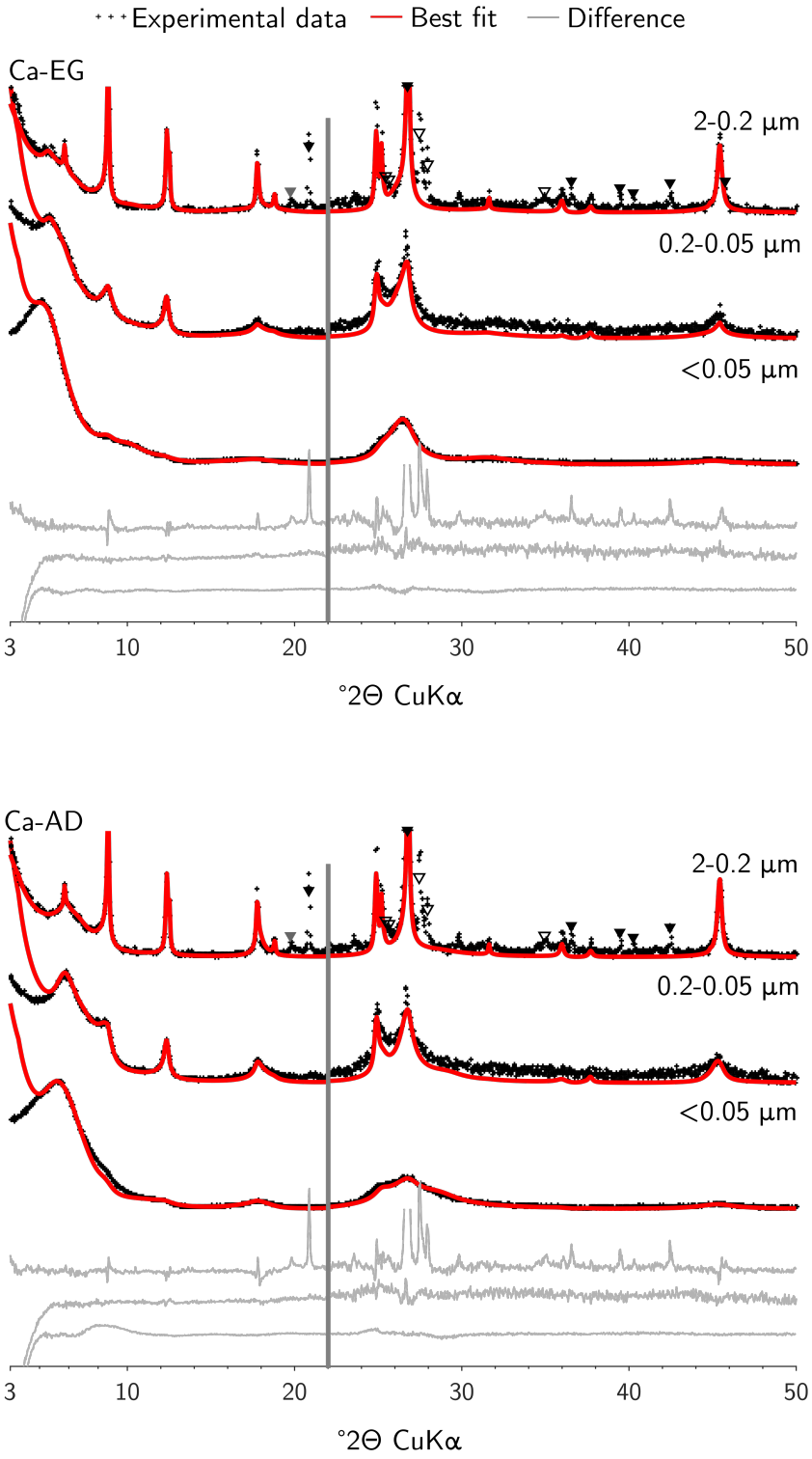

Figure A.22: 2014 CU

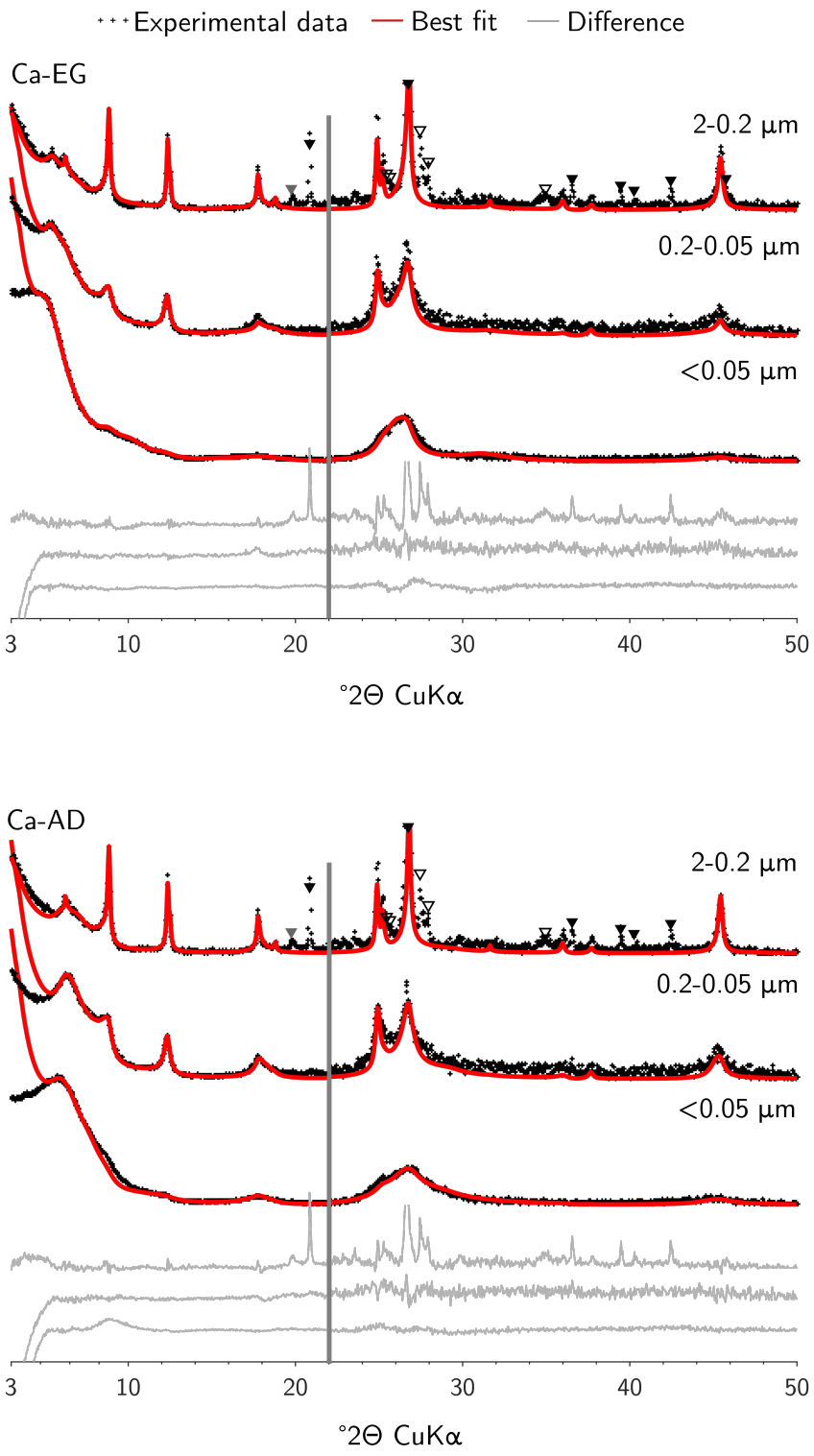

Figure A.23: 2014 RF

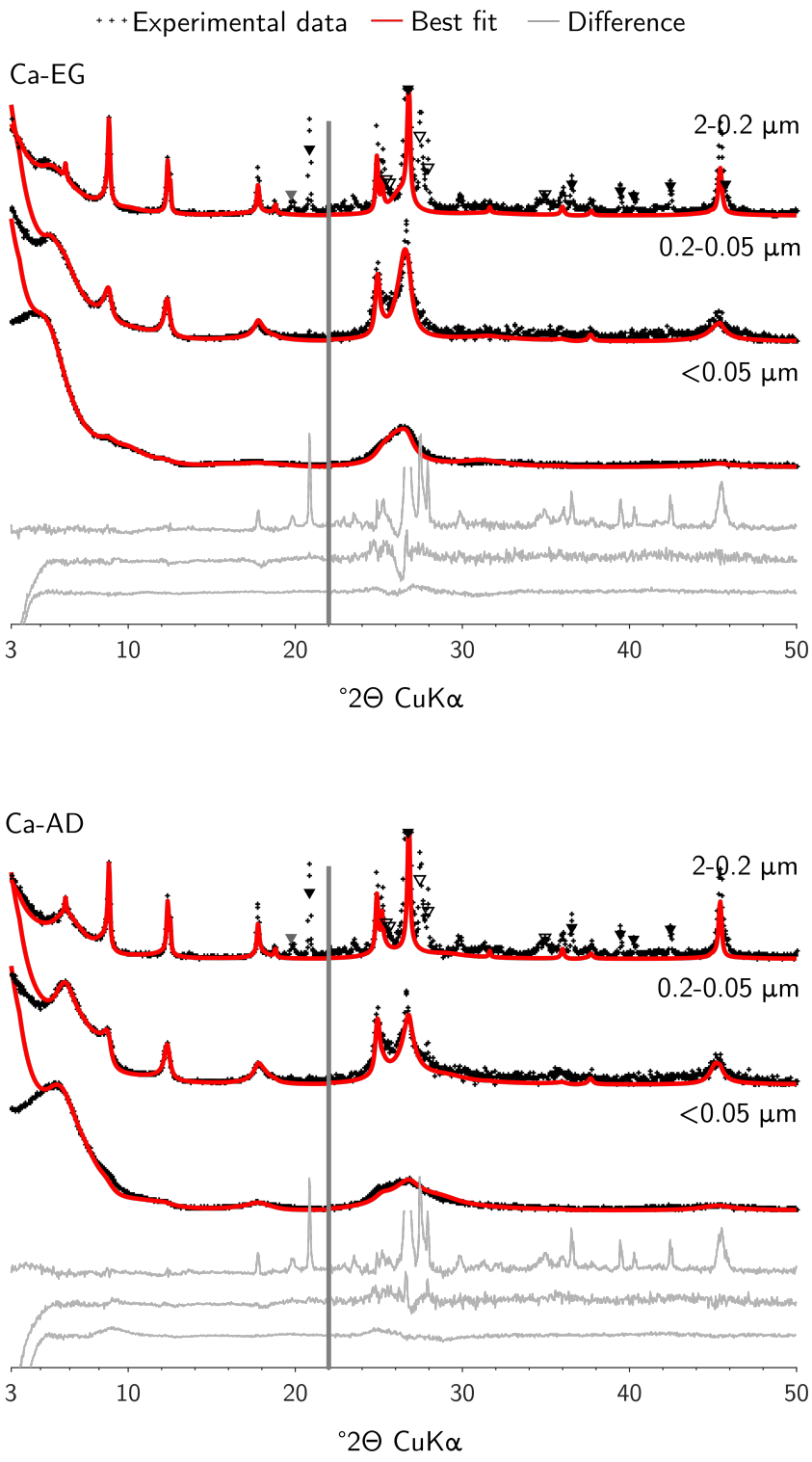

Figure A.24: 2014 RU

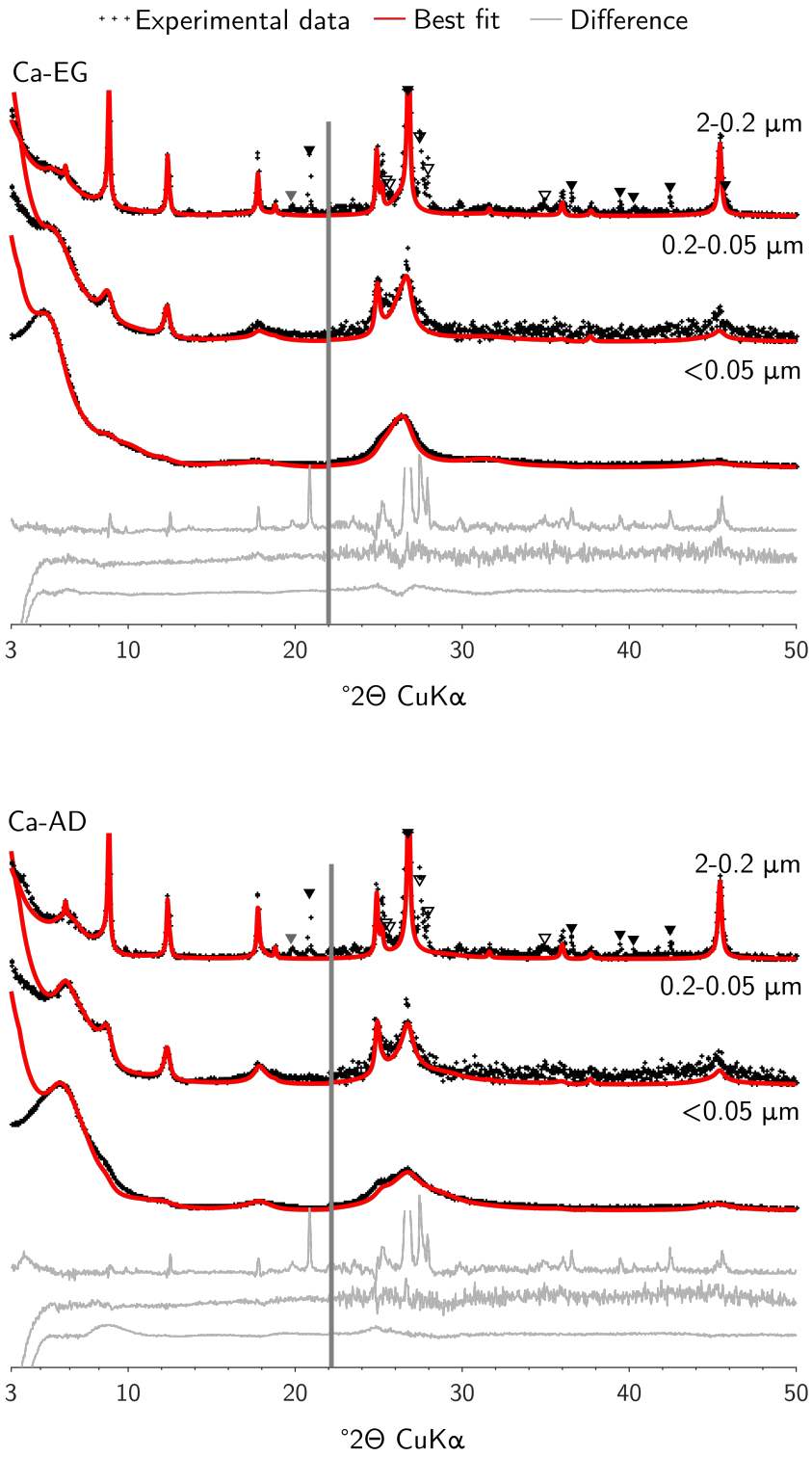

A.6 Structural parameters

The following pages include the layer-type composition and CSD size obtained for each contribution of 2-0.2, 0.2-0.05 and <0.05 μm subfractions of all subplots and years after full-profile XRD fitting using the Sybilla software for both Ca-AD and Ca-EG samples. A single value indicates parameters were unchanged between AD and EG states. The contributions are described in full in Chapter 2. Values for layer-type proportions are given in the form illite-smectite-smectite-chlorite (notation ISSCh). Fe_oh values were allowed to vary between subfractions, however values within each subfraction were consistent between the individual contributions and layer-types with the exception of discrete illite and chlorite phases. Values were used as follows: <0.05 $|mu$m ∼1.56, 0.2-0.05 μm ∼0.80 (discrete illite ∼0.00), 2-0.2 μm ∼0.00. Values are presented for samples in the order 1904-2014.

		1904 CU						**1904 RU**					
		2-0.2 μm		0.2-0.05 μm		<0.05 μm		2-0.2 μm		0.2-0.05 μm		<0.05 μm	
		AD	EG	AD	EG	AD	EG	AD	EG	AD	EG	AD	EG
Illite	N	34		22				34		25			
ISSC 90	I/S/S/C												
	N	19		12		10	9	27		14		10	9
ISSC 80	I/S/S/C	92/2/1/5		94/2/0/4		88/6/2/4	88/8/0/4	94/1/0/5		94/0/2/4	94/2/0/4	89/8/0/3	89/8/0/3
	N	19		15	14			14		13			
ISSC 50	I/S/S/C	80/4/2/14	80/6/0/14	80/2/4/14	80/5/1/14			80/4/2/14	80/5/1/14	80/2/4/14	80/4/2/14		
	N	19		9		9		19		9		7	6
ISSC 35	I/S/S/C	50/12/13/25	50/14/11/25	60/6/9/25	56/12/7/25	60/7/11/22	55/14/9/22	56/15/7/22	55/14/6/25	60/6/9/25	55/15/5/25	65/0/13/22	55/16/7/22
	N	10		6		6	6	19		6		4	4
ISSC 0	I/S/S/C	40/40/0/20	40/40/0/20	35/32/13/20	35/30/15/20	45/22/7/26	37/32/6/26	35/40/5/20		35/33/13/20	35/30/15/20	45/20/9/26	40/32/2/26
	N	5		5	5	3	3	6		4		3	3
Kaolinite	I/S/S/C	0/60/40/0		10/45/25/20	10/68/2/20	10/60/18/12	10/78/0/12	0/80/0/20		10/70/0/20		5/66/17/12	0/80/8/12
	N	47		24		19		47		24	27	19	
KI R1	I/S/S/C												
	N	38		28				47		28			
Chlorite	I/S/S/C	18											
	N							36					
IC 6	I/S/S/C												
	N	23		14				23	23	14			
SS	I/S/S/C	10/0/0/90		6/0/0/94				10/0/0/90		6/0/0/94			
	N					2						2	
						100/0						100/0	

		1957 CF						**1957 CU**					
		2-0.2 µm		0.2-0.05 µm		<0.05 µm		2-0.2 µm		0.2-0.05 µm		<0.05 µm	
		AD	EG	AD	EG	AD	EG	AD	EG	AD	EG	AD	EG
Illite	N	36		30				32	31	30			
ISSC 90	I/S/S/C												
	N	19	27	14		9	9	23		14		10	
ISSC 80	I/S/S/C	95/0/0/5	92/0/0/8	95/1/0/4		89/7/0/4	89/7/0/4	94/0/0/6	94/0/0/6	95/1/0/4		89/4/2/4	89/5/1/4
	N	21		15				14	15	14			
ISSC 50	I/S/S/C	75/8/3/14	75/7/4/14	76/2/8/14	76/10/0/14			75/0/11/14	75/5/6/14	76/2/8/14	76/10/0/14		
	N	14		9		8	7	14		9		8	
ISSC 35	I/S/S/C	45/17/13/25	45/20/9/25	55/12/8/25	50/16/9/25	60/7/11/22	52/17/9/22	45/8/22/25	45/19/11/25	60/6/9/25	58/14/3/25	60/7/11/22	55/16/7/22
	N	9		6		4		10		6		4	
ISSC 0	I/S/S/C	35/45/0/20	35/41/4/20	35/39/6/20	35/37/8/20	33/23/17/26	30/39/5/26	35/42/3/20	35/39/6/20	40/30/10/20	38/25/17/20	40/18/17/25	30/35/9/26
	N	6	5	5		3		7	6	5	6	3	
Kaolinite	I/S/S/C	0/70/10/20	0/80/0/20	5/63/12/20	5/75/0/20	0/78/10/12	0/85/3/12	0/70/10/20	0/80/0/20	5/63/12/20	10/65/5/20	5/70/13/12	0/88/0/12
	N	47		24	27			47		28			
KI R1	I/S/S/C									98/2			
	N	47		28		19		47		28		19	
Chlorite	I/S/S/C												
	N	23						28	23				
IC 6	I/S/S/C												
	N			14				27		14			
SS	I/S/S/C			6/0/0/94				10/0/0/90	4/0/0/96	6/0/0/94			
	N					2						2	
						100/0						100/0	

		1957 RF						**1957 RU**					
		2-0.2 µm		0.2-0.05 µm		<0.05 µm		2-0.2 µm		0.2-0.05 µm		<0.05 µm	
		AD	EG	AD	EG	AD	EG	AD	EG	AD	EG	AD	EG
Illite	N	36		22				36		22			
ISSC 90	I/S/S/C												
	N	27		14		10	9	27		12		10	9
ISSC 80	I/S/S/C	94/0/1/5	94/1/0/5	90/6/0/4		89/4/0/7	89/7/0/4	94/0/1/5	94/1/0/5	90/6/0/4	90/5/1/4	89/4/0/7	
	N	19	23	15				23		15	14		
ISSC 50	I/S/S/C	78/2/6/14	78/5/3/14	75/7/4/14	75/8/3/14			75/0/11/14	75/5/6/14	75/3/8/14	75/8/3/14		
	N	19		9		7		14		9		7	
ISSC 35	I/S/S/C	45/20/10/25	45/18/12/25	54/7/14/25	54/14/7/25	62/0/16/22	54/13/10/22	45/12/18/25	45/17/13/25	60/5/10/25	54/12/9/25	62/0/16/22	54/13/10/22
	N	9		7		4		10		7		4	
ISSC 0	I/S/S/C	35/43/2/20	35/45/0/20	35/43/2/20	35/31/14/20	42/20/11/26	30/39/5/26	35/37/8/20	35/45/0/20	35/33/12/20	35/30/15/20	42/20/11/27	30/35/9/26
	N	7		6	5	3		6		5		3	
Kaolinite	I/S/S/C	0/60/20/20	0/80/0/20	5/65/10/20	0/77/3/20	5/65/18/12	0/88/0/12	0/80/0/20		10/50/20/20	10/68/2/20	5/58/25/12	0/85/3/12
	N	47		28				47		28			
KI R1	I/S/S/C	98/2						98/2					
	N	38		28		19		47		28		19	
Chlorite	I/S/S/C												
	N	32						36					
IC 6	I/S/S/C												
	N	23		14				23		14			
SS	I/S/S/C	10/0/0/90		3/0/0/97				10/0/0/90		6/0/0/94			
	N					2						2	
						100/0						100/0	

		1980 CF						**1980 CU**					
		2-0.2 μm		0.2-0.05 μm		<0.05 μm		2-0.2 μm		0.2-0.05 μm		<0.05 μm	
		AD	EG	AD	EG	AD	EG	AD	EG	AD	EG	AD	EG
Illite	N	36		30				36		30			
ISSC 90	I/S/S/C												
	N	19	27	14		9		23		14		9	
ISSC 80	I/S/S/C	95/0/0/5		95/1/0/4		91/5/0/4	89/7/0/4	95/0/0/5		95/1/0/4		90/0/6/4	90/5/2/4
	N	21		15	14			23		15	14		
ISSC 50	I/S/S/C	80/6/0/14	80/2/4/14	76/2/8/14	76/10/14			75/6/5/14		76/2/8/14	76/10/0/14		
	N	23		9		8	7	21		9		8	7
ISSC 35	I/S/S/C	50/15/10/25	55/12/8/25	50/17/8/25	60/0/18/22	50/20/8/22	45/19/11/25	60/6/9/25	58/14/3/25	60/7/11/22	50/21/8/22	62/0/16/22	54/13/10/22
	N	19		6		4	3	10	11	6		4	3
ISSC 0	I/S/S/C	35/40/5/20	35/45/0/20	30/43/7/20	30/42/8/20	33/20/21/26	30/44/0/26	35/38/7/20	35/41/4/20	40/30/10/20	38/30/12/20	40/20/14/26	35/33/7/26
	N	6	5	8	7	3		7		6		3	
Kaolinite	I/S/S/C	0/70/10/20	0/80/0/20	5/57/18/20	0/80/0/20	0/55/23/22	0/75/13/12	0/70/10/20	0/80/0/20	5/60/15/20	5/69/7/20	5/68/15/12	0/79/9/12
	N	47		28				47		28			
KI R1	I/S/S/C			98/2						98/2			
	N	47		28		19		47		28		19	
Chlorite	I/S/S/C												
	N	36						36					
IC 6	I/S/S/C												
	N	19		14				23		14			
SS	I/S/S/C	5/5/0/90		6/0/0/94				10/0/0/90		3/0/0/97			
	N					2						2	
						100/0						100/0	

		1980 RF						**1980 RU**					
		2-0.2 µm		0.2-0.05 µm		<0.05 µm		2-0.2 µm		0.2-0.05 µm		<0.05 µm	
		AD	EG	AD	EG	AD	EG	AD	EG	AD	EG	AD	EG
Illite	N	36		22				36		22			
ISSC 90	I/S/S/C												
	N	27		12		10	9	27		12		10	9
ISSC 80	I/S/S/C	94/0/1/5	94/1/0/5	94/3/0/3		88/3/5/4	88/8/0/4	94/0/1/5	94/1/0/5	90/6/0/4	90/5/1/4	89/4/0/7	89/7/0/4
	N	23		17				23		15	14		
ISSC 50	I/S/S/C	76/6/4/12		78/0/08/14	78/7/1/14			78/6/4/12		70/5/11/14	70/12/4/14		
	N	19		9		7	6	19		9		8	7
ISSC 35	I/S/S/C	45/22/8/25	45/20/10/25	54/7/14/25	53/14/8/25	62/5/11/22	52/18/8/22	50/22/3/25	50/18/7/25	56/9/10/25	52/15/8/25	60/0/18/22	54/13/10/22
	N	19		7		4		19		7		4	
ISSC 0	I/S/S/C	35/43/2/20	35/45/0/20	35/39/6/20	35/33/12/20	42/22/11/26	35/31/9/26	35/45/0/20	30/44/6/20	30/34/16/20	40/19/15/26	30/35/9/26	30/35/9/26
	N	6		6	5	3		6		6		3	
Kaolinite	I/S/S/C	0/80/0/20		5/66/9/20	0/80/0/20	5/65/18/12	0/88/0/12	0/80/0/20		5/49/25/20	5/75/0/20	5/61/22/12	0/85/3/12
	N	47		28				47		28			
KI R1	I/S/S/C	99/1						98/2					
	N	47		28		19		47		28		19	
Chlorite	I/S/S/C												
	N	36						36					
IC 6	I/S/S/C												
	N	23		14				23		13			
SS	I/S/S/C	10/0/0/90		6/0/0/94				10/0/0/90		3/0/0/97			
	N					2						2	
						100/0						100/0	

		1997 CF						**1997 CU**					
		2-0.2 μm		0.2-0.05 μm		<0.05 μm		2-0.2 μm		0.2-0.05 μm		<0.05 μm	
		AD	EG	AD	EG	AD	EG	AD	EG	AD	EG	AD	EG
Illite	N	36		30				36		30			
ISSC 90	I/S/S/C												
	N	27		14		10	9	23		14		10	
ISSC 80	I/S/S/C	95/0/0/5		95/1/0/4		89/5/2/4	90/5/1/4	95/0/0/5		95/1/0/4		90/5/1/4	
	N	21		15	14			23		15	14		
ISSC 50	I/S/S/C	80/5/1/14	80/2/4/14	76/2/8/14	73/11/2/14			75/6/5/14		76/2/8/14	73/8/5/14		
	N	27		9		8	7	21		9		8	7
ISSC 35	I/S/S/C	50/15/10/25	60/5/10/25	58/14/3/25	60/7/11/22	50/20/8/22	45/19/11/25	60/5/10/25	56/15/4/25	60/7/11/22	50/19/9/22	62/0/16/22	54/13/10/22
	N	19	23	6		4	3	10	11	6		4	3
ISSC 0	I/S/S/C	35/40/5/20	35/45/0/20	40/30/10/20	38/30/12/20	40/17/17/26	30/42/2/26	35/38/7/20	35/38/7/20	35/34/11/20	36/31/13/20	40/20/14/26	30/37/7/26
	N	6	8	6		3		7		6		3	
Kaolinite	I/S/S/C	0/70/10/80	0/80/0/20	5/60/15/20	0/75/5/20	5/66/17/12	0/79/9/12	0/70/10/20	0/80/0/20	5/60/15/20	0/75/5/20	5/68/15/12	0/79/9/12
	N	47		28				47		28		16	
KI R1	I/S/S/C			98/2						98/2			
	N	38		28		19		38		28		19	
Chlorite	I/S/S/C												
	N	36						32					
IC 6	I/S/S/C												
	N	19		14				23		14			
SS	I/S/S/C	5/5/0/90		3/0/0/97				10/0/0/90		3/0/0/97			
	N					2						2	
						100/0						100/0	

		1997 RF						**1997 RU**					
		2-0.2 µm		0.2-0.05 µm		<0.05 µm		2-0.2 µm		0.2-0.05 µm		<0.05 µm	
		AD	EG	AD	EG	AD	EG	AD	EG	AD	EG	AD	EG
Illite	N	36		22				36		22			
ISSC 90	I/S/S/C												
	N	27		12		10	9	27		12		10	9
ISSC 80	I/S/S/C	94/0/1/5	94/1/0/5	94/3/0/3		89/6/1/4	89/6/1/4	92/2/2/5		90/6/0/4	90/5/1/4	89/5/1/4	89/7/1/4
	N	23		17				23		15	14		
ISSC 50	I/S/S/C	78/6/4/12		78/0/8/14	78/7/1/14			75/5/6/14		75/4/7/14	70/12/4/14		
	N	19		9		7	6	19		9		8	7
ISSC 35	I/S/S/C	50/16/9/25	50/17/8/25	54/6/15/25	53/14/8/25	60/3/15/22	50/17/11/22	50/18/7/25	56/5/14/25	52/14/8/25	60/0/18/22	54/12/11/22	54/13/10/22
	N	19		7		4		18		7		4	
ISSC 0	I/S/S/C	35/43/2/20	35/45/0/20	35/39/6/20	35/33/12/20	42/22/11/26	30/35/9/26	35/30/15/20	30/37/13/20	30/35/15/20	40/19/15/26	30/38/6/26	30/35/9/26
	N	6		5		3		7		6	5	3	
Kaolinite	I/S/S/C	0/80/0/20		5/66/9/20	0/80/0/20	5/65/18/12	0/88/0/12	0/80/0/20		5/60/15/20	0/80/0/20	5/61/22/12	0/88/0/12
	N	47		28				47		28			
KI R1	I/S/S/C			99/1						98/2			
	N	38		28		19		38		28		19	
Chlorite	I/S/S/C												
	N	32						27					
IC 6	I/S/S/C												
	N	23		14				23		13			
SS	I/S/S/C	10/00/0/90	6/0/0/94					3/0/0/97					
	N					2						2	
						100/0						100/0	

		2013 CF						2013 CU					
		2-0.2 µm		0.2-0.05 µm		<0.05 µm		2-0.2 µm		0.2-0.05 µm		<0.05 µm	
		AD	EG	AD	EG	AD	EG	AD	EG	AD	EG	AD	EG
Illite	N	36		30				36		30			
ISSC 90	I/S/S/C												
	N	19	27	14		10	9	23		14		10	
ISSC 80	I/S/S/C	95/0/0/5	94/0/0/6	93/1/1/5	93/2/0/5	89/5/2/4	89/6/1/4	95/0/0/5	95/0/0/5	93/1/1/5	93/2/0/5	90/5/1/4	
	N	23		15				23		15			
ISSC 50	I/S/S/C	80/5/1/14	78/0/8/14	75/0/11/14	75/11/0/14			75/0/11/14	75/7/4/14	75/0/11/14	75/11/0/14		
	N	21	18	9		7	6	21	23	9		8	7
ISSC 35	I/S/S/C	50/16/9/25	45/17/13/25	60/6/8/25	54/11/9/25	60/3/15/22	50/17/11/22	42/20/12/25	42/17/15/25	58/7/10/25	50/14/12/25	60/7/11/22	52/17/9/22
	N	14	10	8		4		10	11	8		4	3
ISSC 0	I/S/S/C	35/35/10/20	35/45/0/20	30/30/20/20	30/30/20/20	42/21/11/26	30/35/9/26	35/38/7/20	35/38/7/20	30/36/13/20	30/37/13/20	40/22/12/26	30/36/8/26
	N	7		7		4	3	7		7		3	
Kaolinite	I/S/S/C	0/070/10/	0/80/0/20	0/71/9/20	0/70/10/20	5/65/18/12	0/88/0/12	0/70/10/20	0/80/0/20	0/71/9/20	0/80/0/20	5/68/15/12	0/79/9/12
	N	47		28				47		28		19	
KI R1	I/S/S/C			98/2						98/2			
	N	38		28		19		38		28		19	
Chlorite	I/S/S/C												
	N	36	32					36					
IC 6	I/S/S/C												
	N	23		19	14			23		19	14		
SS	I/S/S/C	10/0/0/90		8/0/0/92	6/0/0/94			10/0/0/90		8/0/0/92	6/0/0/94		
	N					2						2	
						100/0						100/0	

		2013 RF						2013 RU					
		2-0.2 µm		0.2-0.05 µm		<0.05 µm		2-0.2 µm		0.2-0.05 µm		<0.05 µm	
		AD	EG	AD	EG	AD	EG	AD	EG	AD	EG	AD	EG
Illite	N	28		22				30		22			
ISSC 90	I/S/S/C												
	N	27		12		10		27		12		10	9
ISSC 80	I/S/S/C	94/0/1/5		95/0/1/4	95/1/0/4	89/6/1/4		92/2/1/5		91/5/0/4	91/4/2/4	89/6/1/4	
	N	23		17				23		15			
ISSC 50	I/S/S/C	78/0/12/10	78/6/6/10	78/0/8/14	78/8/0/14			75/5/6/14		75/2/10/14	75/11/0/14		
	N	19		9		8	7	19		9		8	7
ISSC 35	I/S/S/C	50/16/9/25	50/18/7/25	54/6/15/25	53/14/8/25	60/7/11/22	54/18/6/22	50/20/5/25	50/18/7/25	58/8/9/25	50/13/12/25	60/9/9/22	54/17/7/22
	N	19		8		4	3	18		7		4	3
ISSC 0	I/S/S/C	35/45/0/20		32/41/7/20	32/34/14/20	40/22/12/26	33/36/5/26	35/30/15/20		30/30/20/20	40/25/9/26	33/33/8/26	30/35/9/26
	N	6		7		3		7		6		4	3
Kaolinite	I/S/S/C	0/80/0/20		5/66/9/20	5/75/0/20	5/68/15/12	0/79/10/12	0/080/0/20	0/50/30/20	0/70/10/20	5/61/22/12	0/75/13/12	0/85/3/12
	N	47		28				47		28			
KI R1	I/S/S/C			98/2						98/2			
	N	38		28		19		38		28		19	
Chlorite	I/S/S/C												
	N	32											
IC 6	I/S/S/C												
	N	23		14				27		13			
SS	I/S/S/C	10/0/0/90		6/0/0/94				1/0/0/99		3/0/0/97			
	N					2						2	
						100/0						100/0	

		2014 CF						2014 CU					
		2-0.2 µm		0.2-0.05 µm		<0.05 µm		2-0.2 µm		0.2-0.05 µm		<0.05 µm	
		AD	EG	AD	EG	AD	EG	AD	EG	AD	EG	AD	EG
Illite	N	36		30				32		30			
ISSC 90	I/S/S/C												
	N	19	27	14		10	10	21	23	14		10	9
ISSC 80	I/S/S/C	94/0/0/6		92/4/0/4		90/5/1/4		92/2/0/6		93/1/1/5	93/2/0/5	89/5/1/4	89/6/1/4
	N	23		15	14			23		15			
ISSC 50	I/S/S/C	78/6/2/14	78/8/0/14	78/2/7/14	78/7/1/14			75/4/7/14	75/6/5/14	75/0/11/14	75/0/11/14		
	N	21	18	9		8	7	21		9		7	6
ISSC 35	I/S/S/C	50/15/10/25	45/17/13/25	55/4/16/25	52/14/10/24	60/7/11/22	52/19/7/22	42/16/17/25	42/16/17/25	58/7/10/25	50/14/12/25	63/1/13/22	53/16/9/22
	N	14	10	6		4	3	7		8		4	3
ISSC 0	I/S/S/C	35/40/5/20	35/45/0/20	30/33/17/20	30/34/16/20	40/17/17/26	35/33/7/26	30/43/7/20	30/42/9/20	30/29/21/20	30/32/18/20	43/21/11/26	33/33/7/26
	N	7		8		3		7		8		4	3
Kaolinite	I/S/S/C	0/70/10/20	0/80/0/20	0/55/25/20	0/75/5/20	5/66/17/12	0/79/9/12	0/70/10/20	0/55/25/20	0/78/2/20	5/65/18/12	0/88/0/12	0/85/3/12
	N	47		28				47		28			
KI R1	I/S/S/C			98/2						99/1			
	N	38		28		19		38		28		19	
Chlorite	I/S/S/C												
	N	36	32					36					
IC 6	I/S/S/C												
	N	23		14				23		14			
SS	I/S/S/C	10/0/0/90		6/0/0/94				10/0/0/90		6/0/94			
	N					2						2	
						100/0						100/0	

		2014 RF						2014 RU					
		2-0.2 µm		0.2-0.05 µm		<0.05 µm		2-0.2 µm		0.2-0.05 µm		<0.05 µm	
		AD	EG	AD	EG	AD	EG	AD	EG	AD	EG	AD	EG
Illite	N	36		22				36		22			
ISSC 90	I/S/S/C												
	N	27		13		10	9	27		12		10	9
ISSC 80	I/S/S/C	94/0/1/5	94/1/0/5	96/0/1/3	96/1/0/3	89/4/2/4	89/6/1/4	92/3/0/5		94/2/0/4	94/1/1/4	89/4/2/4	89/7/1/4
	N	23		19				23		18			
ISSC 50	I/S/S/C	78/0/12/10	78/6/6/10	75/0/11/14	75/8/3/14			75/5/6/14		80/4/2/14	75/5/3/14		
	N	19		9		7	6	19		9		8	7
ISSC 35	I/S/S/C	50/16/9/25	50/18/7/25	54/6/15/25	52/15/8/25	60/3/15/22	50/15/13/22	50/20/5/25	50/18/7/25	56/8/11/25	52/13/10/25	60/6/12/22	54/12/11/22
	N	19		8		4		17		7		4	
ISSC 0	I/S/S/C	35/45/0/20		32/38/10/20	32/30/18/20	42/22/11/26	30/35/9/26	35/36/10/20		30/38/12/20	30/35/15/20	40/20/13/26	30/38/6/26
	N	6		7		3		7		6	5	4	3
Kaolinite	I/S/S/C	0/80/0/20		5/66/9/20	5/75/0/20	5/65/18/12	0/88/0/12	0/80/0/20		0/70/10/20	0/73/7/20	5/66/17/12	0/85/3/12
	N	47		28				47		28			
KI R1	I/S/S/C			98/2						98/2			
	N	38		28		19		38		28		19	
Chlorite	I/S/S/C												
	N	32											
IC 6	I/S/S/C												
	N	23		14				27		13			
SS	I/S/S/C	10/0/0/90		6/0/0/94				1/0/0/99		3/0/0/97			
	N					2						2	
						100/0						100/0	